SAND78-8191
Unlimited Release
UC-62d

Doc 1980/17/00

PHASE II - HELIOSTAT DRIVE MECHANISM

FINAL REPORT

PREPARED FOR

SANDIA LABORATORIES
LIVERMORE, CALIFORNIA

SANDIA CONTRACT NO. 83-0024C

MAY 1980

BY

SOLARAMICS

1301 East El Segundo Boulevard
El Segundo, California 90245

Issued by Sandia National Laboratories, operated for the United States Department of Energy by Sandia Corporation.

Printed in the United States of America
Available from
National Technical Information Service
U. S. Department of Commerce
5285 Port Royal Road
Springfield, VA 22161
Price: Printed Copy $7.25 ; Microfiche $3.00

FORWARD

This final report on the Heliostat Drive Mechanism is submitted in fulfillment of Sandia contract # 83-0024C. Sandia Program Management was provided by Mr. Clayton Mavis. Solaramics personnel contributing to the project included Messrs. W.D. Mitchell, Donald Maxwell, Donald Morden, and J.C. Graddy. The program manager was Mr. H.E. Felix.

TABLE OF CONTENTS

LIST OF FIGURES

LIST OF FIGURES

LIST OF TABLES

INTRODUCTION

The objective of this contract effort has been to design and test the modified azimuth-elevation heliostat drive mechanism generated by SOLARAMICS in the Low Cost Heliostat Preliminary Design Program (contract #ET-78-C-03-1745). The preliminary design has been scaled up to accomodate a larger heliostat of $50m^2$ (524 sq.ft) from the $40m^2$ design.

The design effort has stressed development of a mechanism possessing low initial cost and low maintenance. The basic design concept utilizing 2 linear actuators with bell crank linkages has been retained and refined.

A full scale assembly has been fabricated and tested to evaluate performance characteristics.

1.0 DESIGN CHARACTERISTICS

1.1 Design Criteria

The design criteria has been structured to meet the requirement of specification A10772, Collector Subsystem Requirements summarized below:

- o Operational tracking with wind speed up to 16m/s (35mph)
- o Structural integrity in a non-operational state in a 22m/s (50mph) wind in any orientation
- o Stowage initiation @ 16m/s (35mph) with a maximum wind rise rate of 0.01 m/s^2 (.02 mph/s)
- o Stowed survival in a 40m/s (90mph) wind.

The wind may deviate by up to $\pm$ 10^o from the horizontal for all loading conditions.

- o The drive systems must be capable of positioning the heliostat to stowage, cleaning or maintenance orientation from any operational orientation within 15 minutes.
- o The collector subsystem must maintain structural integrity in any applicable combination of the environments described in Appendix 1 of the subject specification.

The wind loads have been calculated from the coefficients reported in "WIND FORCES ON STRUCTURES" ASCE paper No. 3669. These loads have been utilized in the design calculations and performance analysis reported in Section 1.4.

1.2 Drive Mechanism Design Description

A modified azimuth elevation drive mechanism concept has been developed by SOLARAMICS which embodies an azimuth axis inclined 23^{o} from vertical. The tilted axis is in line with a vector to the tower, and is tilted away from the tower. This concept has the advantage of shifting the location of control singularities outside the operational zone of the tracking requirements. It also reduces the azimuth drive requirement to less than 180^{o} compared to approximately 240^{o} for typical azimuth-elevation systems. The elevation requirement is increased from 180^{o} to 203^{o} to achieve an inverted stowage position.

A unique double bell crank system is utilized to achieve the required angular motions with linear actuators. By attaching the actuator shaft to the functional centerline and the actuator base to a fixed point by one link, and to a rotating crank by another link, a two to one amplification of the rotational motion is achieved. Thus, large angles are achieved with a bell crank system which is normally limited to angles only slightly greater than 90^{o}. The elevation mechanism configuration is shown in Fig.3 and the azimuth mechanism in Fig.4.

A weight summary of the mechanism components is presented in Table 1.

The drive mechanism stiffness was a prime consideration in design for control of natural frequency of the heliostat array and for the performance throughout the operating environmental spectra.

FIGURE 1. HELIOSTAT ASSEMBLY

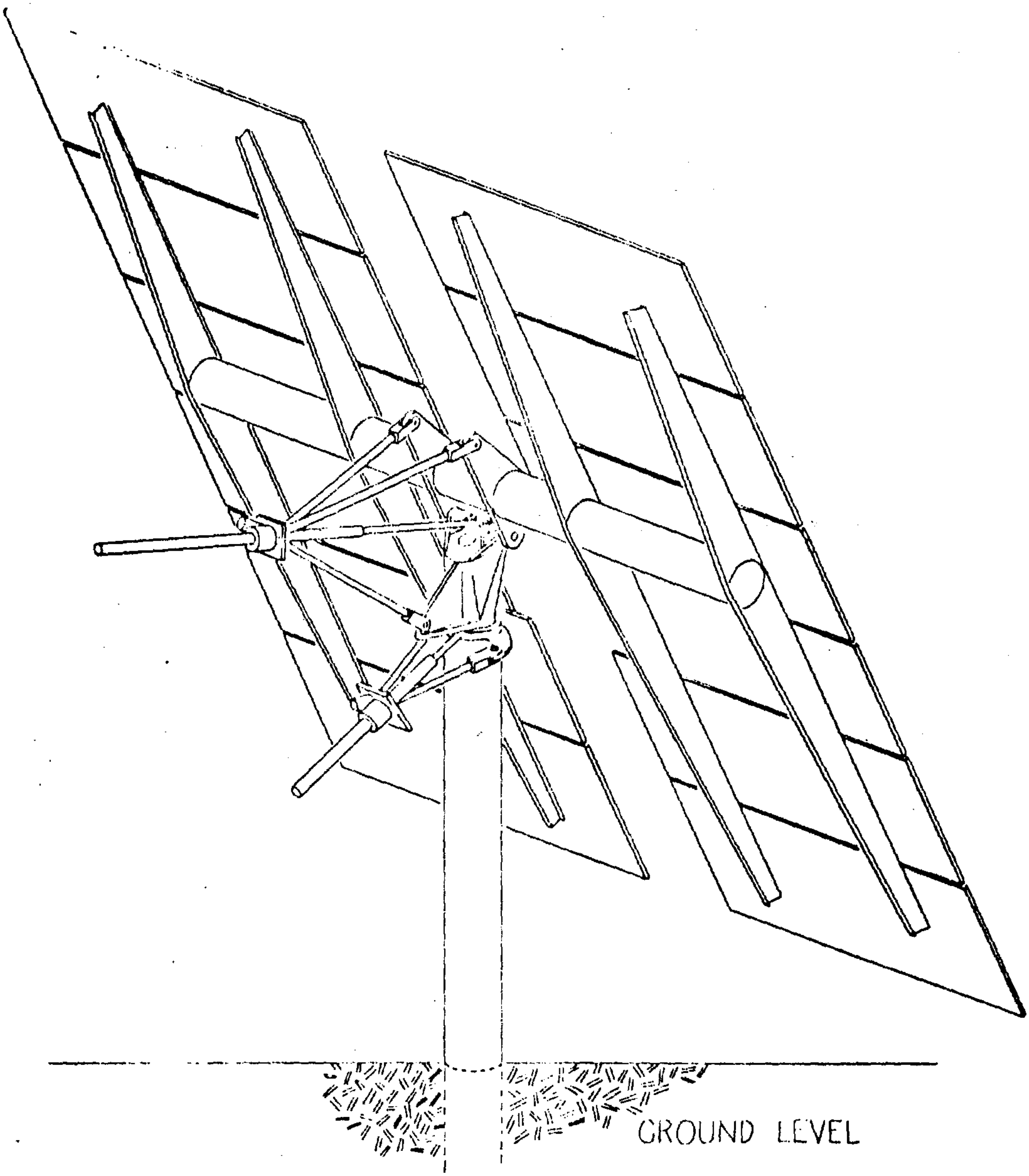

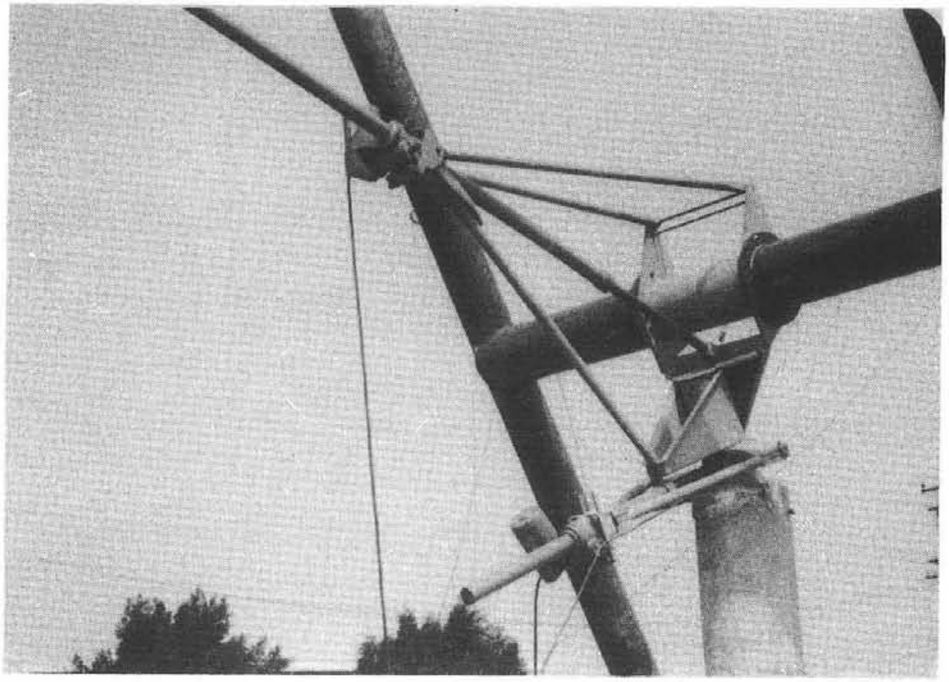

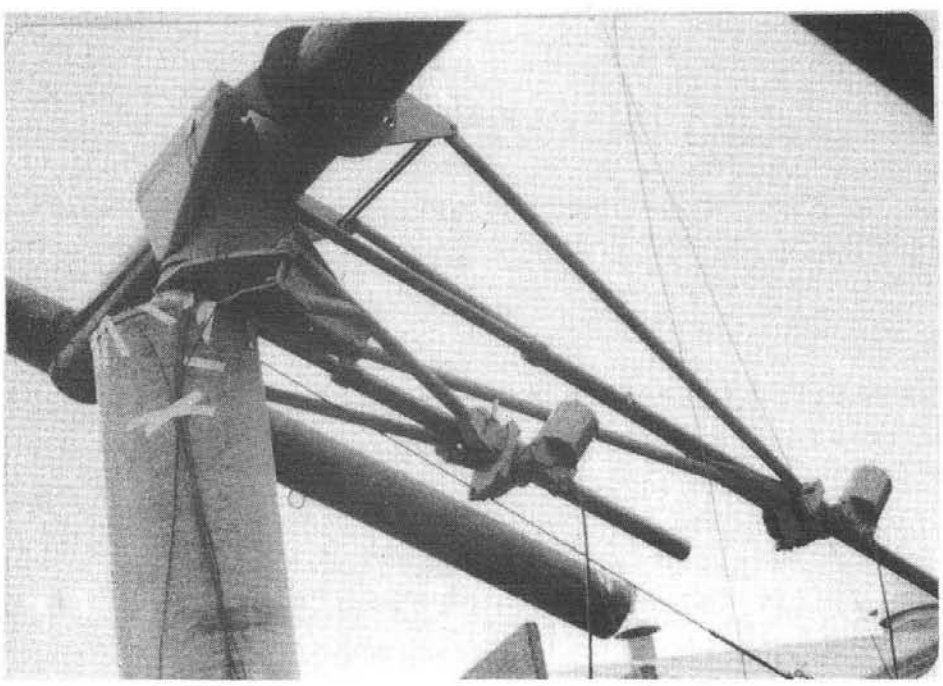

Fig. 2 DRIVE MECHANISM @ 60^{o} ELEVATION &
AT -23o ELEVATION.

FIGURE 3. ELEVATION DRIVE MECHANISM LAYOUT

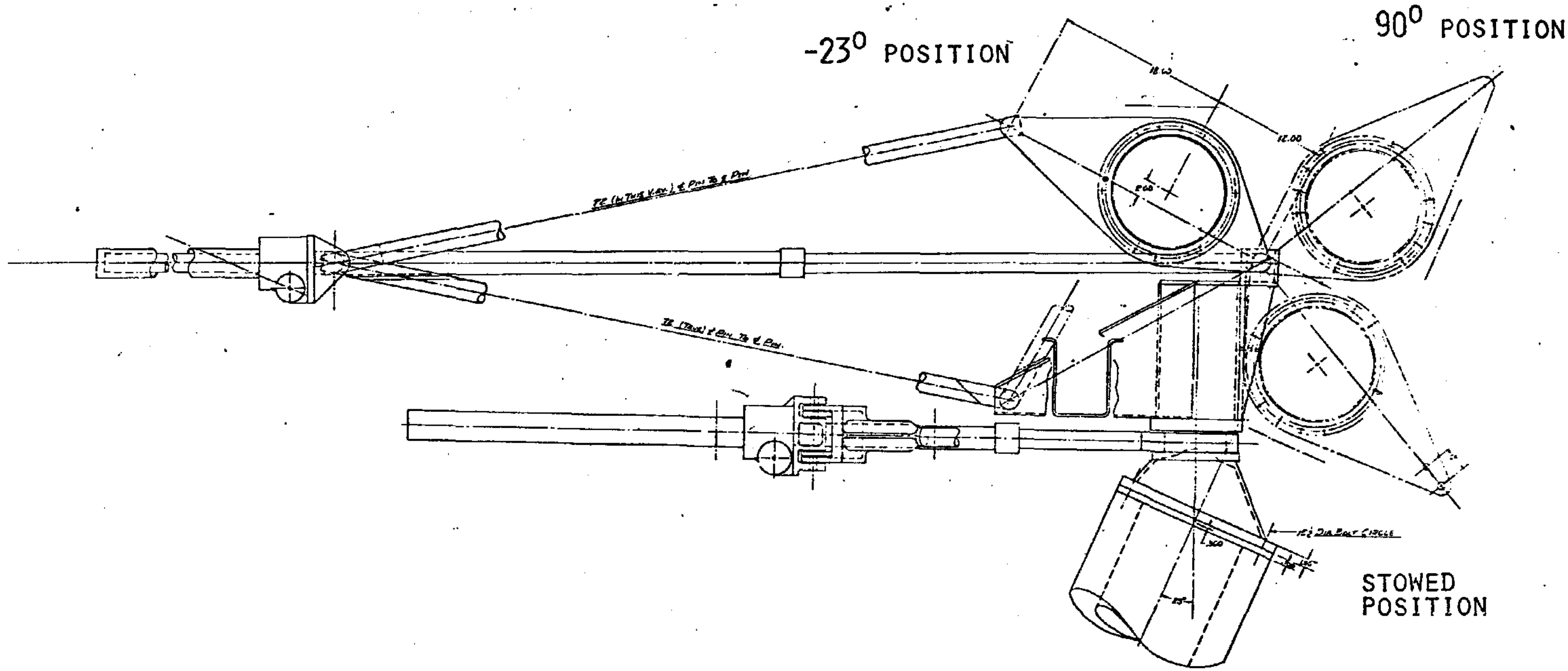

FIGURE 4. AZIMUTH DRIVE MECHANISM (Looking Down)

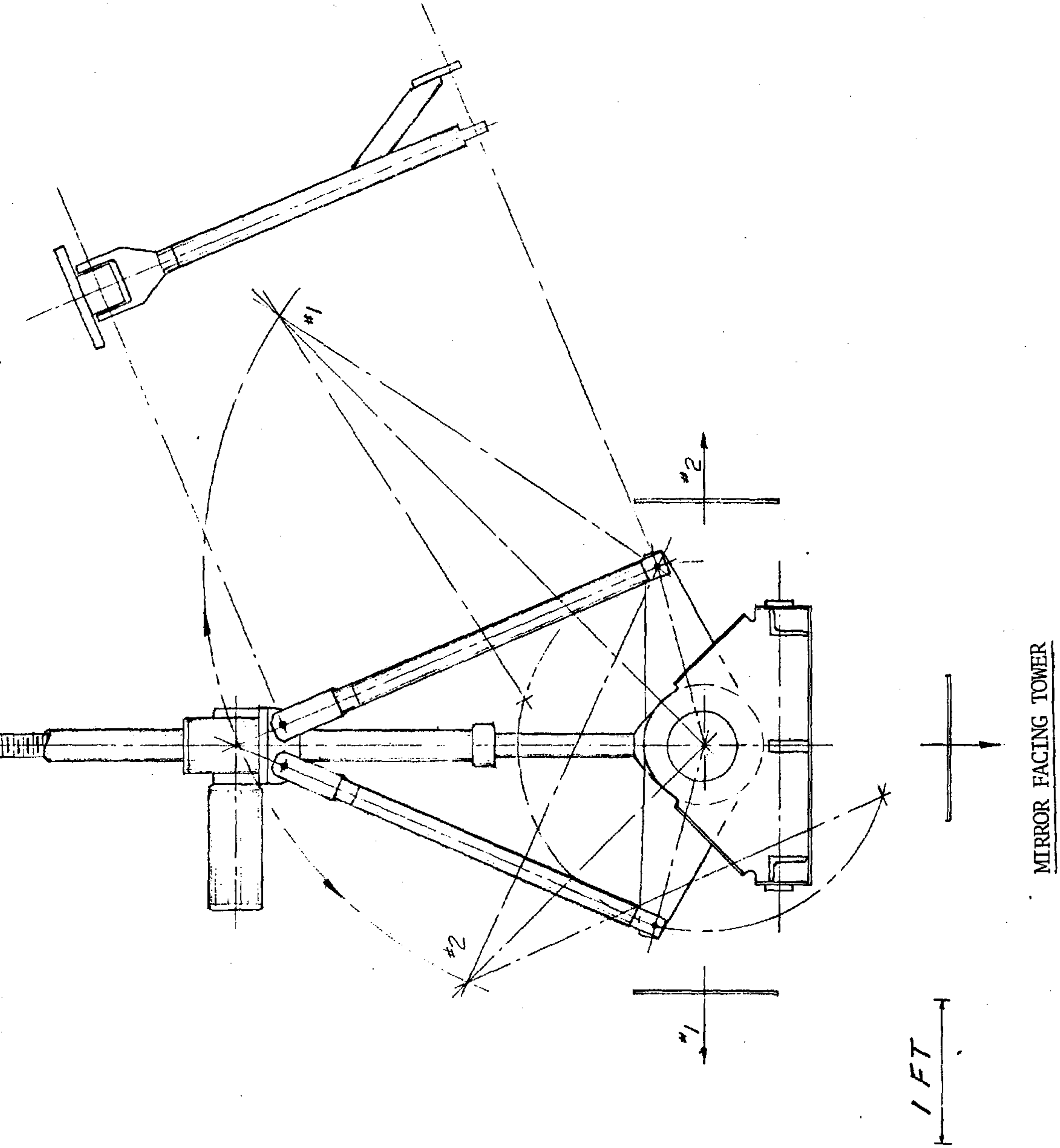

Table 1

DRIVE MECHANISM WEIGHT ESTIMATE

KINGPIN	216 lbs.
TRUNNION	198
CENTER TUBE	41
DRIVE CRANKS	160
UPPER ELEVATION LINKS	202
LOWER ELEVATION LINK	100
ELEVATION ACTUATOR & MOTOR	76
SCREW	56
EXTENSION ROD	70
COVER	15
AZIMUTH DRIVE LINKS	107
AZIMUTH ACTUATOR & MOTOR	72
SCREW	21
EXTENSION ROD	35
COVER	8
COLLAR	20
TOTAL DRIVE MECHANISM	1397 lbs.

1.2.1 Actuators

The advantages of linear actuators chosen for this application include irreversible motion, i.e. self-locking, minimal backlash with adjustment capability for wear, and extensive experience with the design in industrial applications.

Special actuators, specifically for this application, are conceived. The actuators would employ a 2 in. diameter, rolled, modified acme screw thread of 0.2 in. pitch. The screw thread will be roll formed from bar of the required stroke length, then inertia welded to the unthreaded and zinc plated extension shaft.

A single gear reduction of 110 to one by a worm drive is currently planned. The actuator is to be powered by a "three fourths" motor, i.e. a motor without the standard forward bell, which mounts directly on the actuator housing casting. The worm will be an integral part of the motor shaft, roll formed and induction hardened.

The azimuth actuator rate requirement to stow in 15 min. (1.6 in./minute) is only half of the elevation actuator requirement (3.2 in./min.). This is accomplished by utilization of a 875 rpm motor for azimuth drive, and a standard 1750 rpm motor for elevation drive. The clevis fittings for the drive link attachment are an integral part of the actuator housing casting. The actuator features are summarized in Table 2.

1.2.2 Trunnion

The trunnion (Fig. 5) is a welded steel fabrication made up of plate elements. The trunnion contains the elevation hinge pivot and the azimuth axis which rotates on pre-loaded tapered roller bearings on the kingpin. The elevation fixed link pivot and the active azimuth crank pivot are also a part of the trunnion.

TABLE 2

ACTUATOR FEATURES

- MACHINE SCREW SHAFT - 2 IN. DIA.
- 0.2 PITCH, MODIFIED ACME THREAD
- 110 TO 1 SINGLE STAGE GEAR REDUCTION
- PIVOT FITTINGS INTEGRALLY CAST WITH HOUSING
- FULLY ENCLOSED AFT EXTENSION
- FORWARD SCREW ENCLOSED WITH SHIELD & REPLACEABLE GLAND ON SHAFT EXTENSION
- "3/4" MOTOR MCUNTED ON ACTUATOR HOUSING
- 1/3 HP, 1750 RPM MOTOR ON ELEVATION
- 1/4 HP, 875 RPM MOTOR ON AZIMUTH

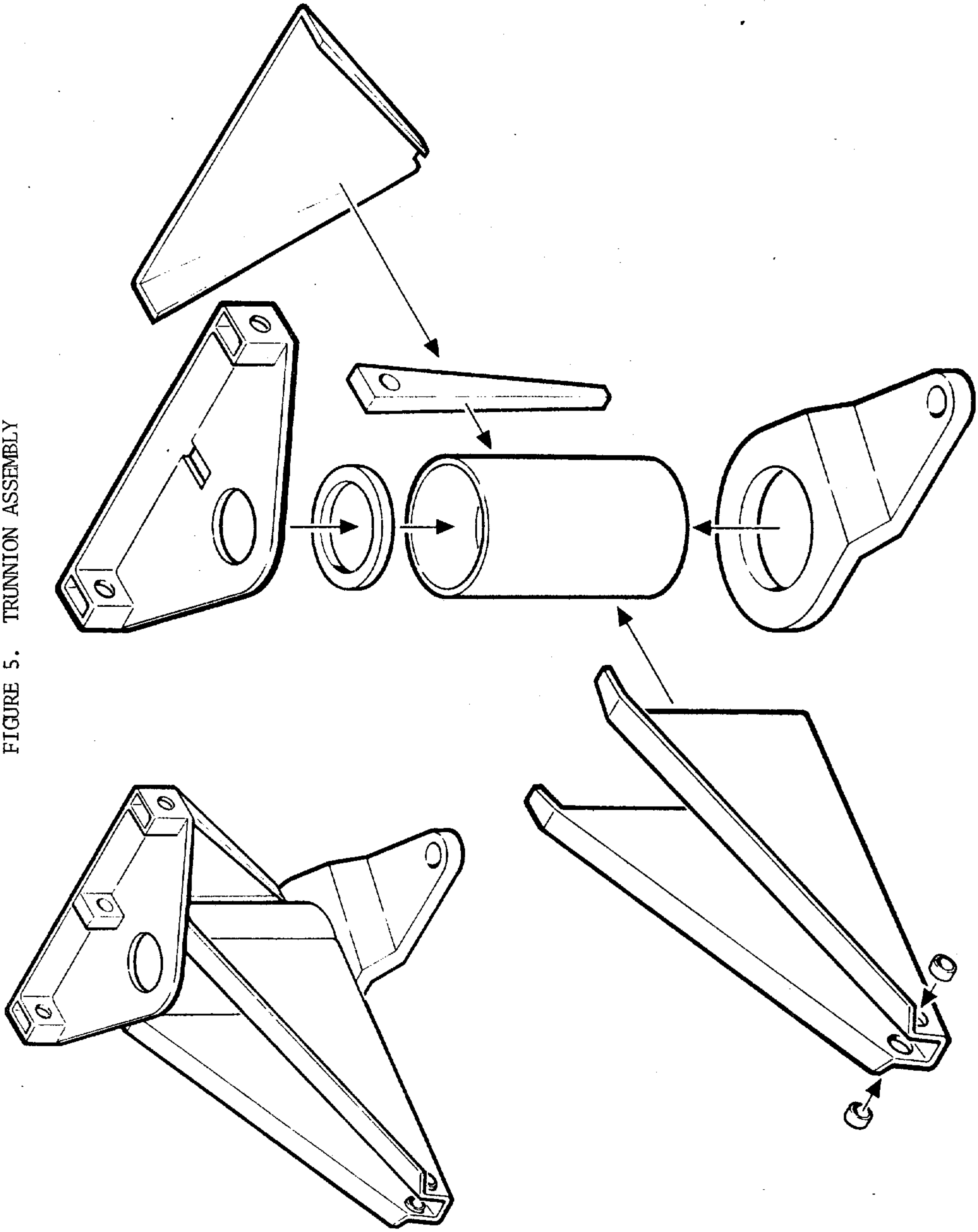

FIGURE 5. TRUNNION ASSEMBLY

FIGURE 6. KINGPIN ASSEMBLY

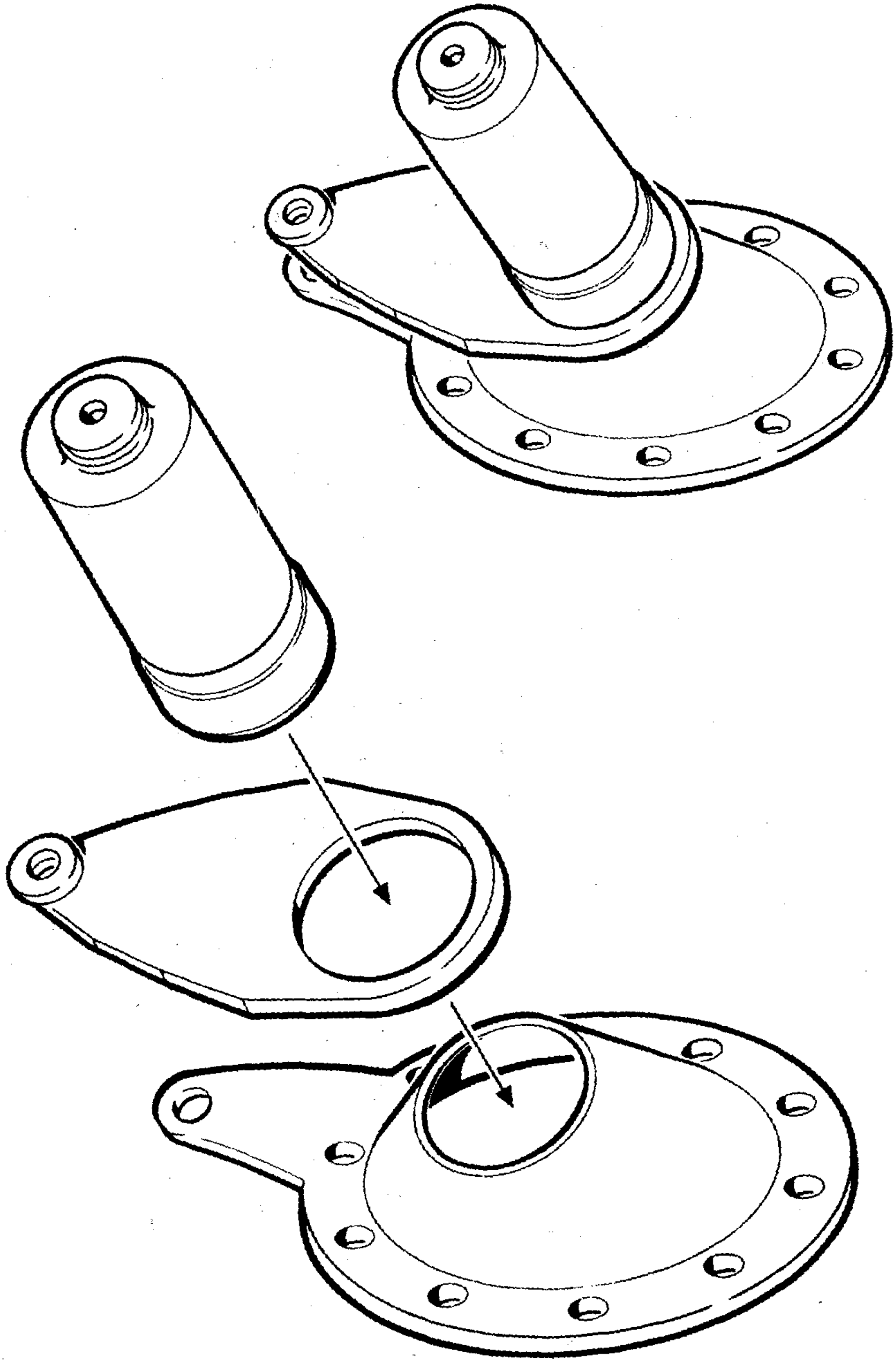

1.2.3 Kingpin

The kingpin (Fig.6) provides the tilted azimuth axis and the structural transition to the pedestal cap. This is accomplished by a 6 in. diameter shaft welded to a tilted, tapered cone and flange forging. The fixed crank for the azimuth linkage and the bearing surface for the azimuth actuator pivot are also provided by the assembly. The three (3) elements are welded together in one set-up with an automated double pass MIG weld. To save material and machining cost, a sleeve is pressed on the 6" diameter shaft for the azimuth collar bearing surface.

1.2.4 Drive Linkage & Bearings

All links are fabricated from 2 in. diameter cold finished merchant bar to which forged end fittings are inertia welded. The forged ends are then milled and bearing holes bored.

A self lubricating bearing fabricated by molding a composite teflon-phenolic material to a steel shell has been chosen for this design. It is produced by Kahr Bearing Co., Division of Sargent Industries. Close tolerance of the installed bearing is accomplished by a broach which is an integral part of the installation tool.

The azimuth rotation is accomplished on a pair of preloaded, tapered roller bearings fitted between the trunnion and kingpin. These bearings support the weight of the heliostat array. Provision is made for supplemental lubrication of these bearings, (Fig.7) which is anticipated at least once during the service life of the assembly, due to breakdown of the initial lubricant.

The azimuth actuator shaft is fitted with a collar, containing a self-lubricating bearing of the composite design described above. The collar rotates about a sleeve on the kingpin and is provided with a thrust bearing of the composite material. The assembly is provided with moisture and dust seals above and below the collar.

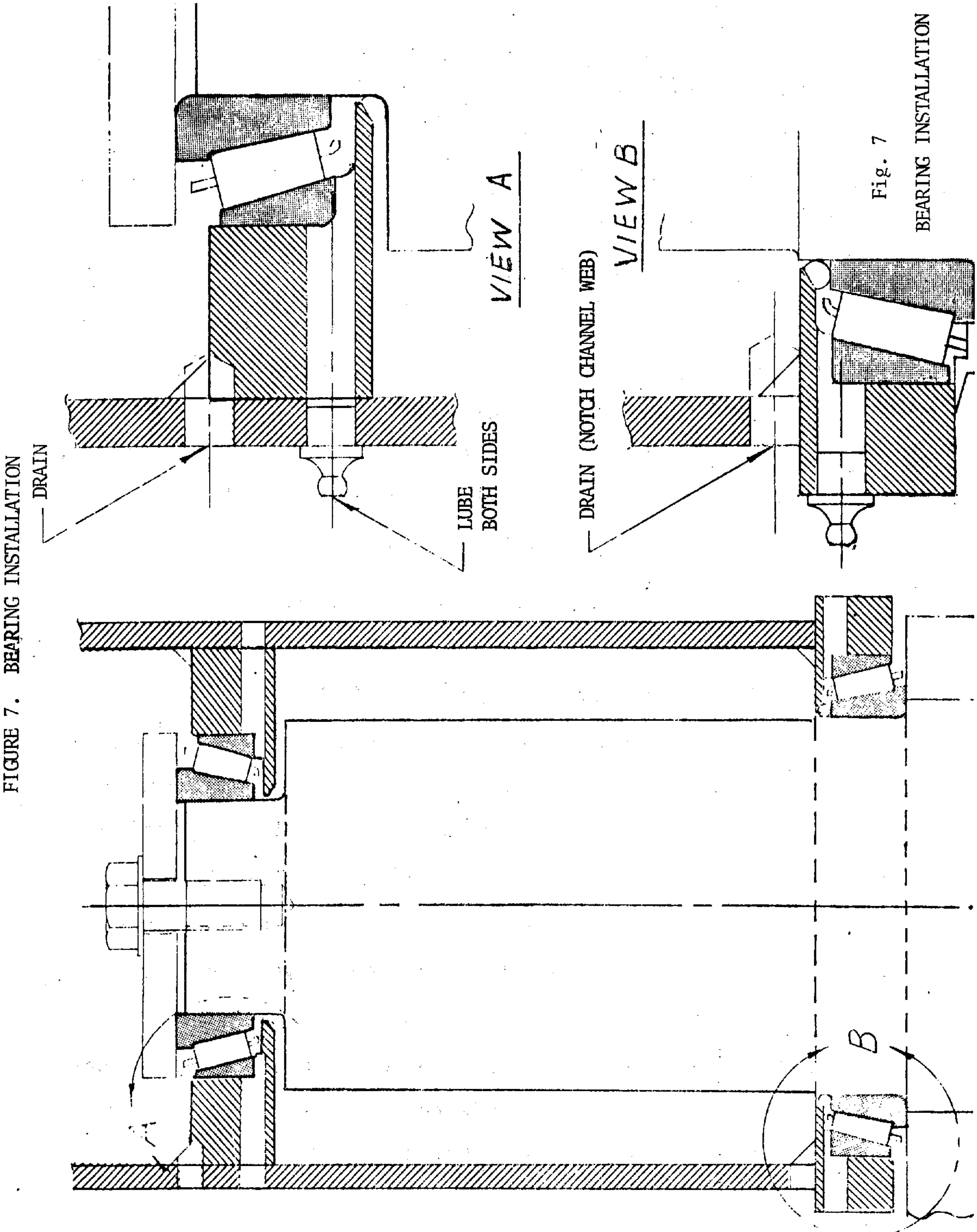
FIGURE 7. BEARING INSTALLATION
DRAIN
LUBE
BOTH SIDES
VIEW A
DRAIN (NOTCH CHANNEL WEB)
VIEW B
Fig. 7
BEARING INSTALLATION
A
B

The drive link/pivot fitting assembly, Fig.8, is fitted with thrust bearings of the self lubricating composite and fine surface finish stainless steel thrust washers. The assembly is sealed with "O" rings to exclude moisture and dust.

1.2.5 Center Torque Tube

The center section of the array main cross tube is a part of the drive mechanism assembly, providing the pivot bearings for the elevation axis and the crank arms for the elevation drive mechanism. The center torque tube assembly consists of a welded steel tube with two plates welded to each end, with provision for a field joint attaching the array frame, Fig.9.

1.2.6 Environmental Protection Features

The exposed metal surfaces are coated with cold galvanizing compound consistency of a fine zinc powder, and an organic binder. The deposited coating contains 95% zinc powder by weight in the dried film.

The motors, and actuator gear boxes are totally enclosed. The actuator shafts are enclosed on the aft extension by a closed tube and on the forward extension by a tube and shaft seal. A drain hole is provided on the forward extension tube to allow accumulated moisture to drain.

The trunnion interior is provided with two drain holes to allow any moisture accumulation to escape. The tilted axis design enhances the drainage effectiveness.

The linkage devices and pin joints are semi-sealed, reducing moisture and dust accumulation. However, the bearing design selected is resistant to this form of degradation, witnessed by their usage in earth-moving equipment.

FIGURE 8. ELEVATION LINKAGE CLEVIS

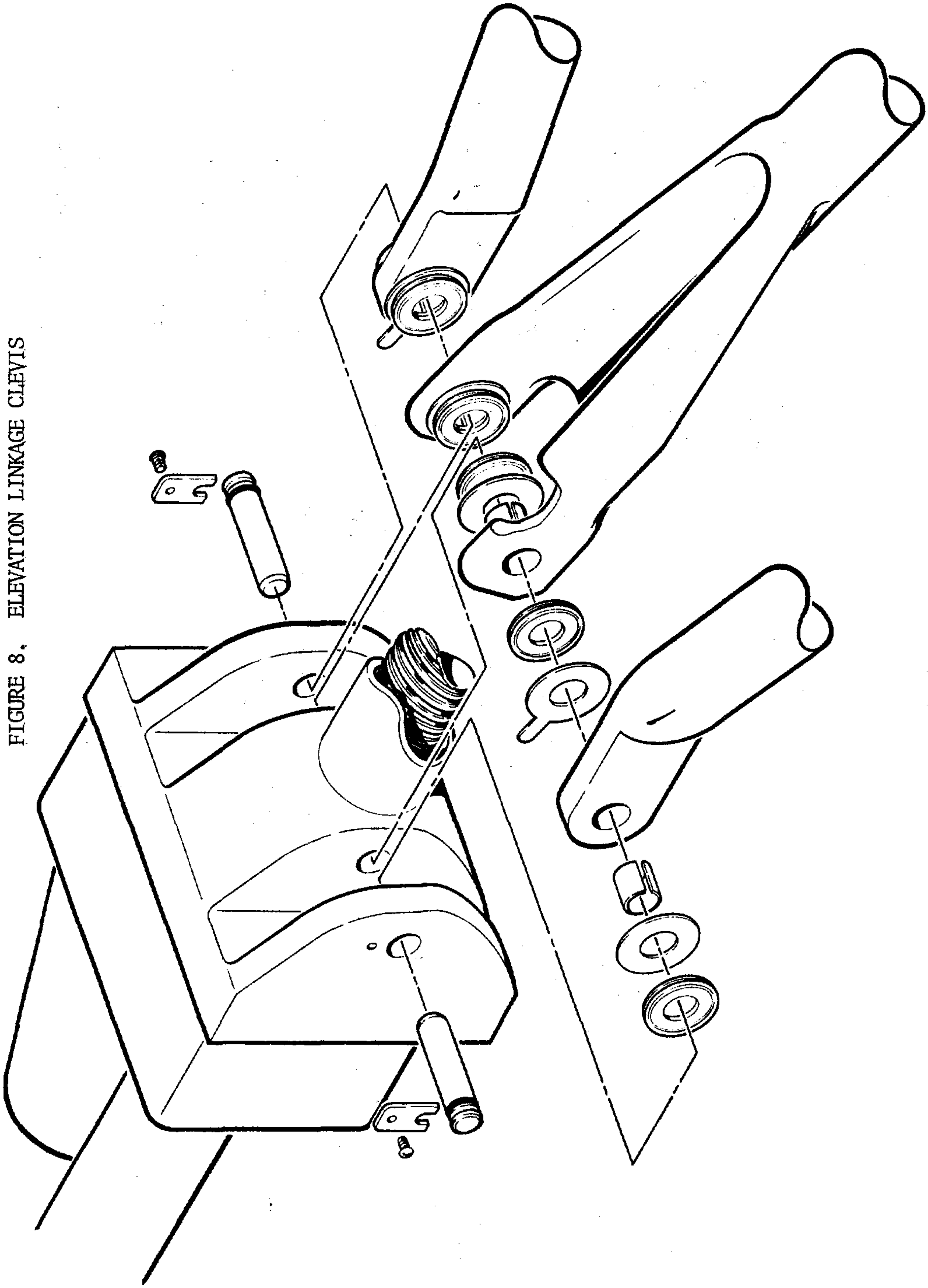

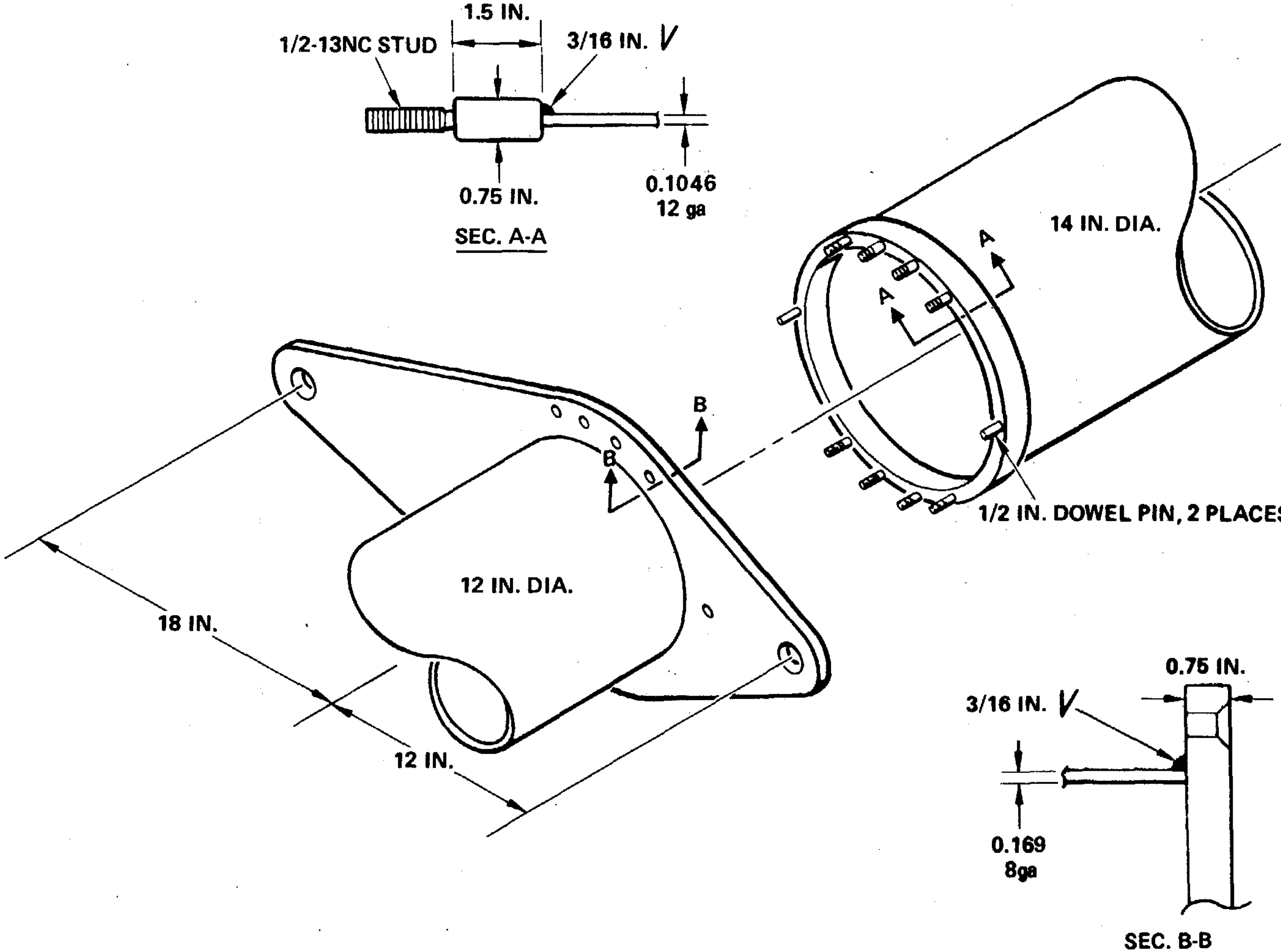

FIGURE 9. CENTER TORQUE TUBE AND FIELD JOINT

1.3 Load Criteria

1.3.1 Wind Aerodynamic Loading

The pertinent pressure coefficients for heliostat aerodynamic loading have been extracted from the ASCE paper referenced in 1.1 and are presented in Figure 10 . The wind profile as a function of elevation, $V_H = V_1 \left(\frac{H}{H_1}\right)^{.15}$, has been employed in the load calculation to determine the effective wind velocity, where:

V_H = Wind velocity at height H.

V_1 = Reference velocity.

H_1 = Reference height ; 10 m(30 ft)

The elevation mechanism moment due to 22 m/s wind, including variation of ± 10° from the horizontal, is presented in Fig.11 , representing the survival wind loading requirement. At stowage with wind speed of 40 m/s the maximum elevation moment is 221,200 in.lbs. at the elevation hinge line.

The moments have been calculated as follows:

$$M = \frac{1}{2} \rho V_H^2 A\, h(.5 - C_{cp})(C_L \cos \alpha + C_D \sin \alpha)$$

Where:

A	= 524 ft² area		H_R	=	Reference Height
h	= 24 ft. chord		H	=	14 ft. height
α	= angle of attack		C_L	=	Lift coefficient
V_H	= Velocity at height H		C_D	=	Drag coefficient
C_{cp}	= center of pressure coefficient				

FIGURE 10. AERODYNAMICS COEFFICIENTS
(Ref: ASCE Paper #3269
Wind Forces on Structures)

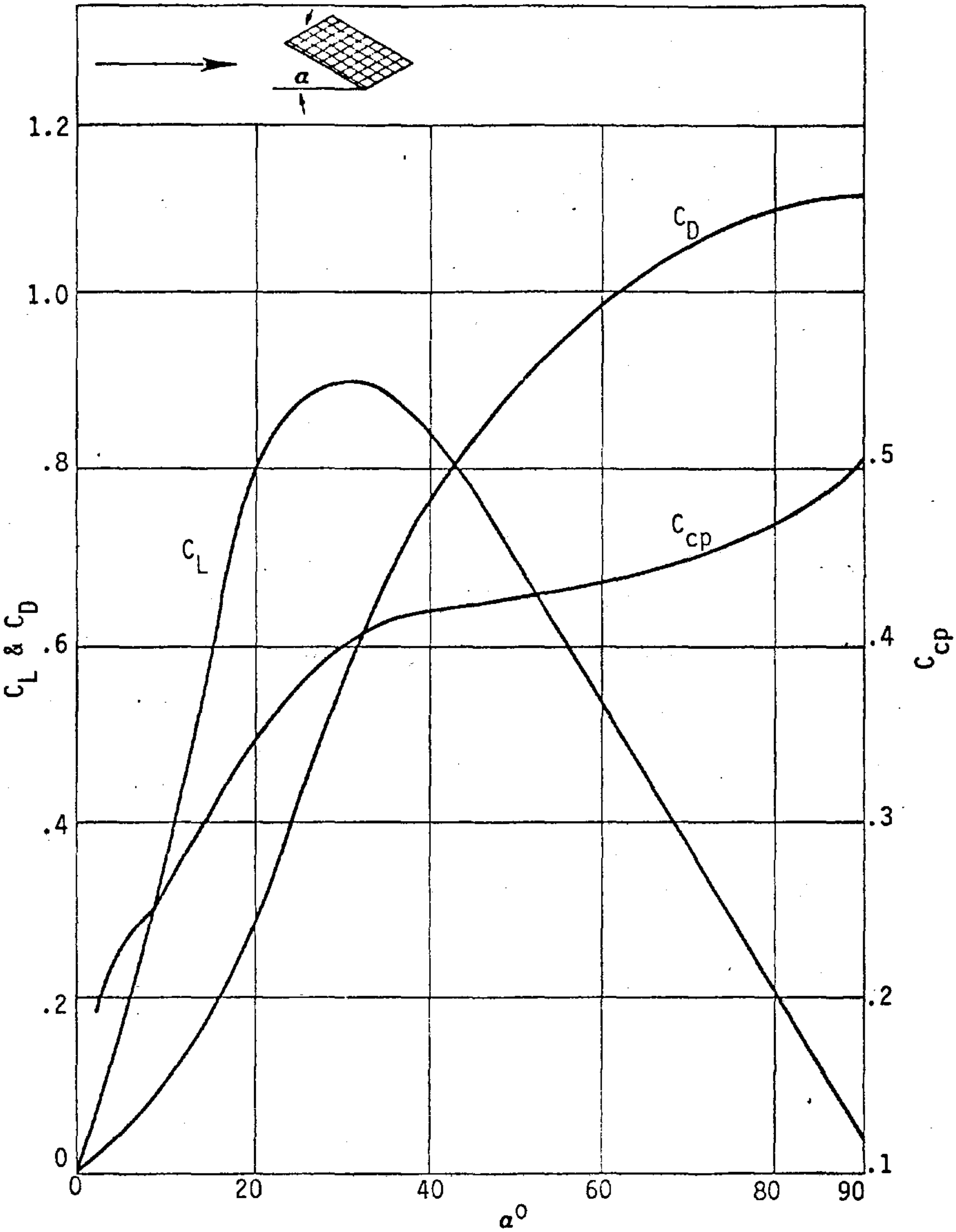

FIGURE 11. ELEVATION MOMENT DUE TO 22m/s WIND @ ± 10° FROM HORIZONTAL

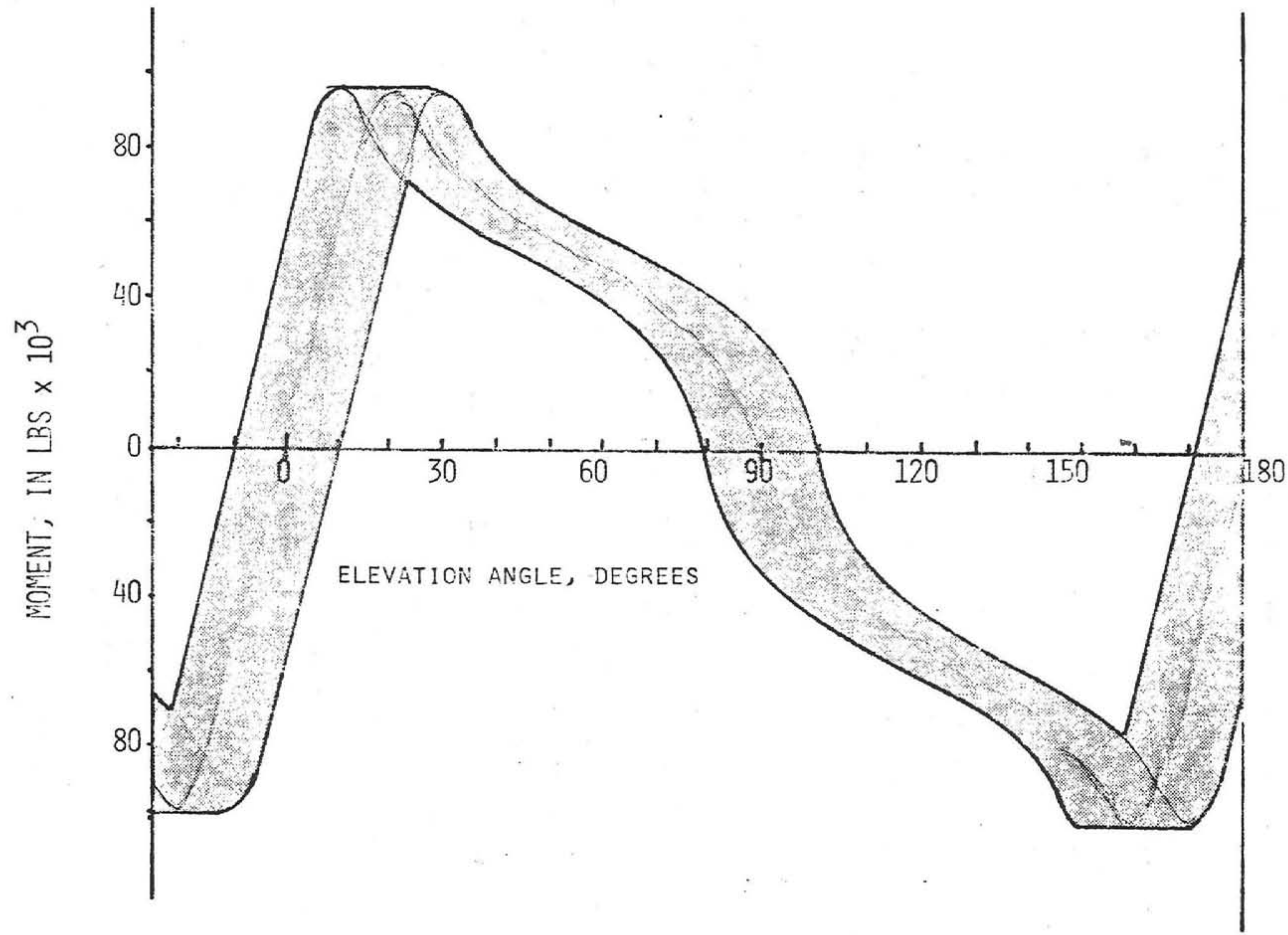

Table 3. ELEVATION MOMENTS

α	C_D	CL	Ccp	M_{16}	M_{22}	M_{40}
10	.106	.36	.26	33,920	64,133	212,000
15	.18	.60	.30	47,460	89,730	
20	.28	.80	.34	51,390	97,163	
25	.42	.88	.375	46,190	87,331	
30	.58	.9	.4	40,530	76,627	
35	.67	.89	.413	36,710	69,403	
40	.75	.85	.42	34,360	64,959	
50	.88	.70	.428	30,670	57,991	
60	.98	.54	.438	26,290	49,698	
70	1.06	.38	.45	21,340	40,342	
80	1.1	.22	.465	14,880	28.125	

The azimuth moment at 22 m/s wind velocity is 97,160 in. lbs. at any azimuth position since the wind direction is fully variable. This maximum occurs at an angle of attack of 20^o and an elevation angle of 67^o . The moment for tracking requirements (16 m/s)wind is 51,390 in. lbs. and for pointing error requirements (12 m/s) is 28,900 in.lbs.

1.3.2 Gravitational Loads

The gravitational loads have been calculated on the basis of Solaramics preliminary design heliostat with a weight distribution as follows:

Mirror facets @ 4.2#/ft^2 x 528 ft^2	= 2196 lbs.
Structural frames	721 lbs.
Main cross tube	621 lbs.
Elevation upper links (2)	108 lbs.
Actuator gear box & motor	55 lbs.
Actuator drive shaft	72 lbs.
Lower link	54 lbs.

These weights result in the elevation hinge line gravitational moments

FIG. 12. COMPOSITE ELEVATION MOMENT @ 16 m/s WIND @ 10° FROM HORIZONTAL

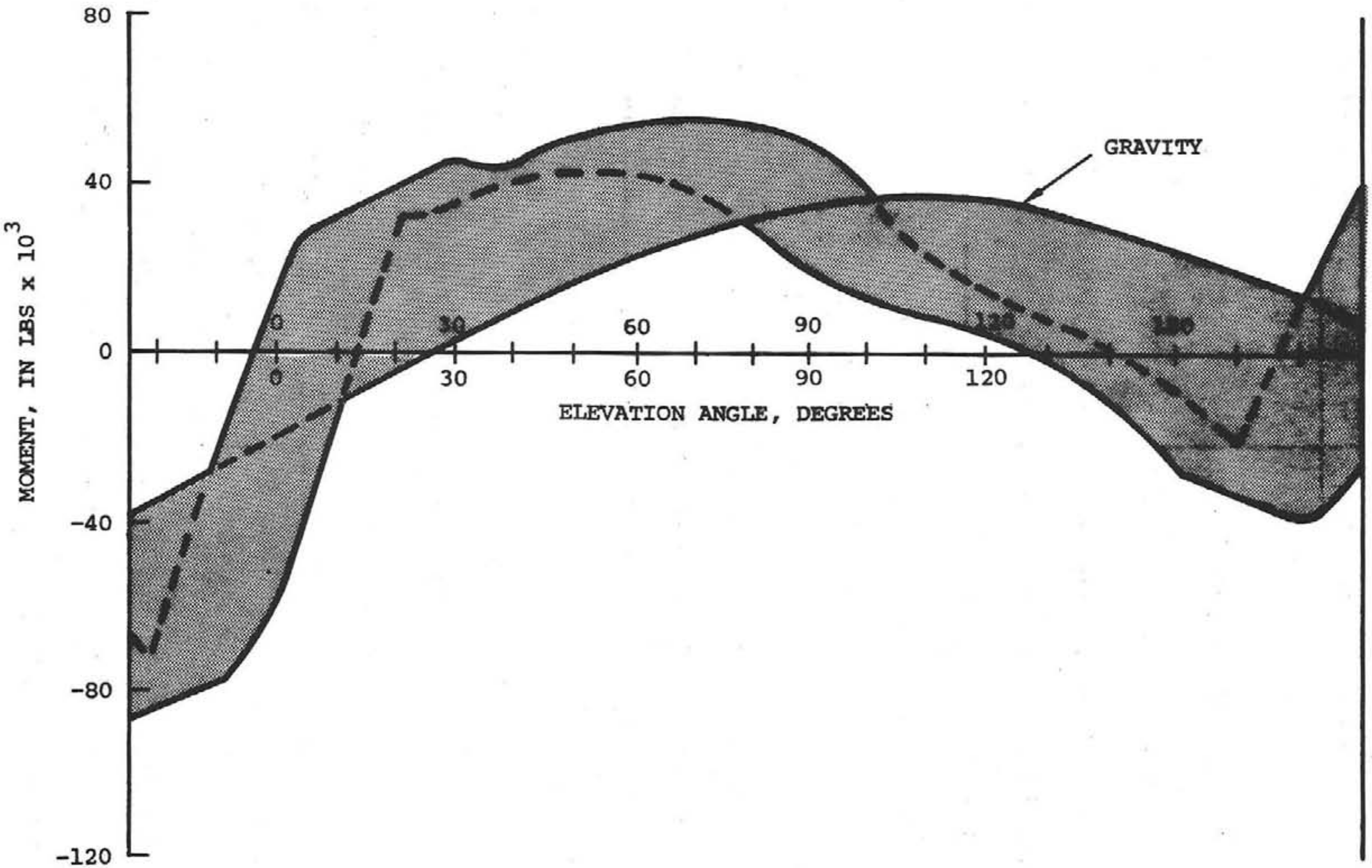

presented in Fig. 12 .

1.3.3 Combined Loading

The combined gravity and wind loading limits at 16 m/s wind, the tracking requirement, is presented in Fig. 12.

1.4 Mechanism Characteristics

1.4.1 Elevation Mechanism

The analytical design characteristics of the elevation mechanism (Fig. 13) are discussed in this section, the physical test characteristics are presented in Section 3 .

The elevation mechanism is shown schematically in Fig.13 together with the functional equations. The solid links are 72 inches pivot to pivot, and the crank arms are 30 inches. The actuator extension is 93.93 inches at 23^{o} elevation, 48.95 inches at + 80^{o} stowed position. The stroke length is 47.98 inches. The angular rotation is slightly non-linear with stroke, and is shown graphically in Figure 14 . Also shown is the angular rotation rate, milliradians per inch of stroke as a function of elevation angle.

The maximum elevation rate is 0.173 mr per motor shaft revolution.

The stiffness of the elevation drive mechanism varies with the position, increasing from 4.76×10^{7} in lbs/rad at -23^{o} to 8.9×10^{7} in lbs/rad at 30^{o}, then decreasing to 2.1×10^{7} in lbs/rad at storage. The mechanism backlash is 0.8 mr at -23^{o} position, decreasing to 0.5 mr at 30^{o} elevation. The backlash consideration is most critical at low actuator load (gravity only) position, i.e. 10 to 30^{o} elevation. Excessive backlash would permit dynamic oscillation at low variable wind conditions resulting in impact loading on linkage bearings.

The backlash calculation is based upon .0010 in. diametral bearing tolerance and .005 in. actuator screw backlash. Corresponding installation

Fig. 13

ELEVATION LINKAGE ANALYSIS

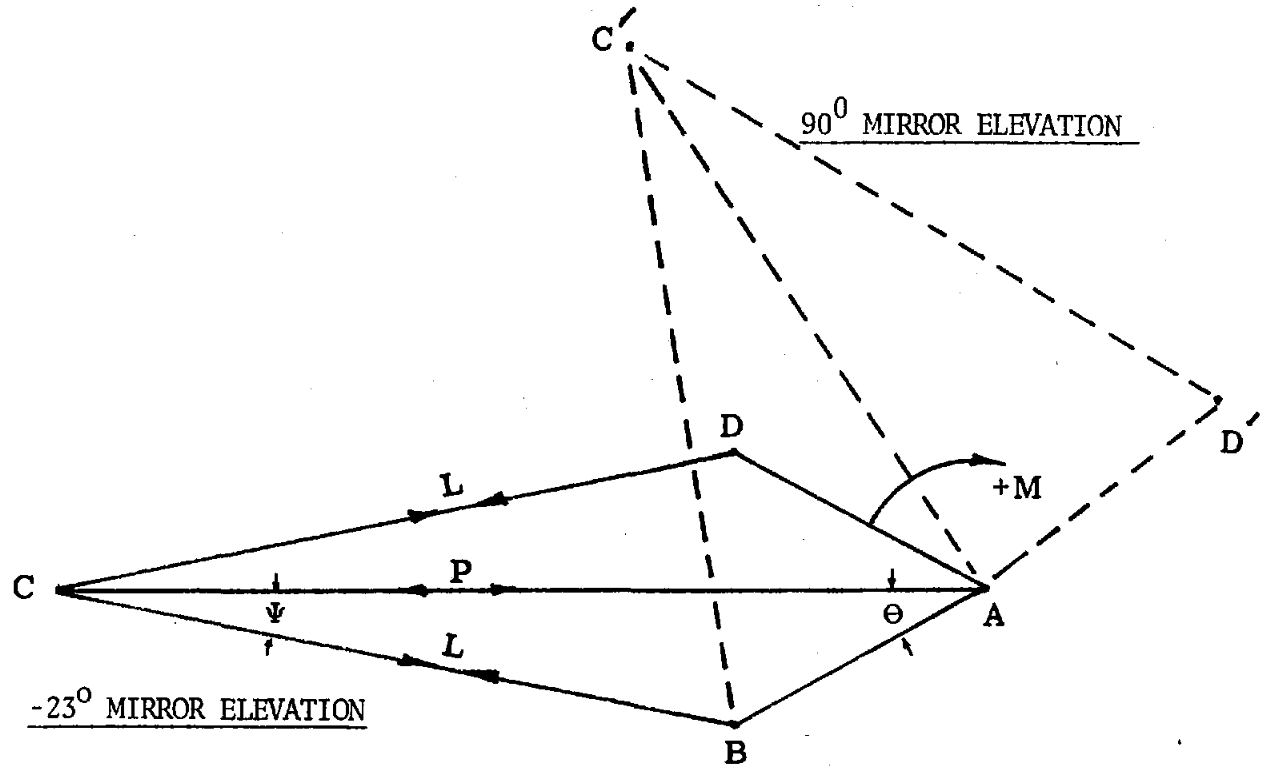

$\overline{AB}$	=	30 in.	$\overline{AC}$	= ACTUATOR LENGTH, VARIABLE
$\overline{AD}$	=	30 in.	M	= APPLIED MOMENT
$\overline{BC}$	=	72 in.	P	= ACTUATOR FORCE
$\overline{CD}$	=	72 in.	L	= LINK FORCE

$$\overline{AB}\ \sin\theta = \overline{BC}\ \sin\Psi$$

$$\overline{AC} = \overline{AB}\cos\Theta + \overline{CB}\ \cos\Psi$$

$$L = \frac{P}{2\cos\Psi} \quad ; \quad M = L \cdot \overline{AC}\ \sin\Psi$$

$$M = \frac{P \cdot \overline{AC}}{2}\ \tan\Psi$$

Table 4

Elevation Mechanism Characteristics

Mirror Elev.	θ°	Ψ°	$\overline{AC}$ in.	$\frac{M}{P}$	$\frac{L}{P}$	$\frac{L}{M}$	Rate Mr/in. Stroke
-23	28.5	11.468	96.927	9.831	.5102	.0519	101.7
-20	30	12.024	96.401	10.267	.5112	.0498	97.4
0	40	15.53	92.351	12.836	.5190	.0404	77.9
20	50	18.614	87.517	14.738	.5276	.0358	67.85
40	60	21.152	82.149	15.892	.5361	.0337	62.92
60	70	23.050	76.512	16.278	.5434	.0334	61.43
80	80	24.226	70.869	15.944	.5483	.0344	62.72
100	90	24.624	65.452	15.000	.5500	.0367	66.67
120	100	24.226	60.450	13.60	.5483	.0403	73.53
140	110	23.050	55.991	11.912	.5434	.0456	83.95
160	120	21.152	52.149	10.088	.5361	.0531	99.12
180	130	18.613	48.95	8.243	.5276	.0640	121.3

Stroke = (96.927 - 48.95) = 47.977 in.

FIGURE 14. ELEVATION ACTUATOR - STROKE AND RATE

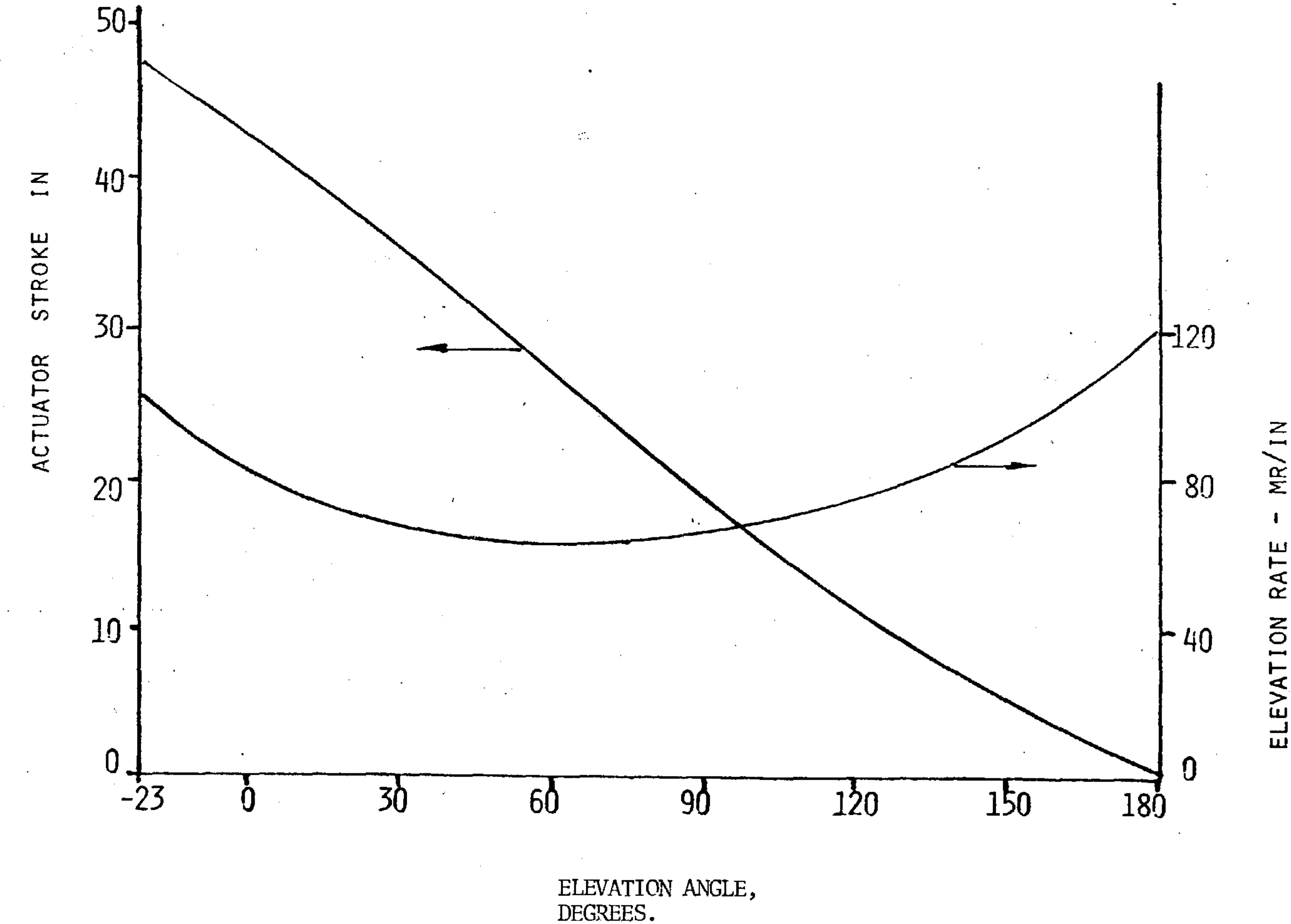

FIGURE 15. ELEVATION ACTUATOR FORCE

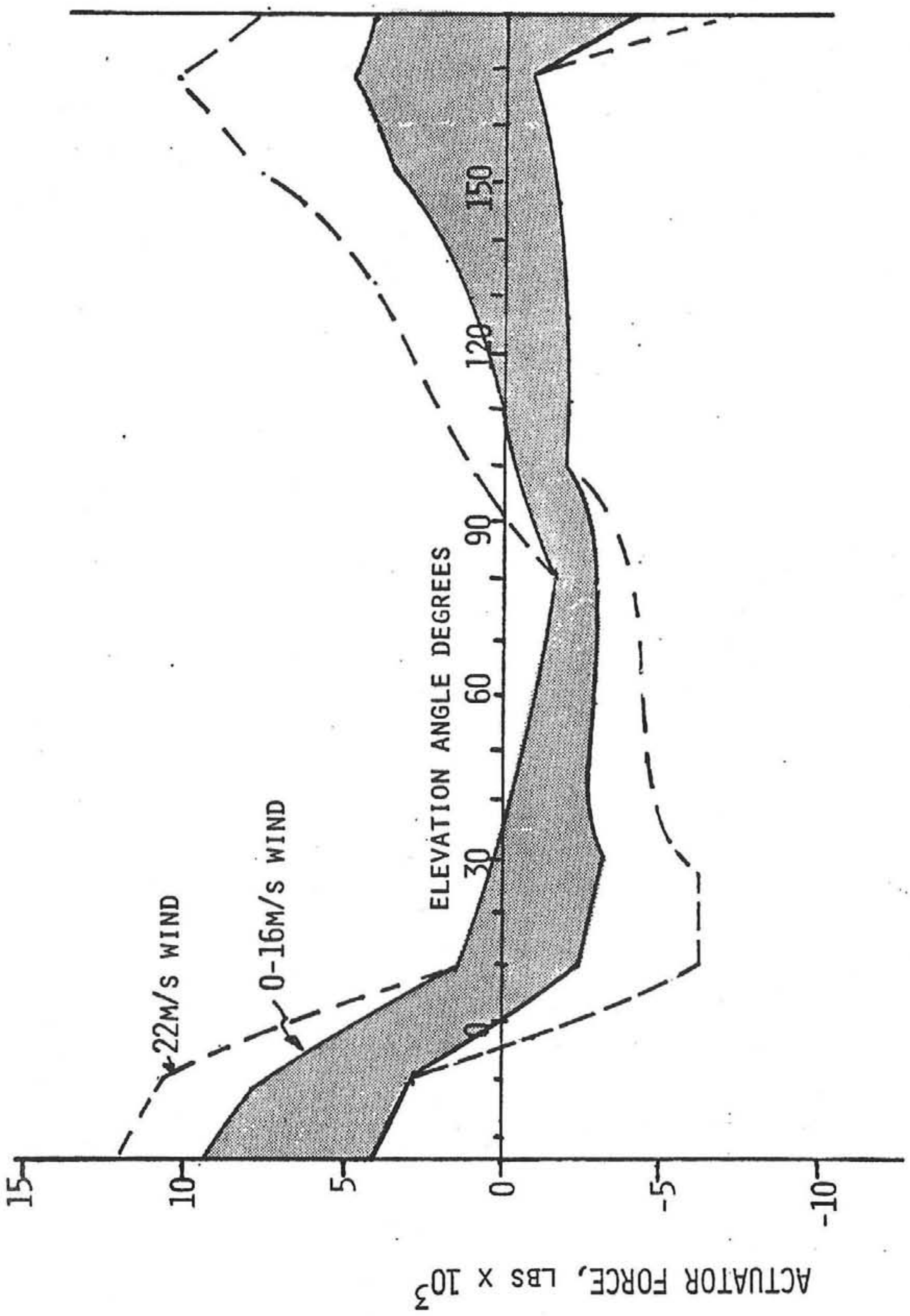

tolerances are 0-.0012 and .003-.005 in. respectively.

The maximum load experienced by the mechanism is 221,200 in lbs. moment at 40 m/s wind condition in the stowed position, resulting in 27,510 lbs. actuator force. The critical loading for drive start-up, operation occurs at -23^{o} elevation and 16 m/s wind (ref.Fig.15) and required 8739 lbs. actuator force. A somewhat higher actuator running force requirement of 10,693 lbs. exists at approximately 170^{o} elevation as a result of wind rise to approximately 24 m/s during stow operation. The above requirements establish the motor starting and stall torque requirements. The survival loads on the actuator are also shown in Fig 15, for the 22 m/s requirement at any orientation.

1.4.2 Azimuth Mechanism

The azimuth mechanism is shown schematically in Fig. 16 together with the function equations. The link lengths are 38.5 inches and crank arms are 15.5 inches. The maximum actuator, pivot to pivot extension is 51.13 in., and the minimum is 28.33 inch. The resulting stroke is 22.8 in. Since the azimuth stow position is at 0^{o}, the maximum stroke to stow is 11.5 inches, which must be accomplished during the first 113^{o} of elevation drive. This requires a minimum actuator stroke rate of 1.38 in/min. The maximum azimuth rate is 0.326 mr per motor shaft revolution.

To maintain commonality of gear trains in the actuators a stroke rate of 1.6 in/min. is achieved with a ½ speed (875rpm) motor. Since the wind direction is infinitely variable, the maximum design conditions occur at an elevation angle of 67^{o} with the array parallel to the azimuth axis and linkage forces exist at the two extremes, i.e. +90^{o} and -90^{o} . The actuator force requirements & the stroke characteristics are shown in Figures 17 & 18. The maximum start-up force is 9577 lbs. at 16 m/s and maximum survival load is 18,110 lbs. at 22 m/s wind.

FIGURE 16. AZIMUTH MECHANISM

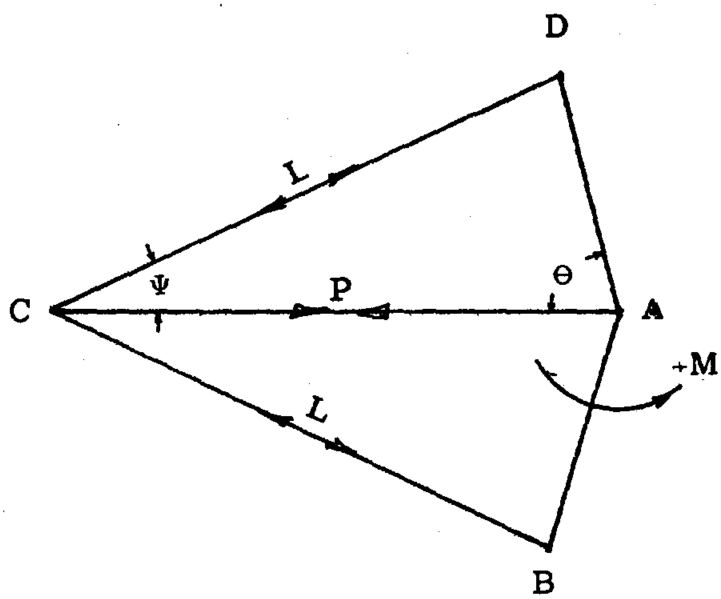

MIRROR FACING TOWER

$\overline{AD} = \overline{AB} = 15.5$ in.

$\overline{BC} = \overline{CD} = 38.5$

$\overline{AC}$ = ACTUATOR LENGTH

M = APPLIED MOMENT

D = ACTUATOR FORCE

L = LINK FORCE

$$\overline{AB} \; \text{Sin}\,\Theta = \overline{BC} \; \text{Sin}\,\Psi$$

$$\overline{AC} = \overline{AB} \; \text{Cos}\,\Theta + \overline{CB} \; \cos\Psi$$

$$L = \frac{P}{2\cos\Psi} \; ; \qquad M = L \cdot \overline{AC} \; \text{Sin}\,\Psi$$

$$= \frac{P}{2} \; \overline{AC} \; \text{Tan}\,\Psi$$

Table 5

AZIMUTH MECHANISM CHARACTERISTICS

Mirror Angle Degrees	θ	Ψ	$\overline{AC}$ in	M/P	L/M	Rate Mr./in. Stroke
-90	30	11.612	51.13	5.254	.0972	190.32
-70	40	14.998	49.062	6.572	.0787	152.1
-50	50	17.963	46.586	7.552	.0696	132.4
-30	60	20.405	43.834	8.153	.0654	122.6
-10	70	22.229	40.939	8.366	.0663	121.7
10	80	23.358	38.036	8.213	.0663	129.0
30	90	23.740	35.242	7.75	.0705	129.0
70	110	22.230	30.337	6.199	.0871	161.3
90	120	20.405	28.334	5.270	.1012	189.7

Stroke = (51.13 - 28.334) = 22.796 in

Maximum Wind Moments = 97,163 in lbs (see Wind Loading Anal.)
@ 22 m/s

Max. Actuator Force = $\frac{97,163}{5.254}$ = 18,493 lbs.
(Rated Load = 10 tons)

Max. Linkage Load = 97,163 x .1012 = 9,832 lbs

Stress in Link @ Bearing End

$$A = 1.125 \text{ in}^2$$

$$\Pi = \frac{P}{A} = \frac{9,832}{1.125} = 8,740 \text{ psi}$$

Margin of Safety = High

FIGURE 17. AZIMUTH DRIVE CHARACTERISTICS

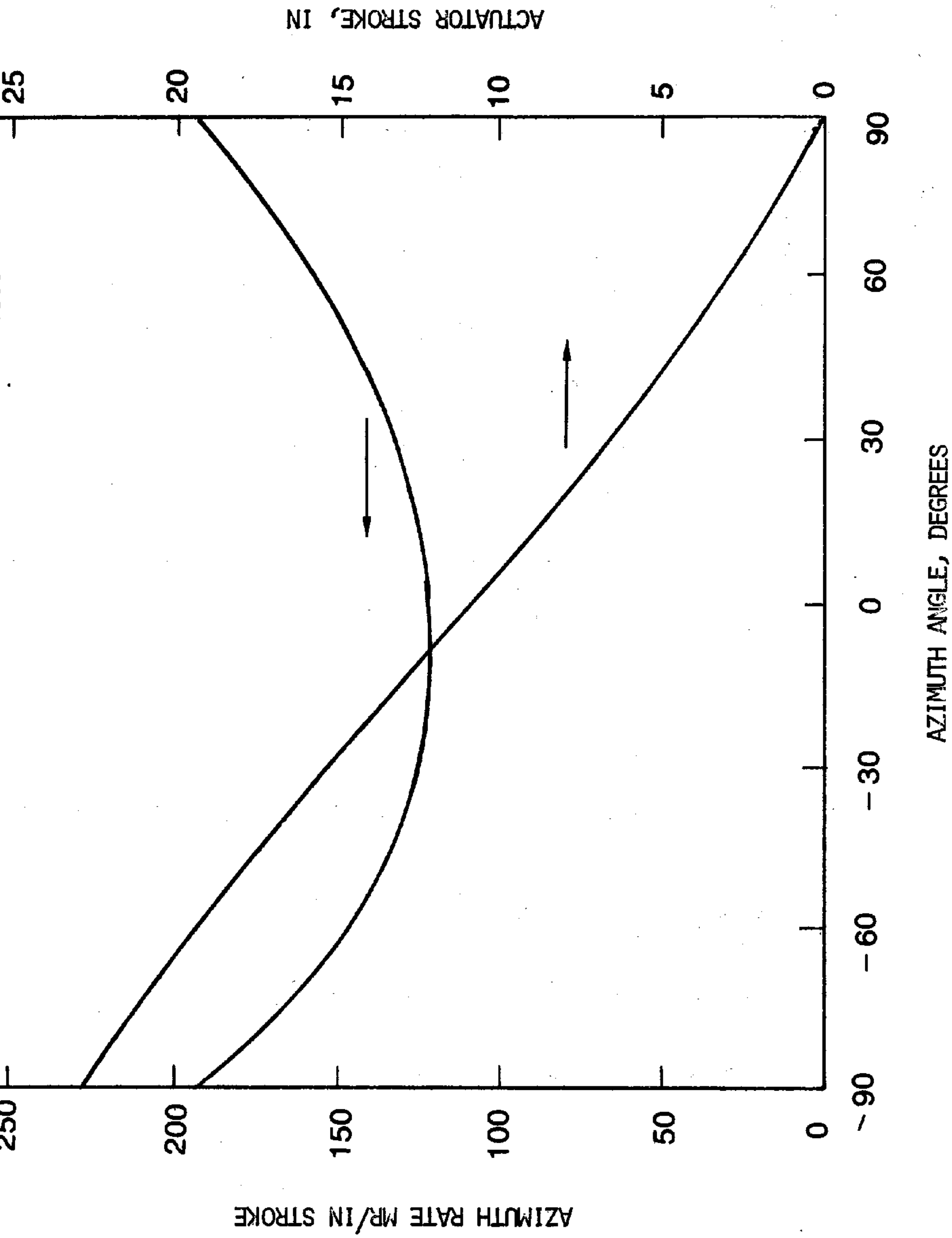

FIGURE 18. AZIMUTH ACTUATOR FORCE

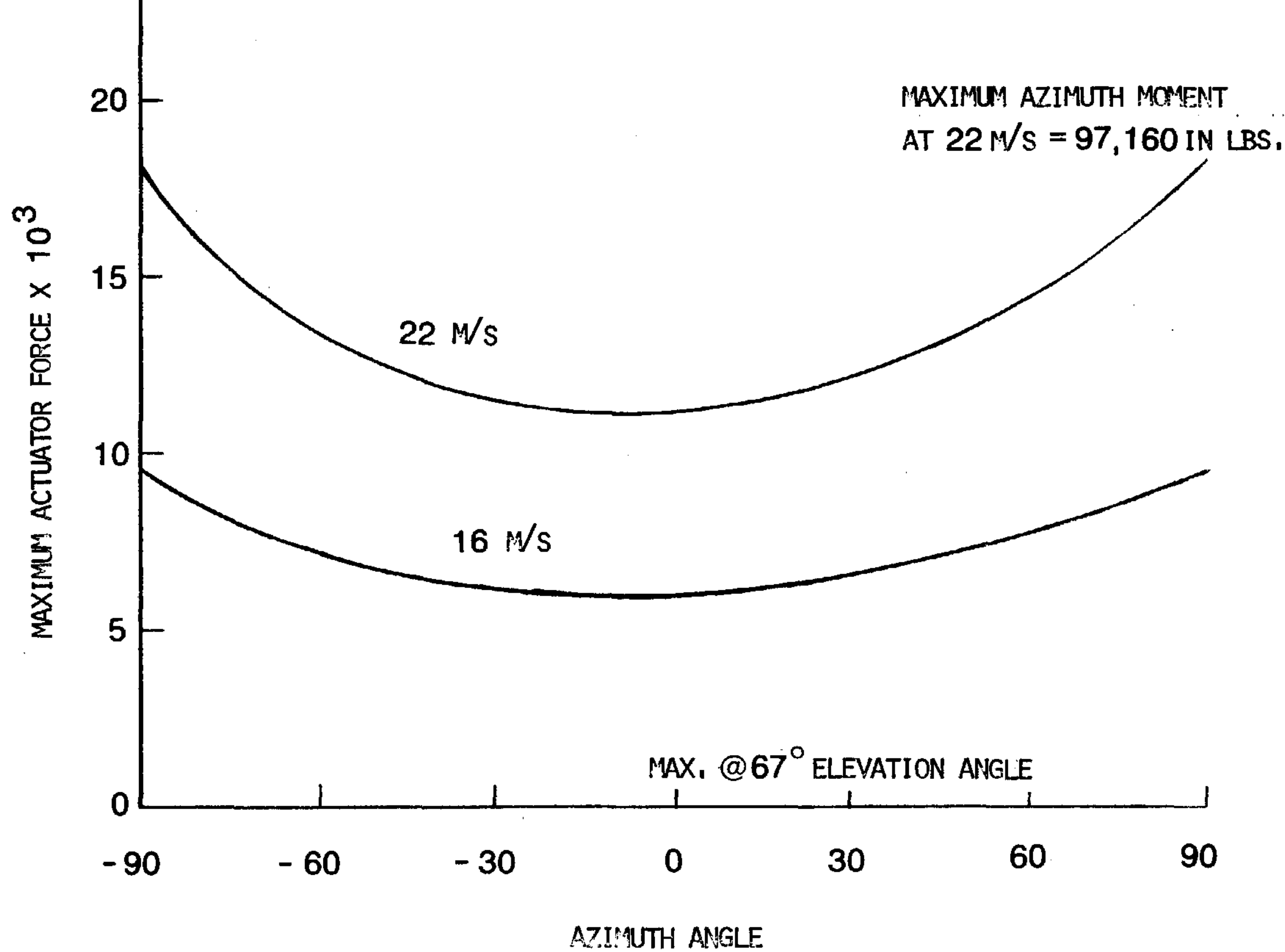

Calculated backlash of the azimuth mechanism is 0.9 mr at 0^{o} increasing to 1.5 mr at the maximum extremities when calculated on the bearing tolerances discussed in Section 1.3.1

2.0 DESIGN TRADE-OFFS

In the generation of the design presented in Section 1.2, a number of trade-offs were examined. Some of the more significant of these are discussed in this section.

2.1 Actuator Selection

A number of trade-offs were considered in the actuator design, such as:

- machine screw vs. ball screw
- screw shaft diameter
- motor interface
- environmental seals
- single reduction vs. double reduction
- gear selection

2.1.1 Machine Screw vs. Ball Screw

The comparison of characteristics of machine screws and ball screws are summarized in Table 6. The decision to utilize a machine screw was based upon the lower cost, self-locking and environmental considerations. The cost consideration as well as the efficiency is enhanced by rolling the machine screw thread rather than machining, or grinding as required for the ball screw. Also the failure of a ball screw actuator can be catastrophic in the loss of the ball retainer cage.

2.1.2 Travelling Nut vs. Translating Screw

The translating screw designs are amenable to incorporation of the backlash adjusting nut whereas the travelling nut designs are not. The backlash adjustment feature is considered necessary for control of system backlash. Also the load path length, and therefore the deflection under load is approximately twice as great with the travelling nut design. The lubrication is better provided and controlled in the translating screw design since all of the lubrication is confined in the gear box. The advantage of the travelling nut design is that it permits use of smaller gears of the spiroid or helicon design since they are located on the end of the shaft and are not constrained by the shaft diameter.

2.1.3 Screw Diameter

While a 1.5 in. diameter screw is capable of carrying the loads imposed by the heliostat, a 2 inch diameter screw was investigated. Analysis of drive linkage stiffness shows a distinct (2:1) advantage for the heavier screw. The heavier screw also permits reduction of the screw pitch from .25 in. to .2 in. reducing the ratio required in the gear reducer. For the rolled thread screw design, the primary cost impact is the additional material required which is approximately $11 per heliostat. Other potential cost impacts occur in the worm gear size, thrust bearings in the actuator, and overall gear housing casting size. These are considered in the discussion on single reduction vs. double reduction gear trains.

The two inch diameter screw is considered necessary, principally for stiffness considerations.

2.1.4 Single Reduction vs. Double Reduction

A single reduction gear train has obvious advantages over a double reduction train from a cost point. With the two inch diameter screw described above with a pitch of 0.2 inches, a gear ratio of 110 to one is required to achieve full stroke in 15 minutes with a 1750 rpm motor on the elevation actuator. Gear ratios of this order are readily achievable with worm, spiroid, or helicon gear sets. It, therefore, appears feasible to perform the elevation control with a single reduction gear train, however the azimuth rate requirement is only one half the elevation rate requirement. It is desirable to reduce the azimuth rate, permitting use of a lower power motor.

TABLE 6: ACTUATOR SCREW TRADE-OFF SUMMARY

BALL SCREW

ADVANTAGES	DISADVANTAGES
.. known life	.. higher cost than machine screw
.. high efficiency for less power consumption	.. backdrives
.. no backlash nut adjustment required	.. failures can be catastrophic
	.. requires clean environment
	.. higher backlash

MACHINE SCREW

ADVANTAGES	DISADVANTAGES
.. self-locking	.. less efficient than ball screw & requires more power
.. less cost than ball screw	.. anti-backlash adjustment is required
.. coupled with anti-backlash nut, there is a wear indicator which signals the useful life of the screw and nut & prevents catastrophic failures	
.. operates better in a less clean environment than ball screw	

The options examined were use of double reduction gear drives, either in the actuator itself, or with a gear motor, or the use of a 875rpm motor. Single gear reduction ratios of 220 to one are not desirable.

Selection of an 875rpm motor appears to be the obvious solution since this can be readily accomplished with very minimal cost impact by doubling the number of poles in the motor. This has the further advantage that the actuator gear trains can be identical for both azimuth and elevation units.

2.1.5 Gear Selection

This trade-off is still open, the gear type options considered include worm, spiroid, and helicon. Material selection and manufacturing processes are to be chosen to obtain best life cycle costs. Powder metal technology is a strong candidate for the gear, and an integral pinion or worm on the motor shaft appears advantageous.

2.1.6 Motor Interface

The initial approach employed a standard "C" flange motor mount integral with the actuator housing in which a splined motor shaft engages a hollow pinion or worm shaft.

By using a "3/4" motor, the forward bell of the motor is not required and the actuator casting is simplified. This concept is in use by Duff-Norton on other high production actuators.

The concept of an integral worm on the motor shaft is also attractive. The advantage is primarily a reduction of parts in the assembly and elimination of a spline coupling. The disadvantage is a more complex motor supplier interface and more difficult motor maintenance replacement. This trade-off is not completed.

2.1.7 Environmental Seals

The major problem of environmental protection exists on the forward screw shaft of the actuator. The aft extension of the screw is totally enclosed in a metal tube, and the actuator gear housing is adequately sealed at the input shaft. The original concept for sealing the forward shaft was use of a telescoping metal protection sleeve. Another option was rubber bellows which was discarded based on life expectancy. By increasing the length of the linkage arms and the actuator shaft it was possible also to seal with a wiper, fixed to the actuator housing by a metal tube, which seals on the unthreaded portion of the screw shaft. The cost impact of increasing the linkage, and shaft length is $.80 per inch with approximately 10" additional length required for a cost of $8 for the elevation mechanism. This is offset by a much lower cost seal configuration and reduction of number of seals required. The major consideration, however, was the significantly improved reliability and maintainability with single wiper design. The wiper and seal is designed as a split seal to facilitate replacement without disconnecting the actuator screw shaft.

2.2 Drive Links

A number of drive link configurations were examined including forged ends welded to tubing, and bar stock with upset ends, subsequently machined or forged, and the solid bar friction welded to forged ends. The major consideration in the linkage design was stiffness, i.e. resistance to in-line loading deflections. To achieve balanced stiffness with the rest of the design, a cross sectional area of approximately 3 sq. inches was desirable. Solid bar has a distinct cost advantage over pipe or tube, the ratio being approximately 1 to 3 per pound unit cost. Since column stability was not a factor, solid bar was the obvious choice. The trade between separate forged ends and integral forged ends on upset bar was also clearly in favor of separate ends for the link lengths required. Inertia, (friction) welding was selected over arc welding because of lower high production costs. Automated arc welding will be lower cost for intermediate production and prototype units.

2.3 Link Bearings

The candidate bearings included ball bearings, bronze (oilite) bushings, and several forms of self-lubricating bearings. Environmental life expectancy, cost, and tolerances were the major parameters considered. Ball bearings could not be expected to survive 30 years due to grease separation and seal failure. They also require larger housings and drive other mechanism costs up. The composite self-lubricating bearing was found to be superior to the impregnated bronze bushings in wear, tolerance to contamination, lubrication life, and compression allowable. This is supported by their increasing utilization in farm machinery and earth moving equipment. The particular self-lubricating bearing was selected, over two others, on its ability to be reamed or broached to size after installation, promising closer tolerance installation which is critical from backlash consideration.

2.4 Trunnion

A cast design and a weld fabricated design were studied. A great deal of effort was expended to minimize the number of parts and to configure the assembly to permit maximum automation of the weld fabrication. The weld fabrication offers lower material cost and higher modulus of elasticity. The lower material cost is offset by the increased labor cost while the machining costs are virtually equal. The weight of the assembly is 184 lbs., and based upon approximately 30¢/lb for torch cut or blanked and formed plate versus 75¢/lb. for ductile iron castings, the material cost differential is $82. Estimates by welding engineers for the configuration shown using automatic equipment and sophisticated holding and positioning fixtures, forecast large scale production labor of 0.6 hours per unit.

The cost and rigidity advantage of the welded design is significant, however the importance of automatic fixturing and welding must be given continued attention in production planning to achieve this advantage.

2.5 Kingpin

The comments on welding versus casting for the trunnion also apply to the kingpin. The spindle is more straight forward as a result of the reduced number of piece parts and the simplified welding (only one automated set-up). The lower cone and flange has been designed as a forging to significantly reduce the number of parts and eliminate two welding operations necessary for an alternate welded design. The alternate welded fabrication was selected for the test unit.

The main shaft for the spindle axis is designed to be machined from solid bar, this being found to be more cost effective than heavy wall mechanical tubing. The diameter was held to the minimum which would meet stiffness objectives in the interest of keeping the tapered roller bearing costs at a minimum. The lower roller bearing selected is a light bearing with a 33,500 lbs. rating (1.5 X Reqmt) having a 5.75 in. i.d. and 7.625 in. o.d. The retail price is $66 (approx. 4 X O.E.M. large quantity cost). The next larger available bearing has a 6.875 in. i.d. and 9.75 in o.d. and costs $124 retail. The next smaller bearing of lower cost has a 4.5 in. i.d. and costs $53 retail. There is an obvious incentive to design around the selected bearing. The smaller bearing results in inadequate stiffness of the main shafts, while the larger bearing and significantly increased o.d. also drives the cost of the hub upward.

3.0 TEST PROGRAM

3.1 Test Set-up

3.1.1 Pedestal Support

The drive mechanism was mounted on a pier/pedestal for support during test. The Solaramics preliminary design pedestal installation was selected on the basis of its design characteristics, cost, and availability. This installation consisted of a hollow, spun cast, prestressed concrete pier, 17 3/4 in. in diameter with a 3½ inch wall. (Fig. 19). The pedestal was installed in a bored hole of 12 ft. depth and an irregular diameter of approximately 20 in. Pole-set, a polyurethane foam material,was injected around the pier in the cavity to set the pier in the bored hole. The soil type was a sandy material, not unlike desert alluvial fill,formed by sand dunes. The geographic area is approximately one half mile inland from the El Segundo beach. The installation was in the Solaramics parking area, covered by a macadam surface. Soil analysis or soil properties were not obtained.

3.1.2 Inertia Fixture

The mirror module array and support structure were simulated by the inertia test fixture shown in Fig. 20 . The inertia fixture was designed to simulate a $50m^2$ array composed of 12-four ft. by eleven ft. mirror modules having a unit weight of 4 lbs/ft^2. The fixture was designed to provide the same static and dynamic moments as the Solaramics preliminary design heliostat. It was fabricated from welded steel pipe, the vertical arms being filled with concrete. The stiffness was purposely designed to be more rigid than the heliostat components or the mechanism assembly to avoid any coupling possibilities to assure validity of the drive mechanism

FIGURE 19. PEDESTAL DESIGN
HOLLOW - SPUNCAST - PRESTRESSED CONCRETE

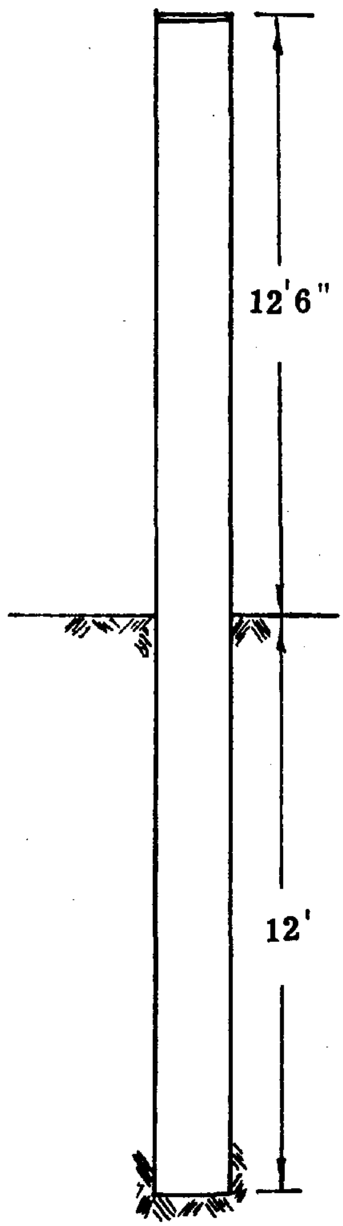

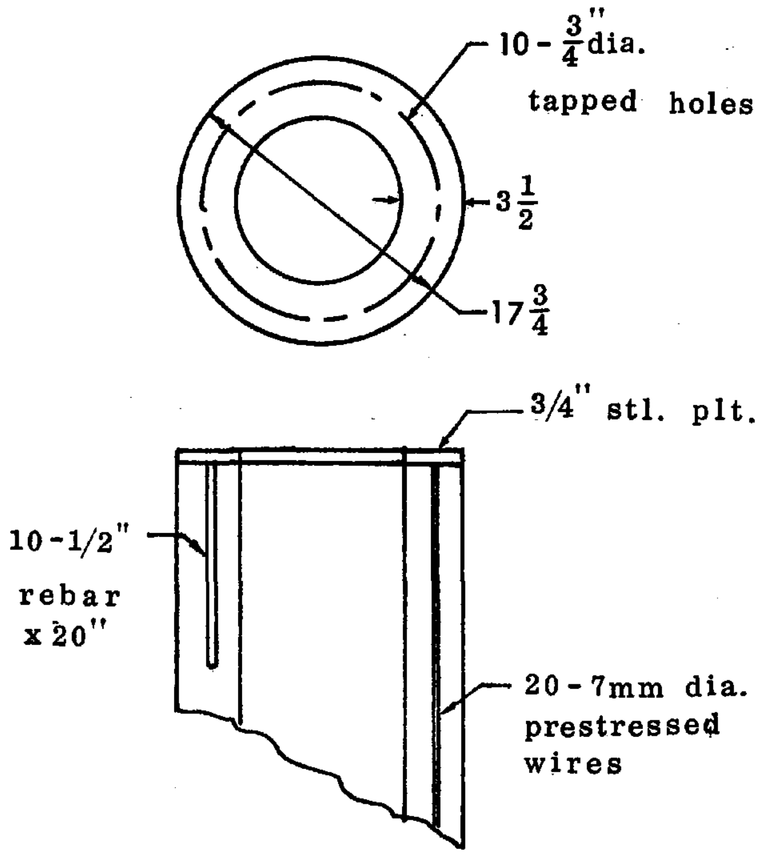

BENDING STIFFNESS, $EI = 2 \times 10^{10}$ LB.IN^2

TORSIONAL STIFFNESS, $GJ = 1.6 \times 10^{10}$ LB.IN^2

FIGURE 20. INERTIA FIXTURE

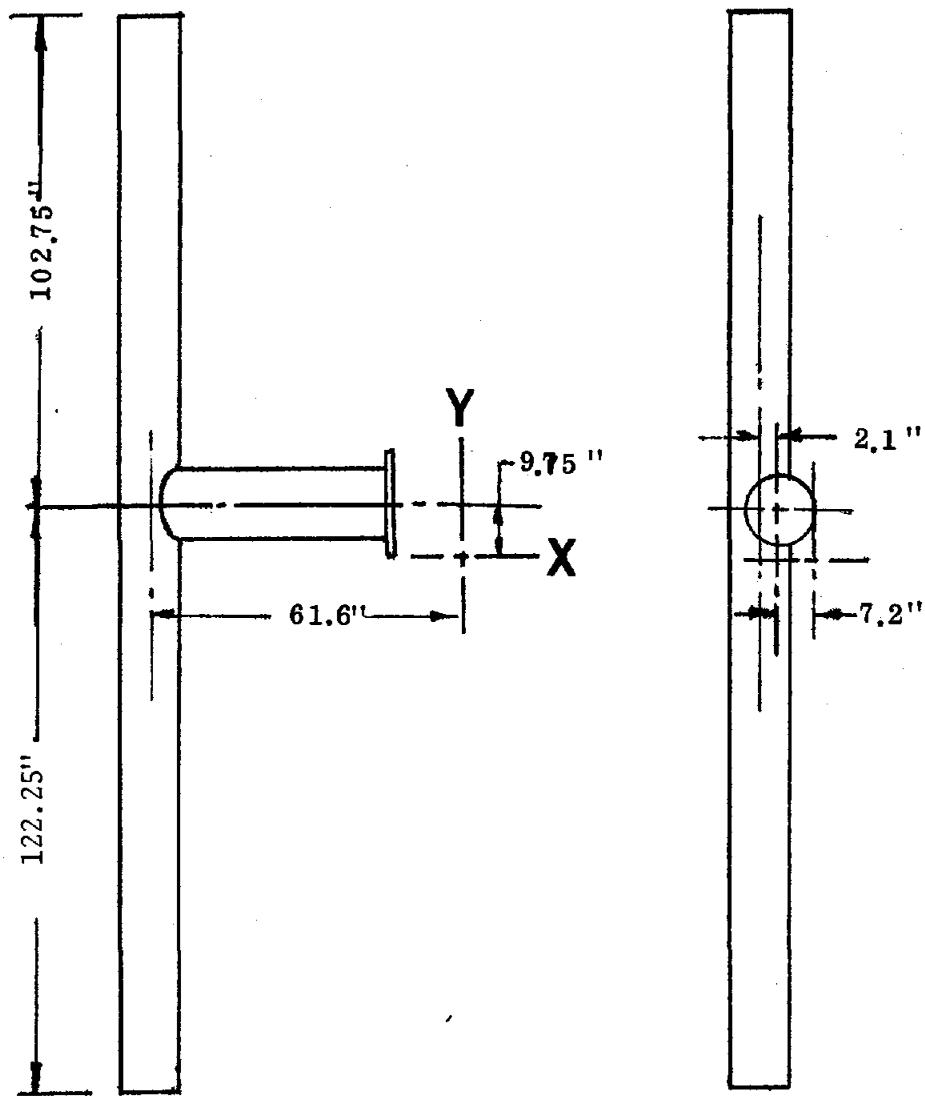

PROPERTIES PER SIDE

WEIGHT	2602 LBS.
Ixx	9.07 $LB\text{-}IN^2$
Iyy	8.72 $LB\text{-}IN^2$

dynamic response tests.

3.2 Test Article Description

The prototype test hardware was designed as closely as possible to the proposed production hardware within cost and schedule limitations. Particular care was exercised to maintain rigidity and tolerance characteristics. The variations of the test hardware from the production design were as follows:

3.2.1 Test Actuators

Cost; design and fabrication lead time precluded the development of the production design actuators. For the test article, commercial actuators; Duff Norton Maxi-pac model M-2709 were utilized. These commercial actuators are equipped with 2 in. diameter drive shafts, duplicating the stiffness characteristics of the production design. The screw pitch was 0.5 in. instead of 0.2 in. and the gear box was a two stage reduction rather than a single stage. The primary gear unit did contain the adjustable backlash nut duplicating the production design.

A specially designed test pivot fitting was bolted to the actuator base flange in lieu of integrally cast pivot fittings which would require new casting patterns and castings which would not have been available within schedule limitations. The bolted pivot fitting was less rigid than the integrally cast fitting, resulting in a slight loss of rigidity in the test, therefore, a conservatively lower frequency response.

The test actuators were fitted with the forward environmental sleeve and seal as well as the aft extension cover tube. However, the forward shaft extension was not cadmium plated as planned for the production actuator.

The test actuator was powered by a 1 horsepower, 1750 rpm, three phase motor which is standard equipment on the Maxi-pac unit. This is a much larger motor than required for the mechanism, however since the larger motor had no effect upon the static or dynamic structural response of the mechanism and was only employed to position the mechanism for test, special fractional horsepower motors were not procured.

3.2.2 Drive Links

The test drive links were fabricated with welded assembly and fittings rather than forged end fittings. The section properties of the production design were maintained. The pivot pin holes were bored by standard machine shop practice without benefit of special tooling.

3.2.3 Trunnion

The test trunnion was fabricated as a welded assembly, the principal variation being the setup and machining operations which were performed by layout and standard machining practice rather than production tools and fixtures. Also all welding was manual rather than automatic. The production design tolerance, on concentricity and parallelism were relaxed for the fabrication of the test unit to standard machining tolerances due to lack of set-up tooling.

3.2.4 Kingpin

A steel weldment was designed to substitute for the forged base transition cone. Wall thickness and strength of the welded cone was matched to the forging design. All welding was manual and machining operations were performed without special tooling. As above, tolerances on parallelism were relaxed.

3.3 Frequency Response

The frequency response was determined by snap-back testing, i.e., applying a load to the array which is instantaneously released. The free system oscillation was then observed by a total of eight piezoelectric accelerometers. Selected accelerometer outputs were processed through a real time frequency analyzer to obtain the drive mechanism response. In addition the response of the mechanism was excited in the lower modes by manual excitation to identify particular modes. Five elevation mechanism positions at 0^{o} azimuth and three azimuth mechanism positions at 67^{o} elevation were evaluated, these are summarized in Table 7 .

The initial tests were performed with the actuator backlash set at approximately .005 in. in the adjustment nut. During the drive torque measurement tests and as a result of further discussion with the supplier of the actuators, it was learned that the backlash adjustment could be reduced to zero and even pre-loaded without significant effect on the drive torque. This technique was applied to the azimuth actuator, resulting in the frequency reported in Table 7 . Since the stiffness of the azimuth linkage is higher at 0^{o} azimuth than at $\pm 90^{o}$, it would be expected that the frequency should be higher at 0^{o}. However there is a gravity bias at $\pm 90^{o}$ which is believed to cause the increased natural frequency by reduction of the tolerance hysteresis in the pivot pin bearings. Conversely the lower natural frequency at 0^{o} azimuth is believed due to hysteresis in the pivot pin bearings. The elevation mechanism was not tested in the reduced backlash condition since the mechanism is gravity loaded at most elevation positions except 30^{o} and 180^{o}.

Table 7

DRIVE MECHANISM

NATURAL FREQUENCY RESPONSE

ELEVATION MODE @ 0^{0} AZIMUTH

EL. ANGLE		HERTZ
-23	------	2.59
0	------	2.75
30	------	2.62
60	------	2.74
180	------	2.33

AZIMUTH MODE @ 67^{0} ELEVATION

-90^{0}	------	1.95
0^{0}	------	1.75
$+90^{0}$	------	1.95

SIMULATED ARRAY INERTIA

I_{ELEV}	------	=	18.2×10^{6} LB - IN^{2}
$I_{AZ.}$	------	=	17.4×10^{6} LB - IN^{2}

3.4 Mechanism Stiffness Tests

Load-deflection tests up to the survival load conditions summarized in Table 8 were performed in five elevation positions, 0^{o} azimuth, and in five azimuth positions, 30^{o} elevation. These tests were performed by ANCO Engineers, an independent testing group. Except as noted, all measurements were made from a transit, mounted on the inertia fixture, Fig. 21. The deflections, therefore, include deflection of the cross tube field joint as well as the pedestal and soil interface. The stiffness characteristics of the pedestal installation were measured separately and are summarized in Table 9 .

Two azimuth linkage configurations were tested, the first utilized a dual pin configuration shown in Fig. 22. The alternate design configuration consisted of a pivot pin located on the actuator screw centerline, Fig. 23. The alternate design appeared to possess a slightly higher rigidity.

All of the load deflection tests were performed with the actuator backlash adjustment set at .003 to .005 in freedom.

3.5 Pointing Error Tests

During the test program review with the contract agency, it was learned that an additional specification for pointing error at 12 m/s wind loading was to be added to the heliostat specification. Therefore, a test to apply ± 28,900 in-lbs moment for multiple cycles was added to the program. The initial pointing error test results are presented in Table 10 . The load was applied by a fixed weight, first in one direction, then in the other for repeated cycles. The elevation mechanism was observed to be well within the 3.5 mr specification, while the azimuth mechanism was not.

FIGURE 21. TRANSIT MOUNTING FOR OBSERVATION OF MECHANISM ROTATION

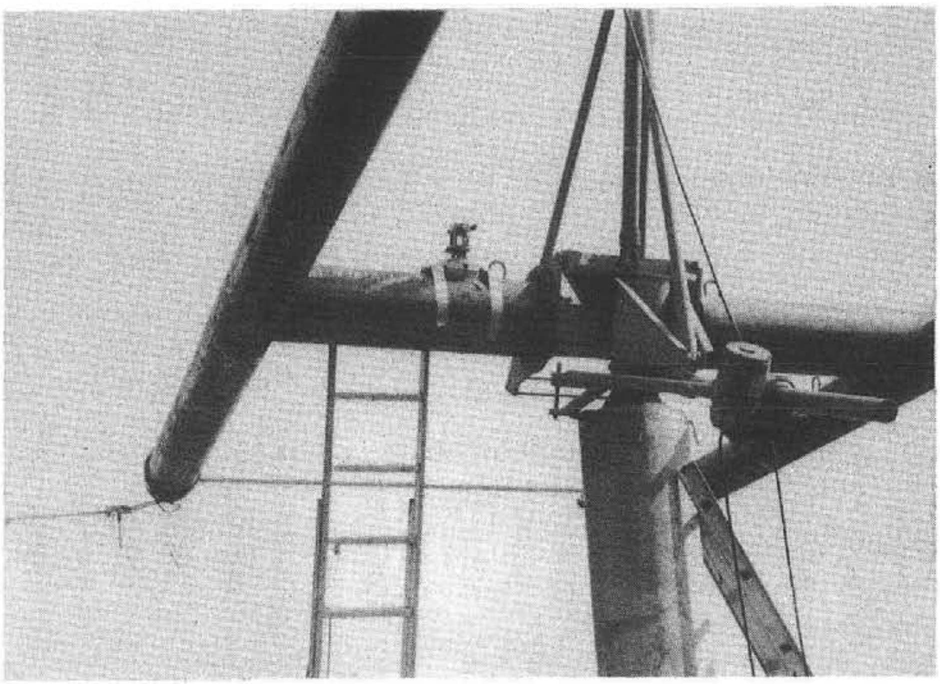

FIGURE 22. DUAL PIN AZIMUTH LINKAGE

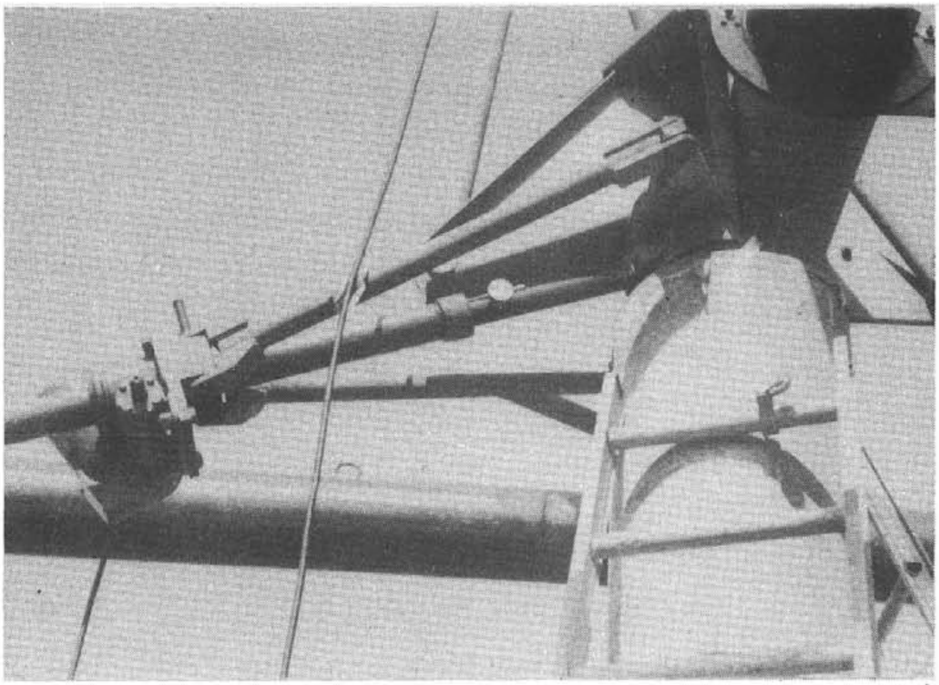

FIGURE 23. SINGLE PIN AZIMUTH LINKAGE

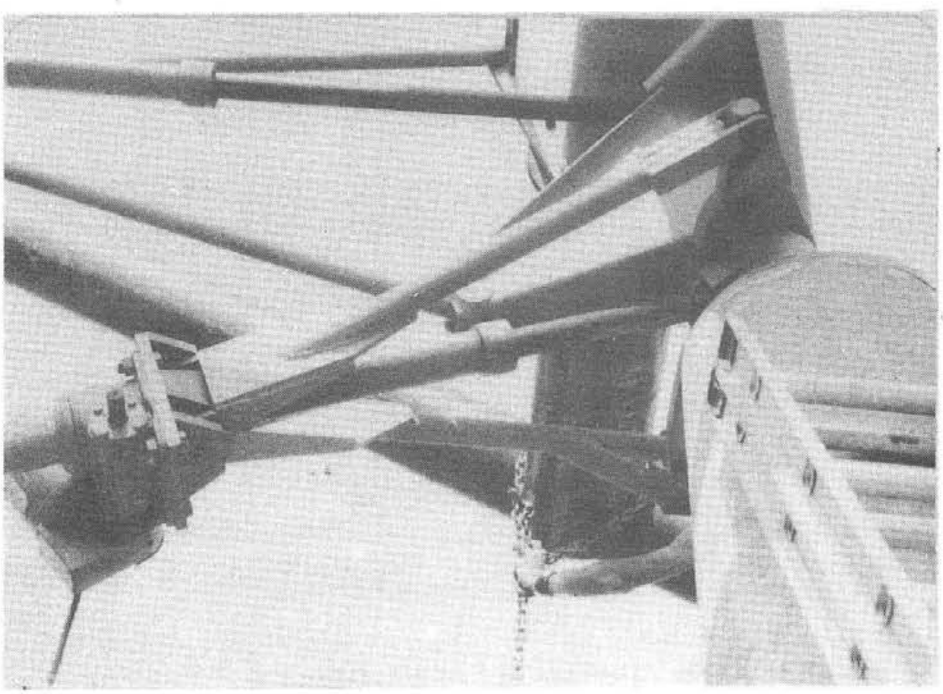

TABLE 8

ROTATIONAL STIFFNESS OF HELIOSTAT INCLUDING PEDESTAL

ELEVATION MECHANISM

Azimuth Position	Elevation Position	Mechanism Stiffness K - in lbs/Rad. +Moment	-Moment	Max.Moment Applied in. lbs.
0^{o}	-23^{o}	--	1.8×10^{7}	- 97,000
0^{o}	0^{o}	1.46×10^{7}	2.0×10^{7}	± 64,100
0^{o}	30^{o}	2.0×10^{7}	--	+ 97,000
0^{o}	60^{o}	3.1×10^{7}	--	49,700
0^{o}	180^{o}	1.2×10^{7}	1.15×10^{7}	212,000

AZIMUTH MECHANISM: DUAL PIN LINKAGE CONFIGURATION

90^{o}	30^{o}	5.7×10^{6}	8.0×10^{6}	± 90,000
45^{o}	30^{o}	8.5×10^{6}	6.9×10^{6}	"
0^{o}	30^{o}	1.06×10^{7}	9.8×10^{6}	"
-45^{o}	30^{o}	7.8×10^{6}	1.2×10^{7}	"
-90^{o}	30^{o}	5.0×10^{6}	7.8×10^{6}	"

AZIMUTH MECHANISM: SINGLE PIN LINKAGE CONFIGURATION

90^{o}	30^{o}	7.3×10^{6}	7.18×10^{6}	"
0^{o}	30^{o}	1.17×10^{7}	1.17×10^{7}	"

AZIMUTH MECHANISM: MEASURED FROM CTR. CROSS TUBE

0	30^{o}	1.6×10^{7}	--	90,000

Table 9

PEDESTAL CHARACTERISTICS

TYPE LOADING	STIFFNESS, Radians/in lb. TEST	ANALYSIS
Cantilever Bending	2.58×10^{-9}	2.99×10^{-9}
Uniform Moment @ Top	13.8×10^{-9}	12×10^{-9}
Torsion @ Top	10×10^{-9}	

Rotation @ Top of Pedestal Due to 12 m/s Wind,

Max. Drag Condition ------------- = 0.34 mr
Max Torsion Condition ------------- = 0.2 mr

Design Properties

Height Above Ground 12.5 ft
Below Ground 12 ft
Torsion Stiffness; $GJ = 1.6 \times 10^{10}$ lb -in^2
Bending Stiffness; $EI = 2.0 \times 10^{10}$ lb -in^2

INITIAL POINTING ERROR TESTS.

PERFORMANCE @ 12 M/S WIND
ELEVATION MECHANISM DEFLECTION.

DATA INCLUDES BACKLASH, PEDESTAL AND FOUNDATION DEFLECTIONS.

ELEVATION ANGLE	APPLIED MOMENT	DEFLECTION
-23°	-28,900 IN LBS	- 1.3 MR
0°	+19,000 IN LBS	+ 1.1 MR
0°	-19,000 IN LBS	- 1.25 MR
30°	+28,900 IN LBS	+ 1.7 MR
60°	+17,250 IN LBS	+ .5 MR

AZIMUTH MECHANISM DEFLECTION

INCLUDES *BACKLASH, PEDESTAL & FOUNDATION DEFLECTIONS

-90°	±28,900 IN LBS.	± 5.4 MR
0°	±28,900 IN LBS.	± 4.1 MR
+90°	±28,900 IN LBS	± 5.61 MR

MEASURED BACKLASH OF AZIMUTH ACTUATOR = .0085 IN.
= 1.6 MR

Techniques to reduce the azimuth pointing error were investigated. The first evaluation was measurement of all relative component contributions and light preload of the backlash adjustment nut (Table 11). Excessive tolerance was located in the pin-pivot joint bearings and the cross tube to trunnion. With the backlash adjustment preloaded the mechanism was very close to the specification requirement at 0^{o}, but still excessive at the extremes, $\pm 90^{o}$. To verify the potential of the structural elements, the rotating pin joints of the azimuth mechanism were welded to eliminate all pin-bearing deflections. This was performed only at the 0^{o} azimuth position, and resulted in a pointing error of $\pm$ 2.35 mr. This sequence of testing is summarized in Table 12 . On the basis of the test experience,it is recommended that the pin and bearing diameter, be increased significantly, (from 3/4 to 1¼ in.), and that better close tolerance installation techniques need to be developed.

Table 11

AZIMUTH MECHANISM

COMPONENT PERFORMANCE

AT 0^{o} AZIMUTH POSITION.

COMPONENT	mr DEFLECTION @ 12 m/s WIND	
	TEST	TARGET
PEDESTAL	.2	.2
CROSS TUBE TO TRUNNION	.85	.5
PIVOT JOINTS	1.25	.36
	2.3	1.06
REMAINDER, TRUNNION CRANKS & ACTUATOR	1.3	1.3
TOTAL MECHANISM	3.6	2.36

Table 12

AZIMUTH MECHANISM

PERFORMANCE @ 12 $^{M}/S$ WIND

AZIMUTH ANGLE	(1)	(2)	(3)
-90^{o}	$\pm$ 5.6 mr.	$\pm$ 4.9 mr.	$\pm$ (3.1)*mr.
0^{o}	4.1 mr.	3.6 mr.	2.35 mr.
$\pm 90^{o}$	5.4 mr.	4.7 mr.	(3.0)*mr.

1) ACTUATOR INSTALLED WITH .004/in, NO LOAD BACKLASH.

2) ACTUATOR INSTALLED WITH BACKLASH NUT LIGHTLY PRELOADED.

3) PIVOT JOINTS TACK WELDED.

ALL VALUES INCLUDE PEDESTAL DEFLECTIONS ($\pm$ .2 mr)

* CALCULATED VALUES.

3.6 Actuator Torque Requirements

The test actuator as described in Section 3.2.1 was a double reduction commercial actuator, fortunately having an exposed shaft extension of the main worm to which a torque could be applied, Fig. 22. With static moments applied to the mechanism, the torque necessary to drive the actuator was measured, both in the direction of force and opposed, Table 13. In no test was there any indication of back drive, there always being a minimum torque of at least 10 in. lbs. required to produce motion in the direction of applied moment. Generally, as the applied moment increased, the torque increased for loading in the direction and opposed to the direction of applied load, as a result of increased friction on the nut/screw interface.

The highest torque experienced was for the -23^{o} elevation angle position which was 260 in. lbs. A torque differential, at this position, of 160 in. lbs. (260 in. lbs. at -104,600 in. lb. moment less 100 in. lbs. at 0 applied moment) resulted from the applied moment of -104,600 in. lbs. The supplier data for this unit indicates that torque required at full load (20,000 lbs actuator force) would be 490 in. lbs. The observed 160 in. lb. torque increment would correspond to an actuator load of 6530 lbs using the above supplier data. The calculated force at this elevation angle is 10,639 lbs. (104,600 in. lbs. moment divided by 9.831 mechanical advantage, Ref. Table 4).

The maximum azimuth torque observed was 190 in. lbs. at an applied moment of 59,400 in. lbs. Using the supplier data indicated above, the indicated actuator force would be 7,755 lbs. The calculated actuator force is 11,271 lbs. (59,400 in. lbs. applied moment divided by the 5.27 mechanical advantage).

In all cases the observed torque was less than the predicted value using the supplier data on torque-force relationship, from which it is concluded that the supplier's published data is conservatively high.

FIGURE 24. WORM SHAFT EXTENSION USED FOR MANUAL POSITIONING AND TORQUE MEASUREMENTS

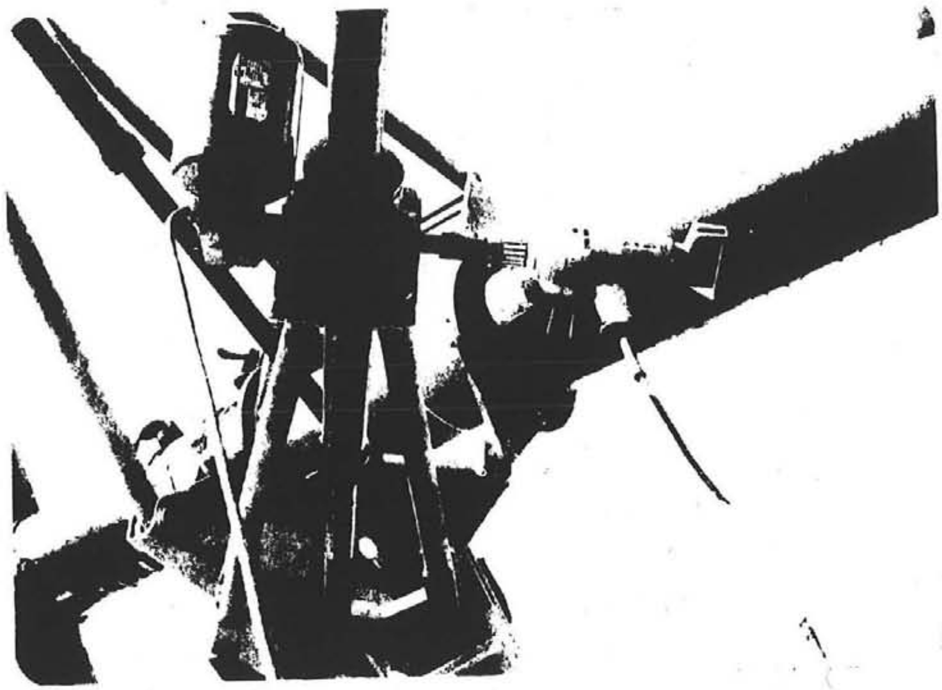

Table 13

ACTUATOR TORQUE MEASUREMENTS

ELEVATION MECHANISM ACTUATOR

0^{o} AZIMUTH

ELEV. ANGLE	APPLIED MOMENT IN.LBS.	ACTUATOR TORQUE IN.LBS.	COUNTER CLOCK WISE
-23^{o}	0	35 cw	100 ccw
	- 34,850 in. lbs.	20 cw	150 ccw
	- 69,700 " "	35 cw	210 ccw
	-104,600 " "	45 cw	260 ccw
30^{o}	0	10 cw	15 ccw
	+104,600 in. lbs.	10 cw	20 ccw
180^{o}	0	60 cw	30 ccw
	+ 34,850 in. lbs.	60 cw	20 ccw
	+ 55,800 " "	80 cw	20 ccw
	+ 83,700 " "	90 cw	20 ccw
	+111,600	80 cw	20 ccw

AZIMUTH ACTUATOR TORQUE MEASUREMENTS

30^{o} ELEVATION

AZIMUTH ANGLE	APPLIED MOMENT IN.LBS.	ACTUATOR TORQUE	
0^{o}	0	10 cw	10 ccw
	39,600 in. lbs.	45 cw	75 ccw
	59,400 " "	60 cw	120 ccw
-90^{o} (shaft extended)	0	20 cw	40 ccw
	39,600 in. lbs.	60 cw	140 ccw
	59,400 " "	95 cw	160 ccw
$+90^{o}$ (shaft closed)	0	40 cw	20 ccw
	39,600 in. lbs.	130 cw	60 ccw
	59,400 " "	190 cw	95 ccw

4.0 CONCLUSIONS & RECOMMENDATIONS

A full scale mechanism has been fabricated and demonstrated having a potential for low cost fabrication. The mechanism was found to meet all the specification requirements with the exception of the azimuth pointing error which could be brought within the requirement with the following design improvements:

1) Increase all pin/bearing diameters at the pivot points from 3/4 in. to 1¼ in. dia.
2) Improve the installation and seating of the self lubricating bearing in their housings prior to reaming to size.
3) Increase the torsional rigidity of the center cross tube by increasing the tube diameter.

The mechanism developed has the capability for inverted stow, the current trend in heliostat design appears to be toward vertical stow. This would reduce the elevation drive requirement to 113° from 203°, permitting additional simplification of the elevation mechanism, with the following

1) reduction of stroke length and corresponding reduction of mechanism linkage lengths.

2) improvement of the elevation mechanism stiffness characteristics by eliminating the less efficient extreme angular positions.

5.0 APPENDIX

"Dynamic Testing of a Heliostat" prepared by the Technical Staff of ANCO Engineers, Incorporated, Santa Monica, California.

5.0 APPENDIX

Final Report

DYNAMIC TESTING OF A HELIOSTAT

Prepared for

SOLARAMICS, INC.
El Segundo, California

Approved by

Quality Assurance

By

The Technical Staff
ANCO ENGINEERS, INC.
Santa Monica, California
(213) 829-9721, 829-2624

November 1979

1.0 INTRODUCTION

To determine the static and dynamic characteristics of the heliostat designed and built by Solaramics, Inc., the series of tests discussed herein were performed on a full-scale unit. Reflector panels were not available at the time of testing; however, their weight and mass distribution was simulated by filling the heliostat's simulated structure with concrete. Several types of tests were performed (1) to determine both elevation and azimuth mechanism stiffness as functions of elevation and azimuth angle and to document backlash and hysteretic effects; and (2) to determine dominant resonant frequencies, modal damping ratios and identify response shape which would permit verification of the mathematical modeling effort or suggest modifications to be made to the mathematical model to bring agreement between experimental and predicted values of loads, moments, and stresses.

Subsequent sections of this report discuss the testing methods used, the results of testing, the analytical techniques used, the analytical results and a comparison of experimental and analytical results.

2.0 TEST METHODS

As mentioned, several test methods were employed to determine the static and dynamic characteristics of the heliostat. Snap back testing was performed at five elevation mechanism positions and at three azimuth angles to identify the heliostat's dominant resonant frequencies and modal damping ratios. Two types of excitation were used. The first relied on monitoring the response of the heliostat to man excitation. In this way lower modes of the heliostat were preferentially excited to permit their identification. This technique proved most successful in identifying modes of vibration that were attributed to backlash in the elevation and azimuth linkages.

The second types of snapback excitation relied on a hydraulic actuator to exert a known static force to the heliostat. Instantaneous release of this force allowed the heliostat to enter free vibration where all modes could be observed. This technique proved most useful in identifying modes of vibration which involved flexure of the heliostat and its individual structural elements. Table 2.1 summarizes the test sequence followed.

A total of eight Endevco piezo electric accelerometers were mounted on the heliostat to monitor its response to induced loads. Accelerometer signals were then passed through amplifiers and strip chart recorders to view the response of the heliostat in the time domain and determine the magnitude of the acceleration response. Selected accelerometer signals were processed through a Spectral Dynamics (SD330A) real time analyzer to view the response of the heliostat in the frequency domain. Spectral plots were then converted to hard copy using an x-y recorder. Example of the time frequency domain response to one snapback test may be seen in Figure 2.1.

Forced vibration techniques using a small (10 kg) split disk eccentric mass shaker to introduce a sinusoidal forcing function were used to confirm resonant frequencies previously identified by snapback techniques and to

TABLE 2.1: HELIOSTAT TEST SEQUENCE

Test No.	Run No.	Test Type	Elevation (°)	Azimuth (°)	Force Direction	Purpose
1	1	Snapback	30°	0°	Vertical	Preliminary investigation of modal response
	2	Snapback	30°	0°	Various	No meaningful data taken
1.4, 0	1	Snapback	60°	0°	Y and Z	Hand excitation to identify resonant frequencies
2.1, 0	1	Snapback	-23°	0°	-30° in -X direction (X-Z plane)	To identify f_i and β_i
2.2, 0	1	Snapback	0°	0°	Same	Same
2.3, 0	1	Snapback	30°	0°	Same	Same
2.4, 0	1	Snapback	60°	0°	Same	Same but force doubled in two cases to note non-linearities
2.5, 0	1	Snapback	180°	0°	Same	Same as 2.1, 0
3.3, 0	1	Snapback	30°	0°	-22° in -Y direction (Y-Z plane)	To identify f_i, β_i and hand excitation to identify "clearance" modes
3.3, -90	1	Snapback	30°	-90°	-30° in -X direction (X-Z plane)	Same
3.3, +90	1	Snapback	30°	+90°	-30° in -X direction (X-Z plane)	Same

TABLE 2.1 (cont'd)

Test No.	Run No.	Test Type	Elevation (°)	Azimuth (°)	Force Direction	Purpose
3.4, 0	1	Snapback	60°	0°	-22° in -Y direction (Y-Z plane)	To identify f_i, β_i and hand excitation to identify "clearance" modes
4.4, 0	1	Snapback	60°	0°	Various (X-Z plane)	Force applied at reflector support beam to document "clearance" modes
5.5, 0	1	Shaker	180°	0°	±Y	MK-11 shaker installed on reflector support beam - 10% and 100% eccentricity
5.5, 0	2	Shaker	180°	0°	±Z	Same
6.1, 0	1	Static	-23°	0°	$-M_Y$	0, -97,000 in.-lb static moment to determine elevation mechanism stiffness
6.1, 0	2	Static	-23°	0°	$\pm M_Z$	±90,000 in.-lb static moment to determine azimuth mechanism stiffness
6.2, 0	1	Static	0°	0°	$\pm M_Y$	±64,100 in.-lb moments as in 6.1, 0 Run 1
6.2, 0	2	Static	0°	0°	$\pm M_Z$	Same as 6.1, 0 Run 2
6.3, +90	2	Static	30°	90°	$\pm M_Z$	Same as 6.1, 0 Run 2
6.3, +90	3	Static	30°	90°	$\pm M_Z$	Same as 6.1, 0 Run 2 but linkage modified

TABLE 2.1 (cont'd)

Test No.	Run No.	Test Type	Elevation (°)	Azimuth (°)	Force Direction	Purpose
6.3, 0	1	Static	30°	0°	$\pm M_Y$	0, +97,000 in.-lb moments to determine elevation mechamism stiffness
6.3, 0	2	Static	30°	0°	$\pm M_Z$	Same as 6.1, 0 Run 2
6.3, 0	3	Static	30°	0°	$\pm M_Z$	Same as 6.3, +90 Run 3
6.3, 0	4	Static	30°	0°	$\pm M_Z$	Same as 6.3, 0 Run 3 but data collected from top of cross head and top of support column
6.3, -45	2	Static	30°	-45°	$\pm M_Z$	Same as 6.1, 0 Run 2
6.3, -90	2	Static	30°	-90°	$\pm M_Z$	Same as 6.1, 0 Run 2
6.4, 0	1	Static	60°	0°	$\pm M_Y$	0, +49,700 in.-lb moment applied about Y axis
6.4, 0	2	Static	60°	0°	$\pm M_Z$	Same as 6.1, 0 Run 2
6.5, 0	1	Static	180°	0°	$\pm M_Y$	±212,000 in.-lb moment applied about Y axis
6.5, 0	2	Static	180°	0°	$\pm M_Z$	Same as 6.1, 0 Run 2

FIGURE 2.1: TIME FREQUENCY DOMAIN RESPONSE TO SNAPBACK TEST 2.4,0

ANCO

ANCO Engineers, Incorporated, 1701 Colorado Avenue, Santa Monica, CA 90404

Test # 2.4,0 Run # 1 Recorded by RSK/JSH Date 6/20/79 Location Ch 6

Input Sens 1 VRMS or ______ db. Transducer Sens X5 Output Sens 0 10 (20) X1 X4 (lin) log

Freq Range 10 Hz Exp. Average ______ Averages ______, Peak hold ✓, Trans Cap ______

Comments: HEAVE-II, 628 lbs pull, 30° off horizontal @ top of pedestal
Heliostat at 60° Elevation, 0° Azimuth

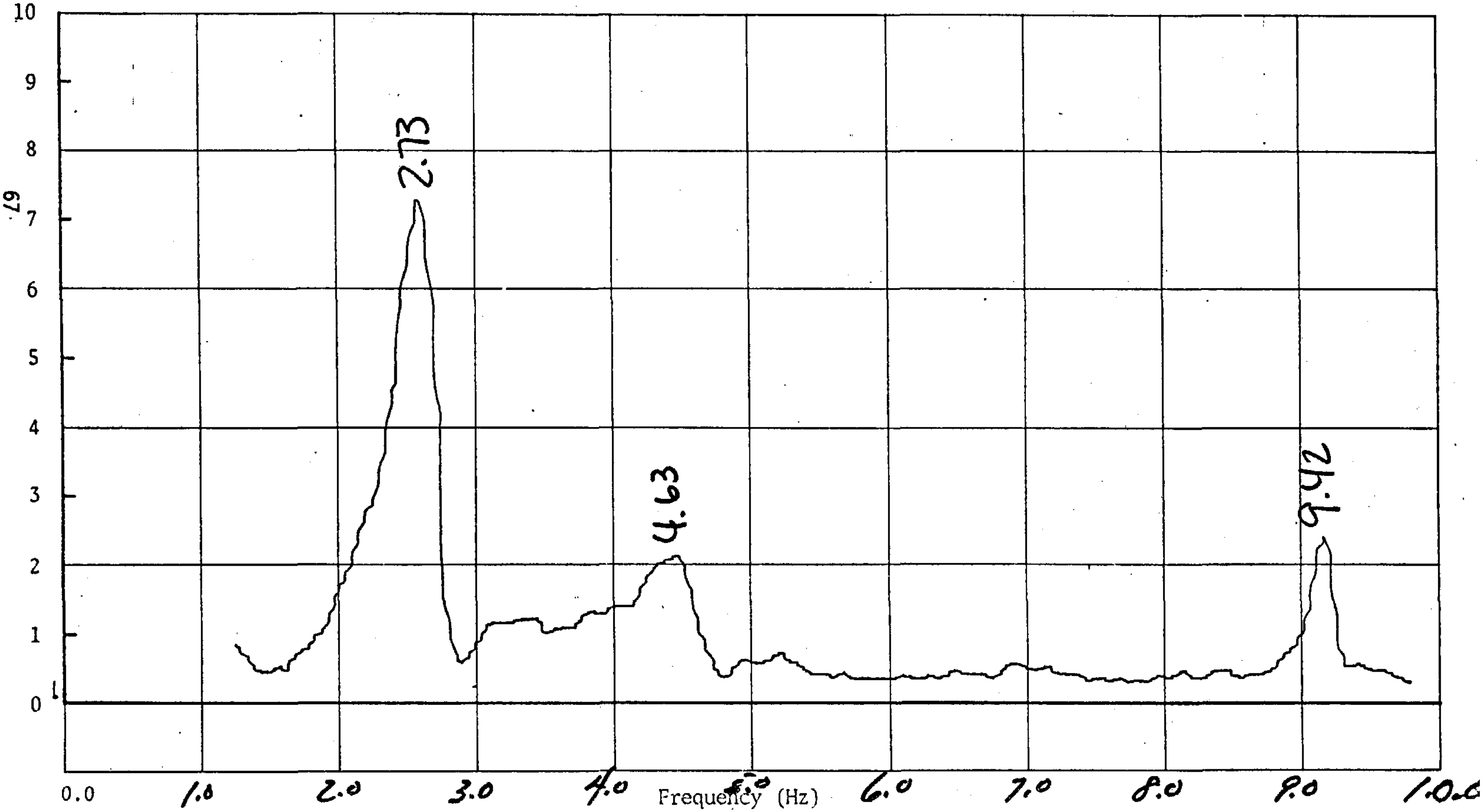

identify response shapes of the heliostat. To identify resonant frequencies the MK-11 shaker was swept slowly through the frequency range of interest while both the time domain and frequency domain response was recorded. Since the force output of the shaker was proportional to the frequency squared, lower modes were difficult to excite. Sufficient force was output above 5 Hz to identify higher modes of vibration. Next the vibrator was set at a resonant frequency and held there while time domain signals were compared in amplitude and phase to determine the response shape and permit modal identification for comparison with predicted mode shapes.

Mechanism stiffness was evaluated by mounting a transit on the heliostat near the cross head (shown in Figure 2.2) and recording the rotations of the heliostat by sighting to a distant point. The applied loads (hence moments) were increased in increments up to the full design moment and then decreased incrementally to document hysteretic effects. Both positive and negative moments were applied to the azimuth mechanism at 5 azimuth angles and at 5 elevation angles. Positive and negative moments were applied to the elevation mechanism at 3 elevation angles, a negative moment at 1 elevation, and a positive moment at 1 elevation (refer to Table 2.1). In addition, deflections between the actuator's housing and arm (hence rotations) were recorded at selected orientations to determine actuator stiffness and heliostat rotation due to actuator stiffness. This was done for both the elevations and azimuth actuators.

Upon review of the rotational stiffnesses calculated about the azimuth linkages certain members were improved to increase the stiffness and a second abbreviated series of tests performed to document the effects of the changes. Data were collected as above with the heliostat oriented at 30^{o} elevation 0^{o} azimuth and at 30^{o} elevation + 90^{o} azimuth. In addition the sighting transit was relocated from near the cross head to the cross head and then to the support column to determine the rotations as functions of applied moment at those locations.

FIGURE 2.2: TRANSIT ON HELIOSTAT CROSS FOR MECHANISM STIFFNESS EVALUATION

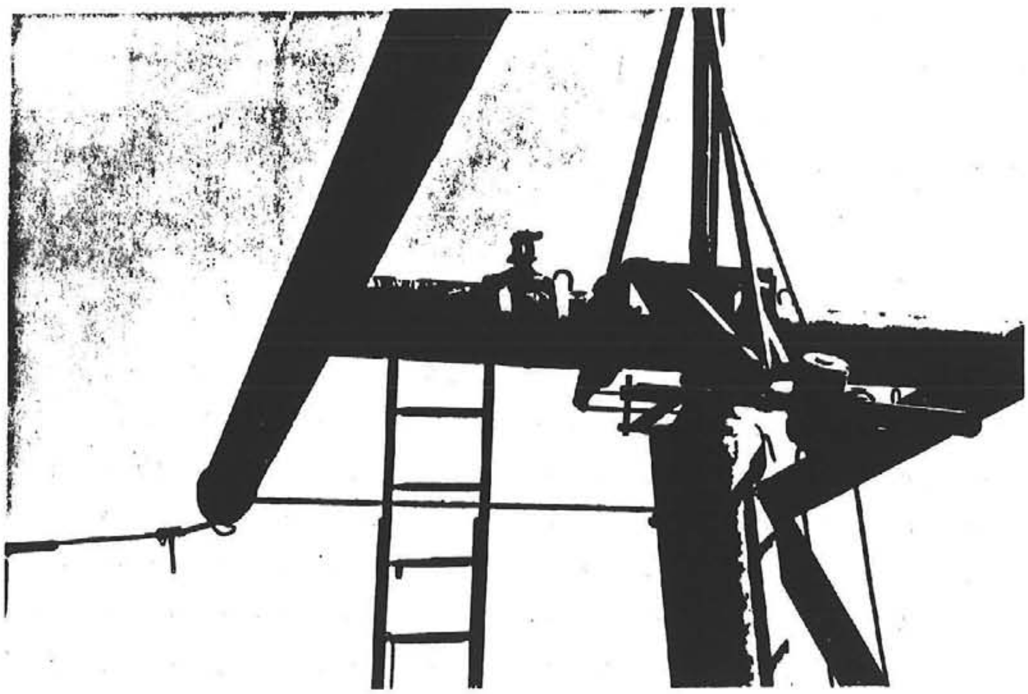

3.0 TEST RESULTS

Testing by snapback and eccentric mass shaker excitation is summarized in Table 3.1 for the five different elevation angles and several different azimuth angles. As can be seen, there is some variation in observed resonant frequency as the elevation of the heliostat is changed from -23° to +180°. This phenomenon was thought to be due to an increase or decrease in rotational stiffness about the cross arm as the elevation mechanism changes position relative to the cross arm.

The lowest resonant frequency was observed at 1.76 Hz at 30° elevation and 0° azimuth. This mode of vibration was identified as rotation of the panel supporting members in their own plane. This mode of vibration was determined to be strongly dependent on azimuth control mechanism stiffness; that is, at ±90° azimuth positions, where the moment resistance of the azimuth linkages are at minimum values, the resonant frequency was observed to decrease correspondingly.

The second mode of vibration observed at 2.7 Hz was described as rotation of the reflective surface about the cross arm. Here some frequency dependence on elevation angle was observed. The third mode was found at about 4.5 Hz at 30° elevation, 0° azimuth. This mode involved translation of the heliostat surface. Bending of the support column was present. At 5.2 Hz bending of the support column parallel to the reflective surface was observed. Bending of the panel supports was found at 8.6 and 9.4 Hz. Estimates of modal damping ratios range between 1.0 and 4.0 percent of critical.

No detailed response shapes were mapped; however, sufficient data were collected during the steady state sinusoidal tests to permit modal identification so that a comparison between experimentally determined resonant frequencies, analytically determined resonant frequencies, and analytically predicted values could be made.

TABLE 3.1: DETERMINED RESONANT FREQUENCIES AND DAMPING RATIOS - RESONANT FREQUENCY (DAMPING RATIO)

Elevation (°)	Azimuth	$f_1(\beta_1)$ Hz(%)	$f_2(\beta_2)$ Hz(%)	$f_3(\beta_3)$	$f_4(\beta_4)$	$f_5(\beta_5)$	$f_6(\beta_6)$
-23°	0°	-	2.59(2.3)	4.2(2.3)	5.68(-)	8.67(∿1.0)	9.71(-)
0°	0°		2.75(2.7)	4.75(2.3)	-	9.15(-)	9.63(-)
30°	+90°	1.24(-)	2.85(1.5)	4.68(-)	5.66(1.7)	9.16(-)	9.63(∿1.0)
30°	0°	1.76(1.9)	2.62(-)	4.52(3.4)	5.21(-)	8.58(1.0)	9.39(1.0)
30°	-90°	1.16(-)	2.85(-)	4.74(-)	5.63(2.0)	9.22(-)	9.62(-)
60°	0°		2.74(4.5)	4.73(2.2)	5.7(-)	8.28(1.0)	9.40(1.0)
180°	0°		2.33(-)	3.83(-)		8.88(-)	9.57(-)

Table 3.2 summarizes values of rotational stiffnesses of the heliostat for the various angles of elevation and azimuth where tests were conducted. As can be seen, average gross elevation rotational stiffnesses range from 1.15×10^7 to 3.1×10^7 in.-lb/radian depending on elevation angle at 0° azimuth angle with the average being 1.8×10^7 in.-lb/rad. These data represent gross rotation of the heliostat due to static loads applied at the extremities of the panel support beams and as such have contributions arising from bending of the support beams, bending of the cross arm, flexure in the elevation actuator, and bending of the support column. To quantify the rotation due to elevation actuator stiffness, a dial indicator was placed between the actuator rod and rod support tube. Measurements were taken during selected tests which indicated that about 22 percent of the gross rotation was due to elevation actuator flexibility.

Average gross rotational stiffnesses taken to determine azimuth stiffness ranged from 5.0×10^6 to 1.6×10^7 in.-lb/rad, again depending on elevation and azimuth angle. This stiffness was observed to be a maximum at 0° azimuth and to decrease as the azimuth angle was increased to ±90°. Again measurements were taken to determine the influence of azimuth actuator flexibility on the gross rotational stiffness. As can be seen, approximately 26 percent of the observed rotation was due to this phenomenon.

In addition, considerable flexure was occurring between the cross head and cross arm connection. This was verified by taking data with the transit on the cross arm and on the cross head in separate but identical tests. This suggests that about 27 percent of the reported gross rotation was due to this flexibility.

Changes were made to the azimuth mechanisms which improved stiffness by another 9 percent. Column flexure was estimated to contribute to approximately 10 percent of the gross rotation. Considerable improvement could be made on the values reported in Table 3.2.

TABLE 3.2: AVERAGE GROSS ROTATIONAL STIFFNESSES OF HELIOSTAT

Azimuth (°)	Elevation (°)	Positive Moment $k=\frac{in.-lb}{rad}$	Negative Moment $k=\frac{in.-lb}{rad}$	Comments
Moments applied to determine elevation mechanism stiffnesses:				
0°	-23°	Not taken	1.8×10^7	
0°	0°	1.46×10^7	2.0×10^7	
0°	30°	2.0×10^7	Not taken	
0°	60°	3.1×10^7	Not taken	
0°	180°	1.2×10^7	1.15×10^7	
Moments applied to determine azimuth mechanism stiffnesses:				
0°	0°	1.1×10^7	1.03×10^7	
+90°	30°	5.7×10^6	8.0×10^6	
+90°	30°	7.3×10^6	7.18×10^6	Modified linkage
+45°	30°	8.5×10^6	6.9×10^6	
0°	30°	1.06×10^7	9.8×10^6	
0°	30°	1.17×10^7	1.17×10^7	Modified linkage
0°	30°	1.60×10^7	Not taken	Measured from cross head
0°	30°	1.0×10^8	Not taken	Measured from top of column
-45°	30°	7.8×10^6	1.2×10^7	
-90°	30°	5.0×10^6	7.8×10^6	
0°	180°	1.5×10^7	9.6×10^6	
45°	30°	4.9×10^7	4.9×10^7	Azimuth actuator
0°	30°	4.1×10^7	4.1×10^7	Azimuth actuator
0°	180°	4.6×10^7	4.6×10^7	Azimuth actuator
0°	30°	9.3×10^7	9.3×10^7	Elevation actuator

All data taken to determine the gross stiffnesses are presented in Figures 3.1 through 3.16. Here hysteretic and backlash effects may be seen. Tables 3.3 through 3.16 present these data numerically.

Results of Solaramics, Inc.'s additional dynamic tests on the drive mechanism are included in Appendix A. The results of these additional tests are separately discussed by Solaramics, Inc. in their report. ANCO did not conduct these tests and therefore is not including any comments.

FIGURE 3.1

Heliostat Rotational Stiffness Characteristics

(–) Moment about y-axis (Elevation Linkage)

–23° Elevation; 0° Azimuth

Test 6.1.0 Run 1

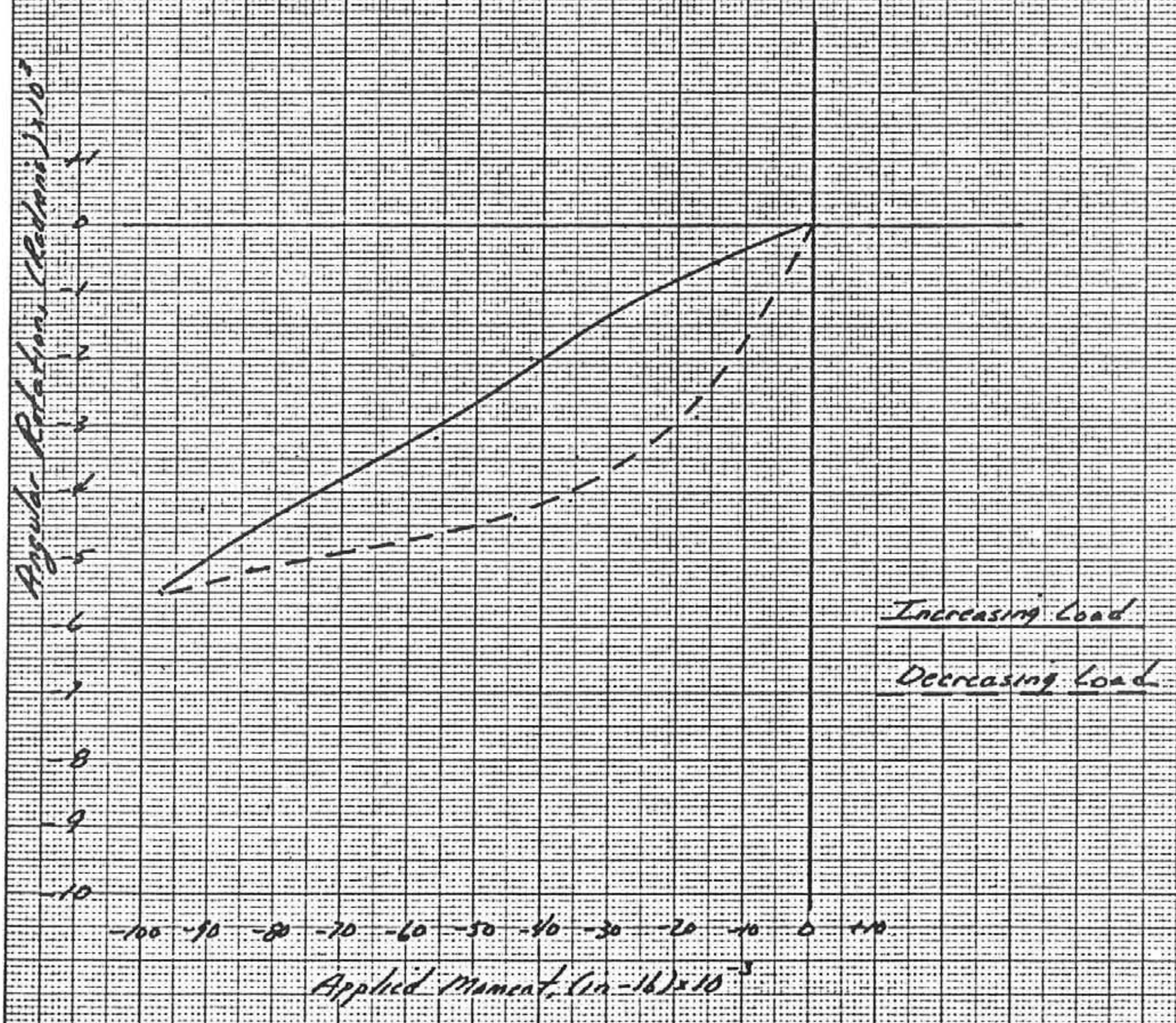

FIGURE 3.2:

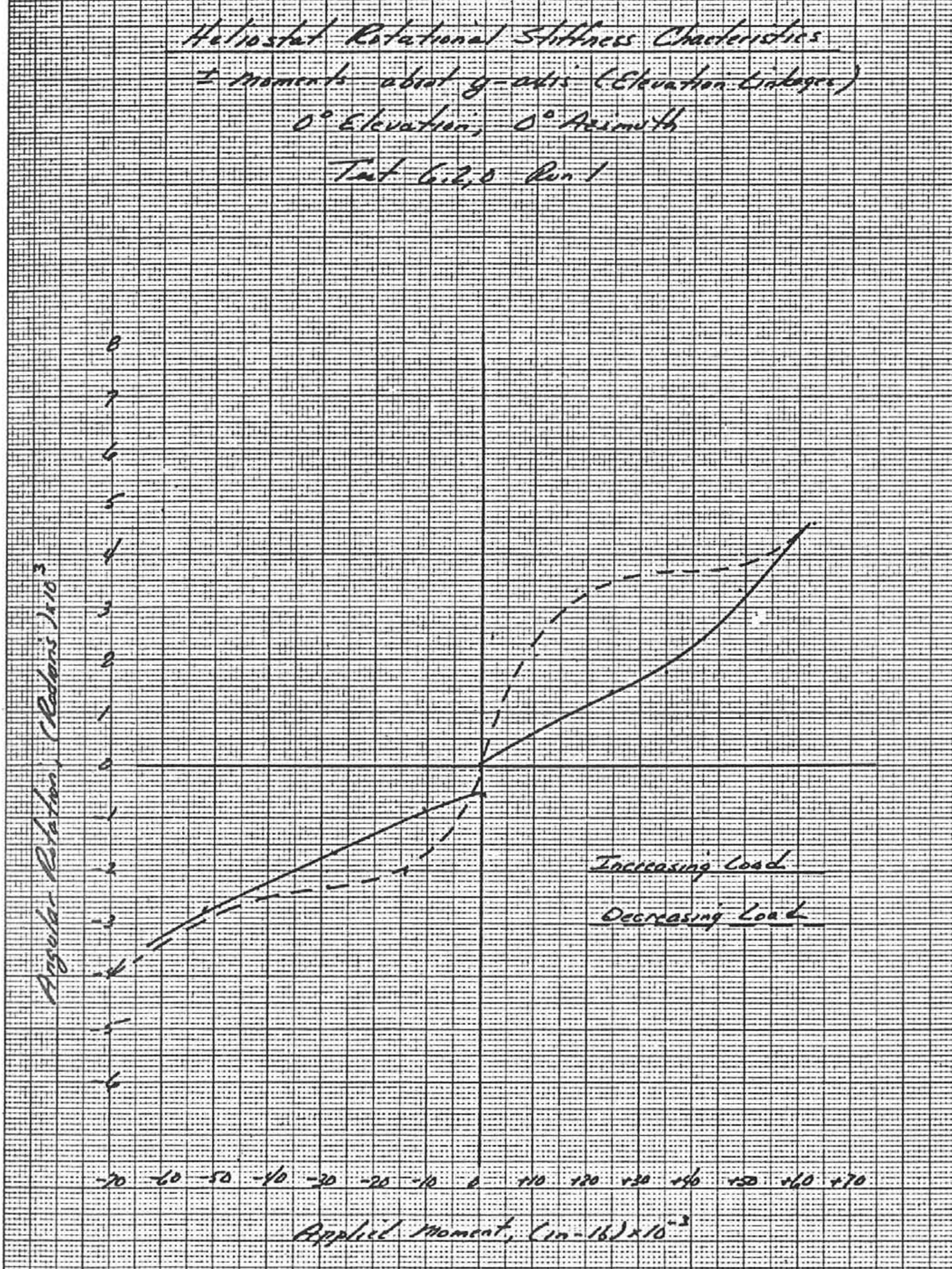
Heliostat Rotational Stiffness Characteristics
± moments about y-axis (Elevation Linkages)
0° Elevation, 0° Azimuth
Test 6.2.0 Run 1
Angular Rotation, (Radians) x10^-3
Applied Moment, (in-lb) x10^-3
Increasing Load
Decreasing Load
8
7
6
5
4
3
2
1
0
-1
-2
-3
-4
-5
-6
-70 -60 -50 -40 -30 -20 -10 0 +10 +20 +30 +40 +50 +60 +70

FIGURE 3.3:

Heliostat Rotational Stiffness Characteristics

+ Moment about y-axis (Elevation Linkages)

30° Elevation, 0° Azimuth

Test 6.3.0 Run 1

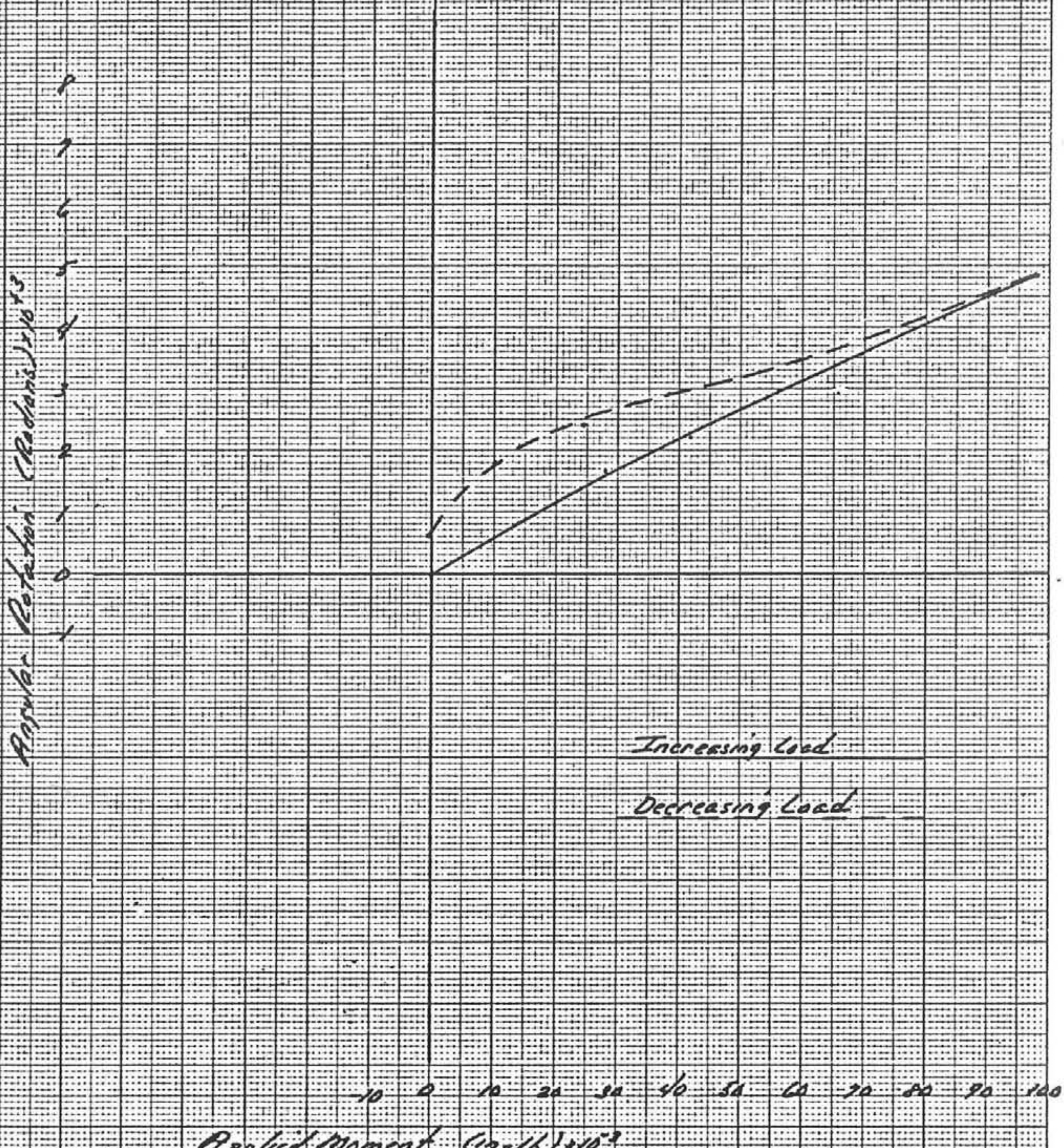

FIGURE 3.4:

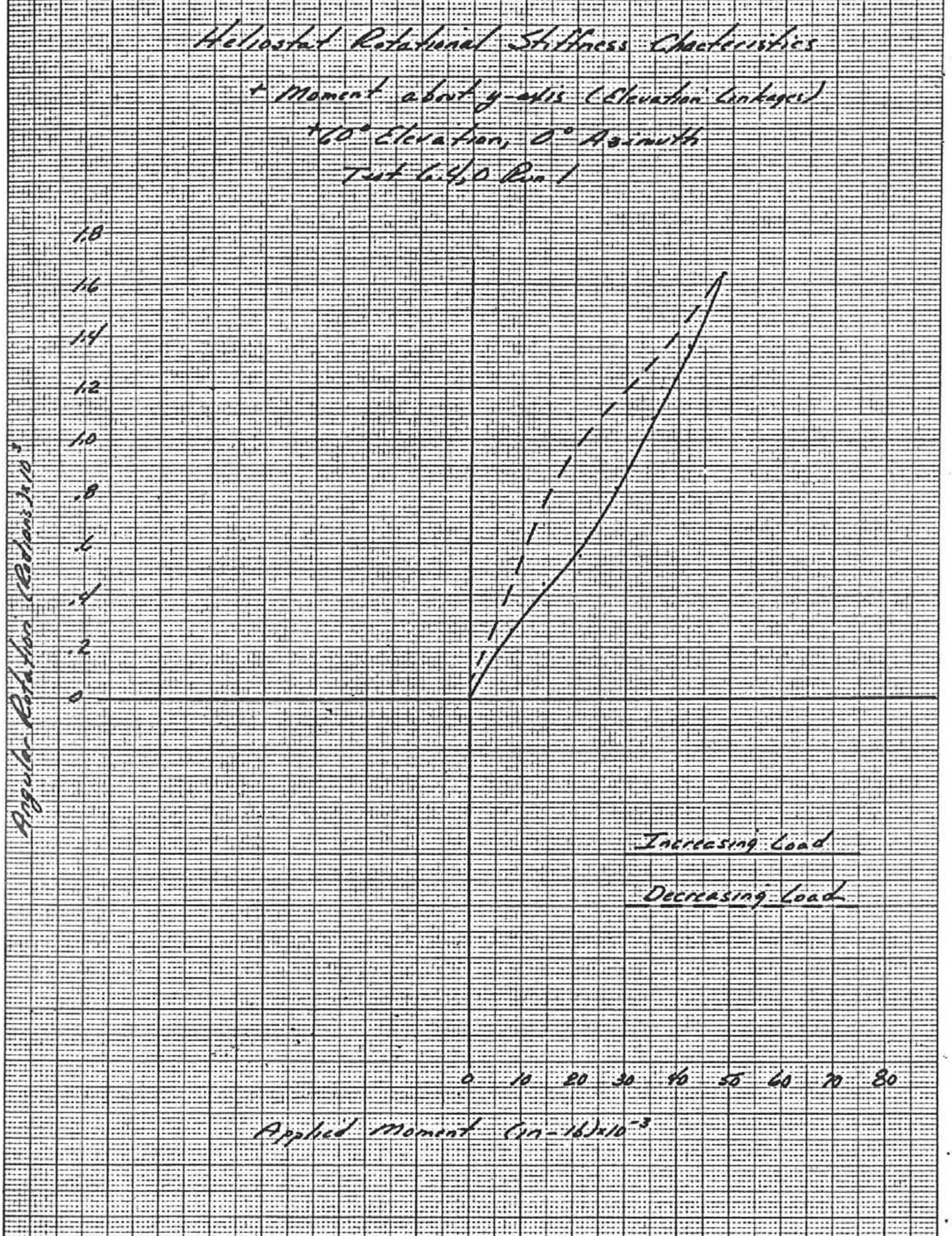
Heliostat Rotational Stiffness Chacteristics
+ Moment about y-axis (Elevation Linkages)
+60° Elevation, 0° Azimuth
Test 6.4.0 Run 1
Angular Rotation (Radians)x10^-3
1.8
1.6
1.4
1.2
1.0
.8
.6
.4
.2
0
Increasing Load
Decreasing Load
0
10
20
30
40
50
60
70
80
Applied Moment (in-lb)x10^-3

FIGURE 3.5:

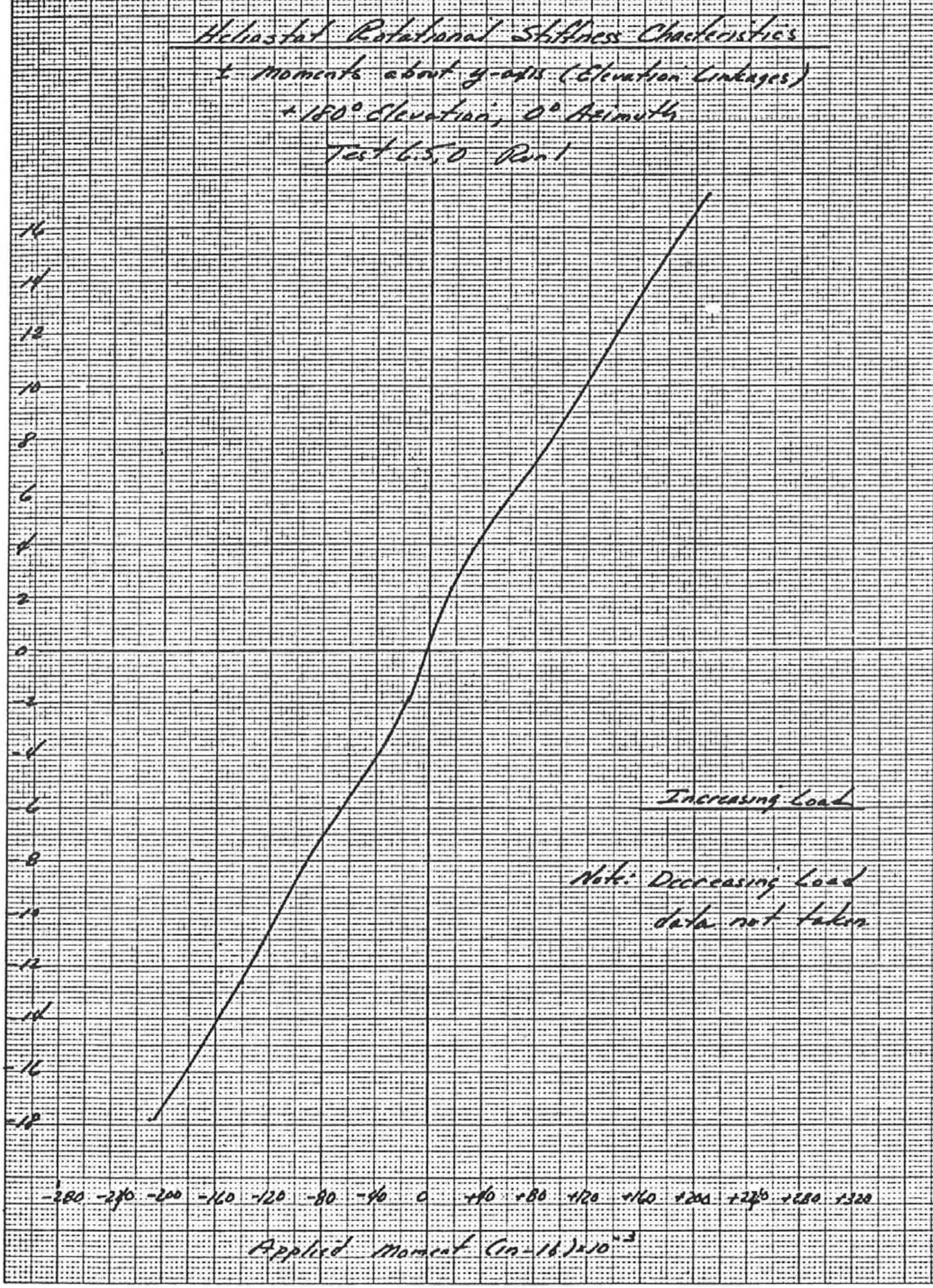

Heliastat Rotational Stiffness Characteristics
± moments about y-axis (Elevation Linkages)
+180° Elevation; 0° Azimuth
Test 6.5.0 Run 1
Angular Rotation; (Radians) x 10^3
16
14
12
10
8
6
4
2
0
-2
-4
-6
-8
-10
-12
-14
-16
-18
-280 -240 -200 -160 -120 -80 -40 0 +40 +80 +120 +160 +200 +240 +280 +320
Applied Moment (in-lb) x 10^-3
Increasing Load
Note: Decreasing Load data not taken

FIGURE 3.6:

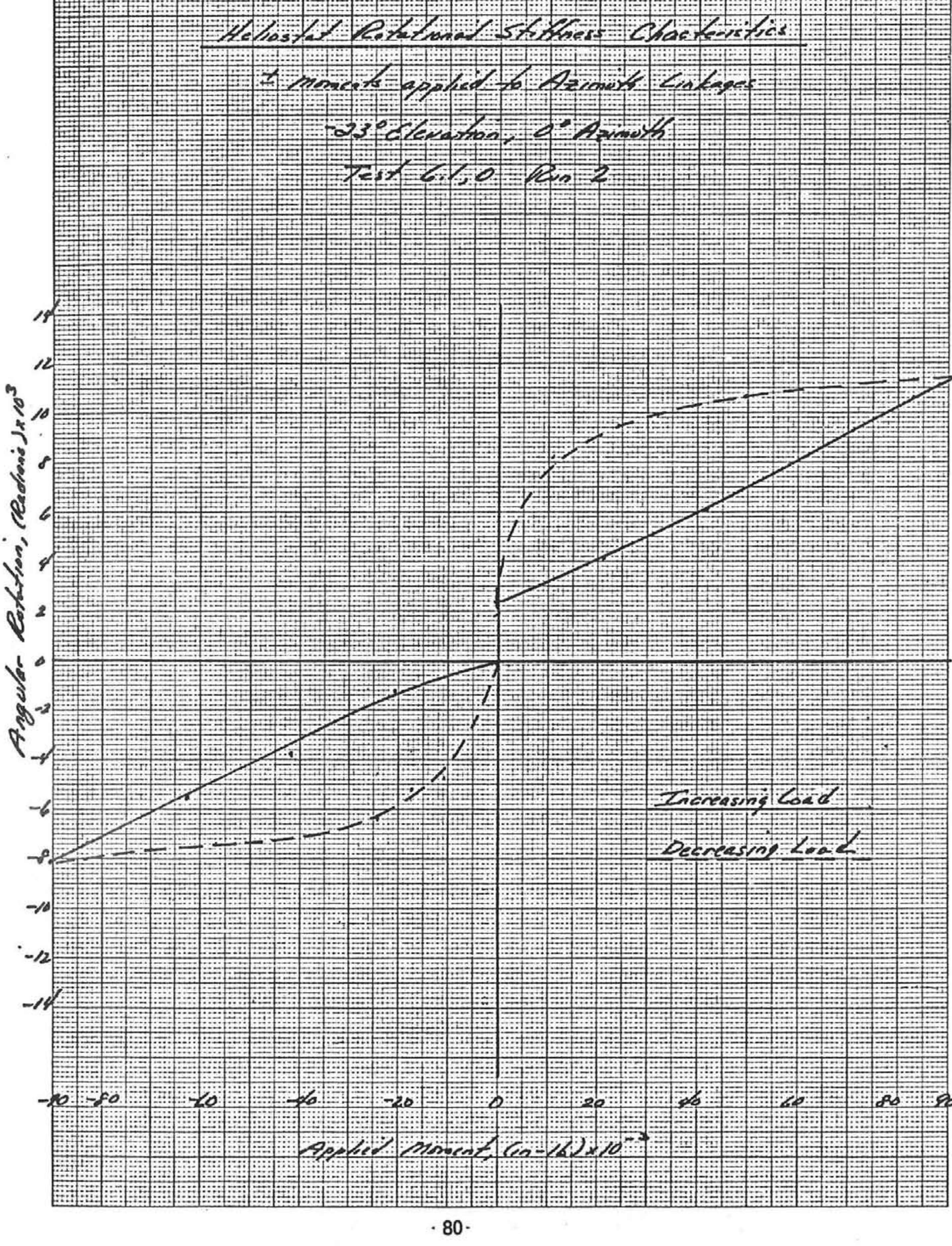
Heliostat Rotational Stiffness Characteristics
± moments applied to Azimuth Linkages
-23° Elevation, 0° Azimuth
Test 6.1,0 Run 2
Angular Rotation, (Radians) x 10³
Applied Moment, (in-lb) x 10⁻³
Increasing Load
Decreasing Load

FIGURE 3.7:

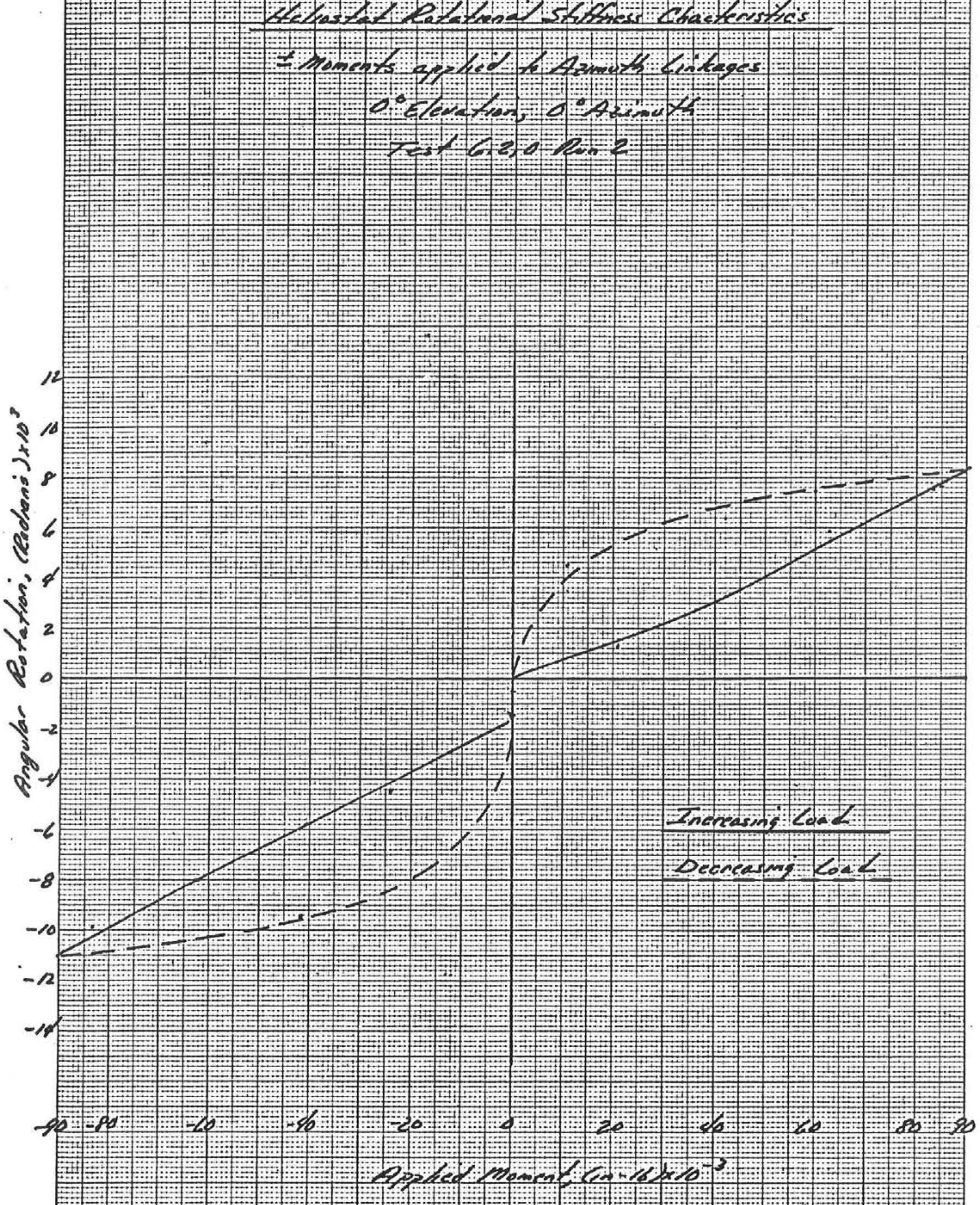
Heliostat Rotational Stiffness Chacteristics
± Moments applied to Azimuth Linkages
0° Elevation, 0° Azimuth
Test 6.2.0 Run 2
Angular Rotation, (Radians) x10³
12
10
8
6
4
2
0
-2
-4
-6
-8
-10
-12
-14
Increasing Load
Decreasing Load
-90
-80
-60
-40
-20
0
20
40
60
80
90
Applied Moment, (in-lb) x10⁻³

FIGURE 3.8:

Heliostat Rotational Stiffness Chacteristics

± Moments applied to Azimuth Linkages

30° Elevation, +90° Azimuth

Test 6.3,90 Run 2

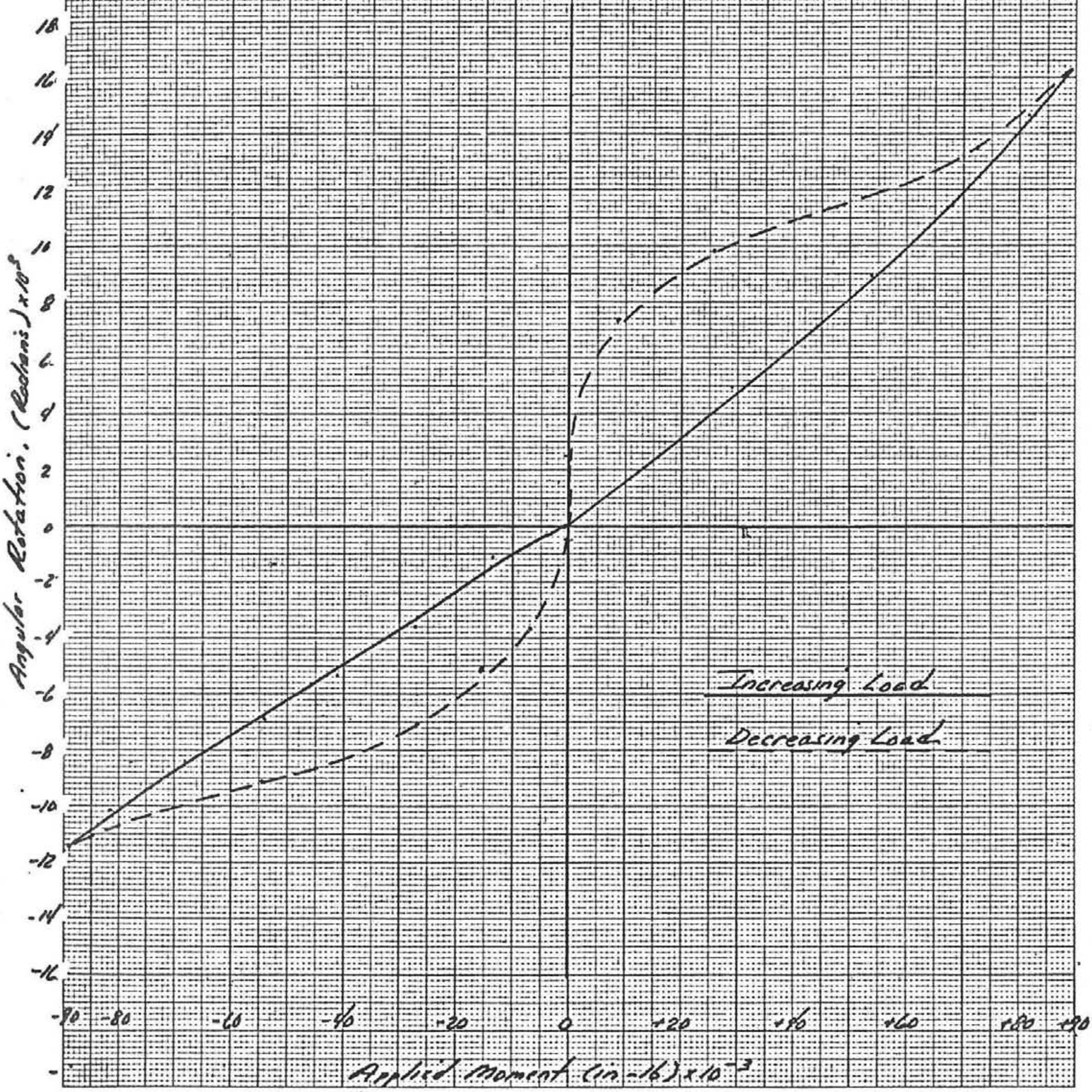

FIGURE 3.9

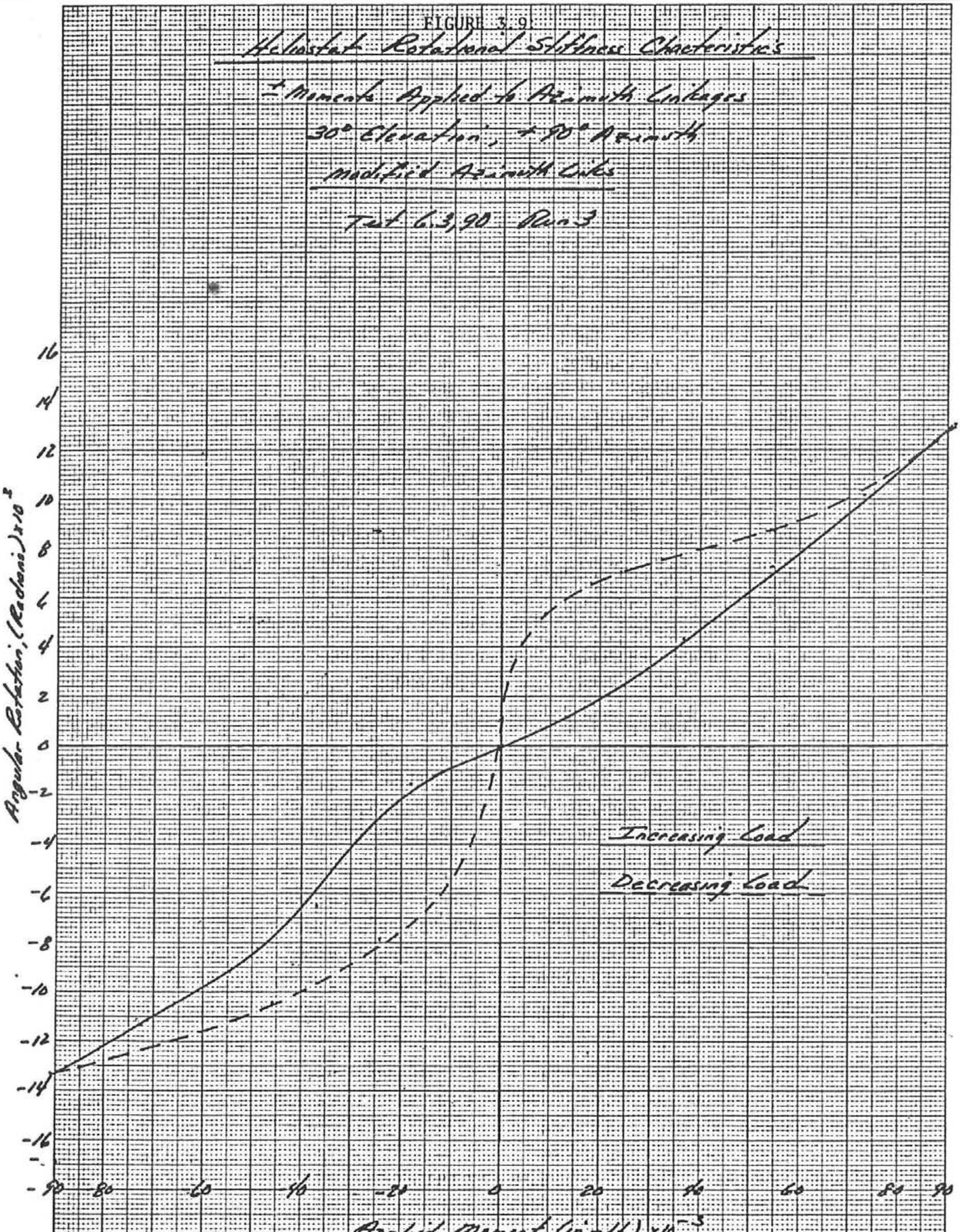
Heliostat Rotational Stiffness Characteristics
± Moments Applied to Azimuth Linkages
30° Elevation; +90° Azimuth
modified Azimuth Links
Test 6.3,90 Run 3
Increasing Load
Decreasing Load
Angular Rotation; (Radians) x10
16
14
12
10
8
6
4
2
0
-2
-4
-6
-8
-10
-12
-14
-16
-90
-80
-60
-40
-20
0
20
40
60
80
90
Applied Moment (in-lb) x10^-3

FIGURE 3.10:

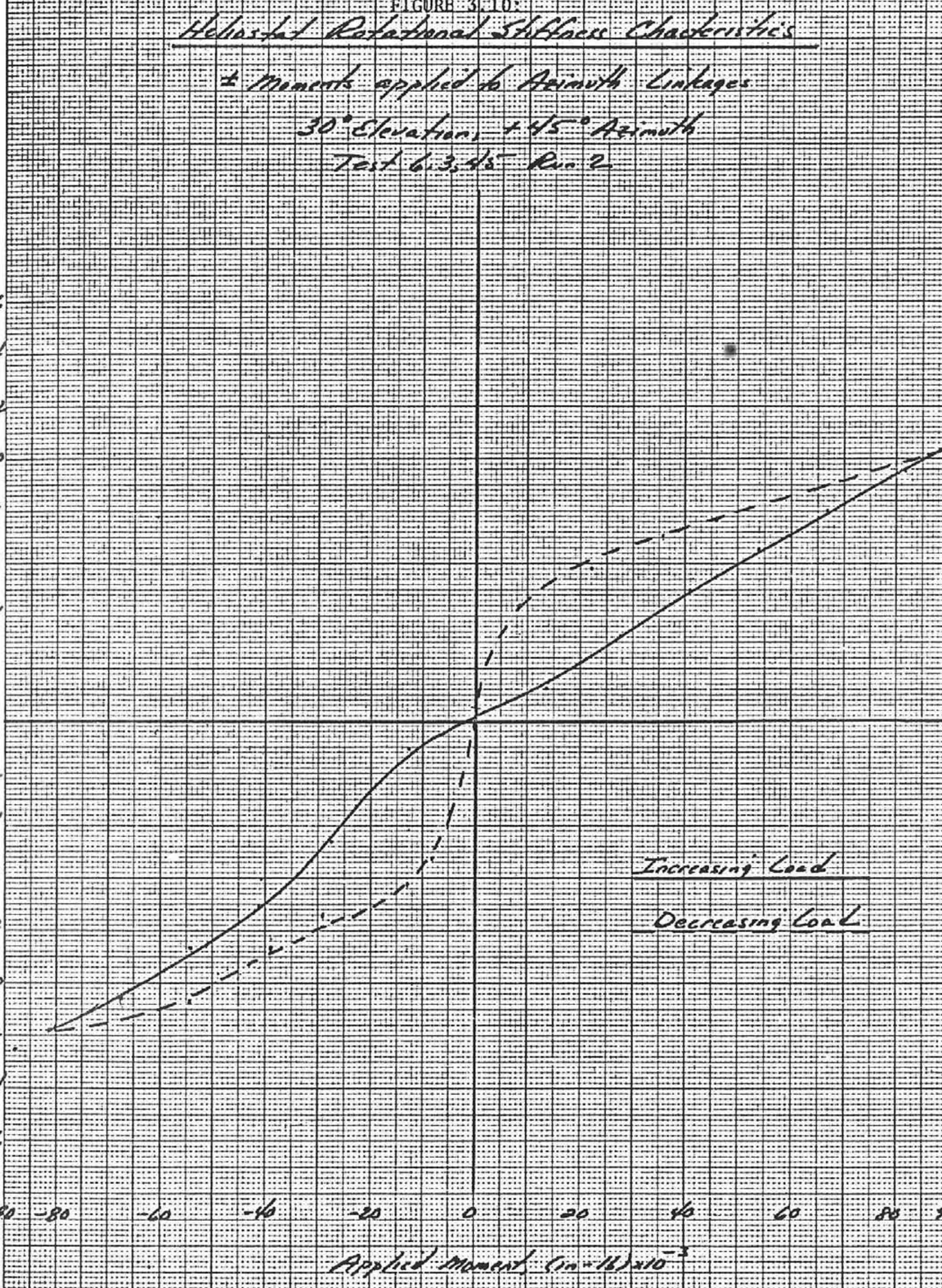
Heliostat Rotational Stiffness Characteristics
± Moments applied to Azimuth Linkages
30° Elevation, +45° Azimuth
Test 6.3.45 Run 2
Angular Rotation, (Radians) x10^-3
16
14
12
10
8
6
4
2
0
-2
-4
-6
-8
-10
-12
-14
-16
-90
-80
-60
-40
-20
0
20
40
60
80
90
Applied Moment, (in-lb) x10^-3
Increasing Load
Decreasing Load

FIGURE 3.11:

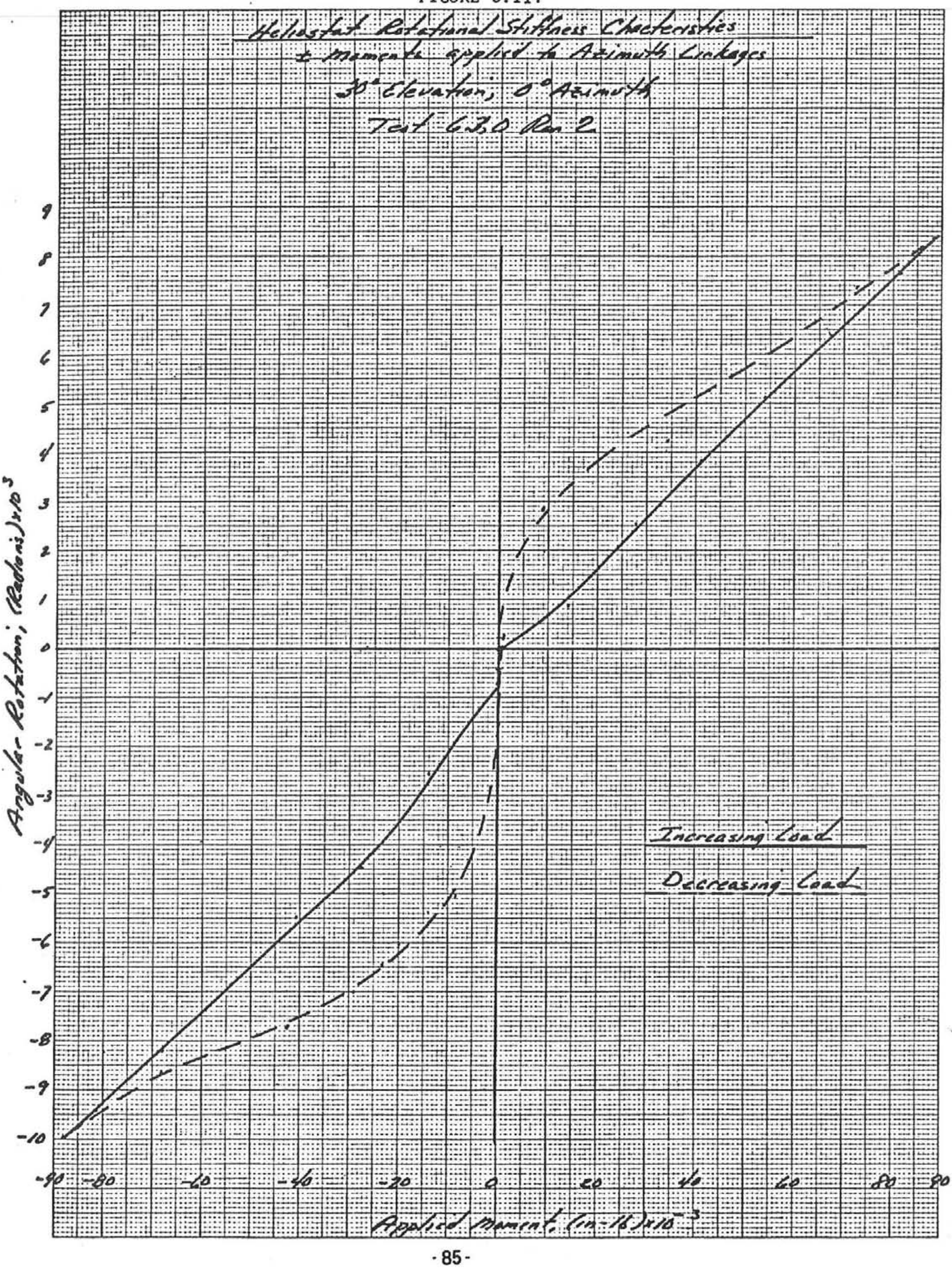
Heliostat Rotational Stiffness Characteristics
± Moments applied to Azimuth Linkages
30° Elevation; 0° Azimuth
Test 6.3.0 Run 2
Angular Rotation; (Radians)x10³
9
8
7
6
5
4
3
2
1
0
-1
-2
-3
-4
-5
-6
-7
-8
-9
-10
-90
-80
-60
-40
-20
0
20
40
60
80
90
Applied Moment, (in-lb)x10⁻³
Increasing Load
Decreasing Load

FIGURE 3.12

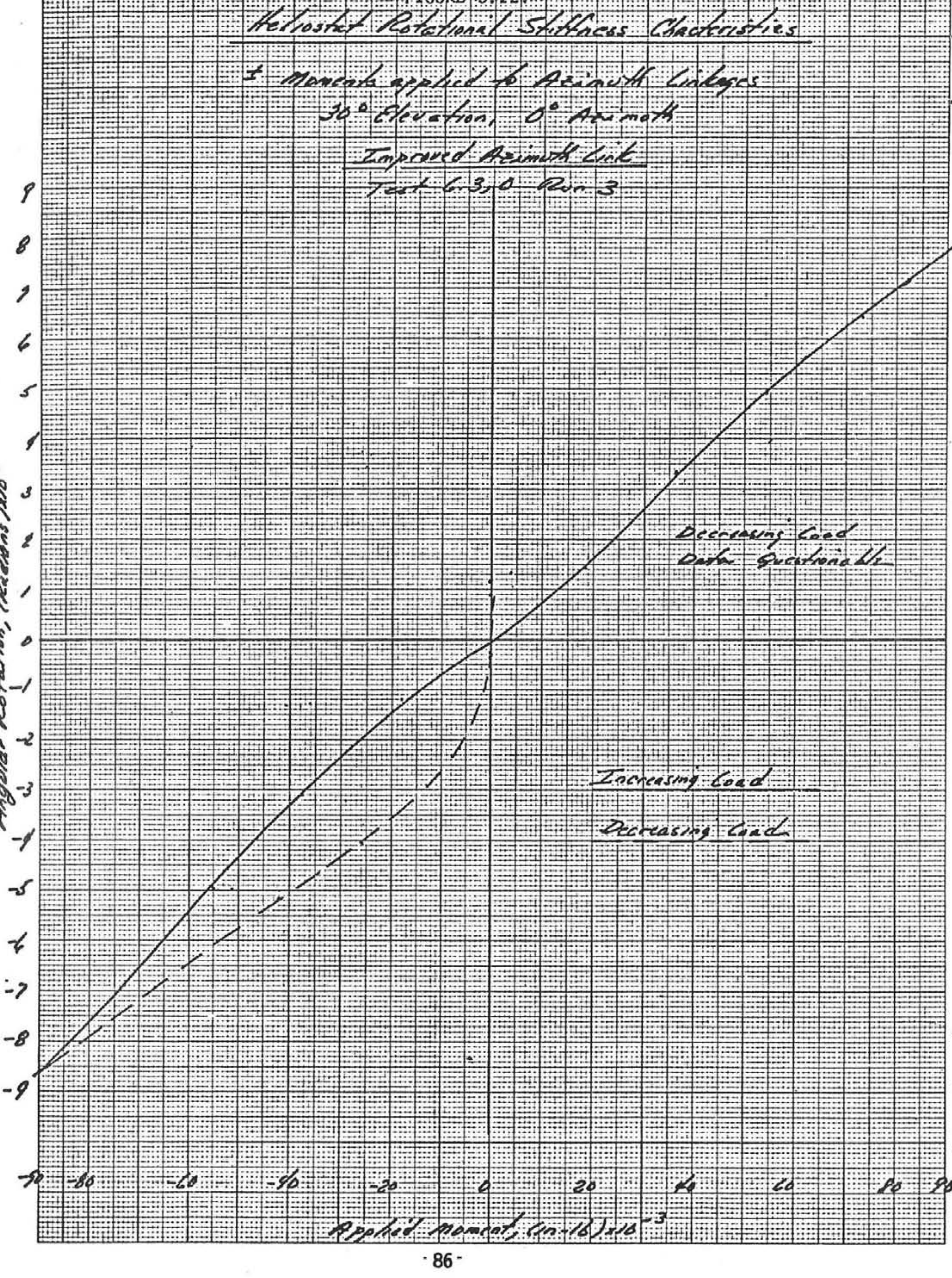
Heliostat Rotational Stiffness Characteristics
± Moments applied to Azimuth Linkages
30° Elevation, 0° Azimuth
Improved Azimuth Link
Test 6.3.0 Run 3
Decreasing Load
Data Questionable
Increasing Load
Decreasing Load
Angular Rotation, (Radians)x10^3
9
8
7
6
5
4
3
2
1
0
-1
-2
-3
-4
-5
-6
-7
-8
-9
-90
-80
-60
-40
-20
0
20
40
60
80
90
Applied Moment, (in-lb)x10^-3

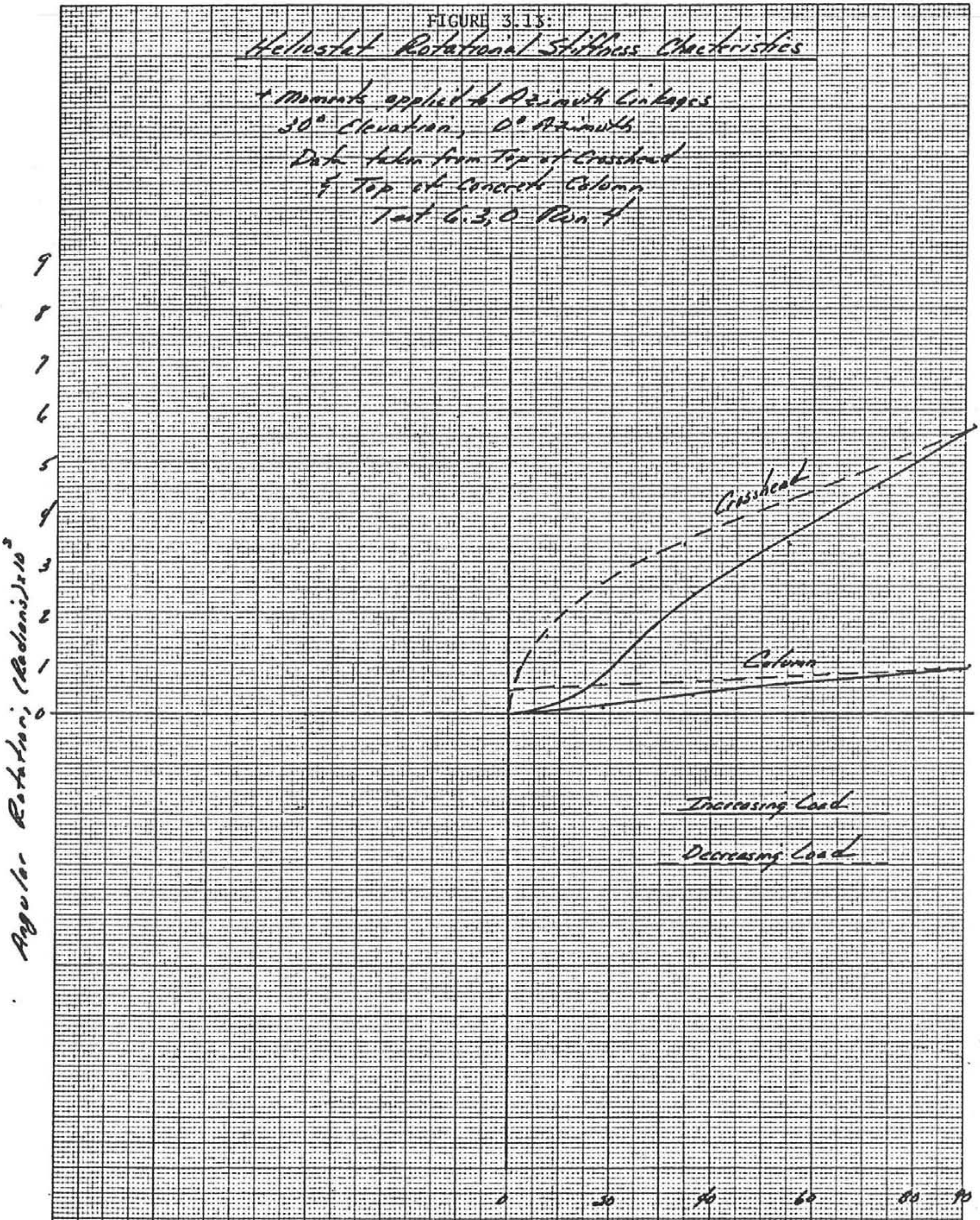

FIGURE 3.13: Heliostat Rotational Stiffness Chacteristics

FIGURE 3.14:

Heliostat Rotational Stiffness Characteristics

± Moments applied to Azimuth Linkages

30° Elevation, -45° Azimuth

Test 6.3, -45 Run 2

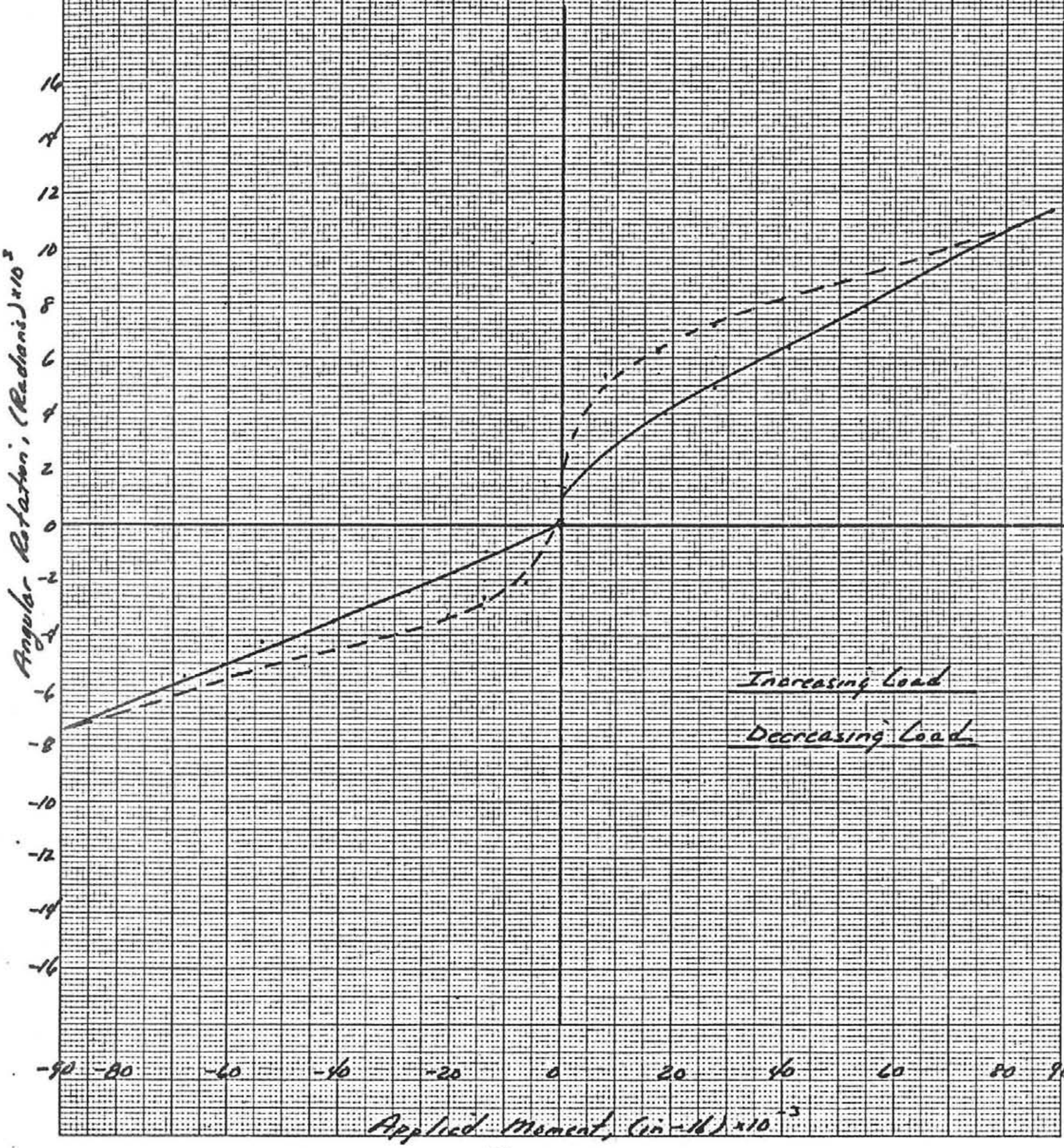

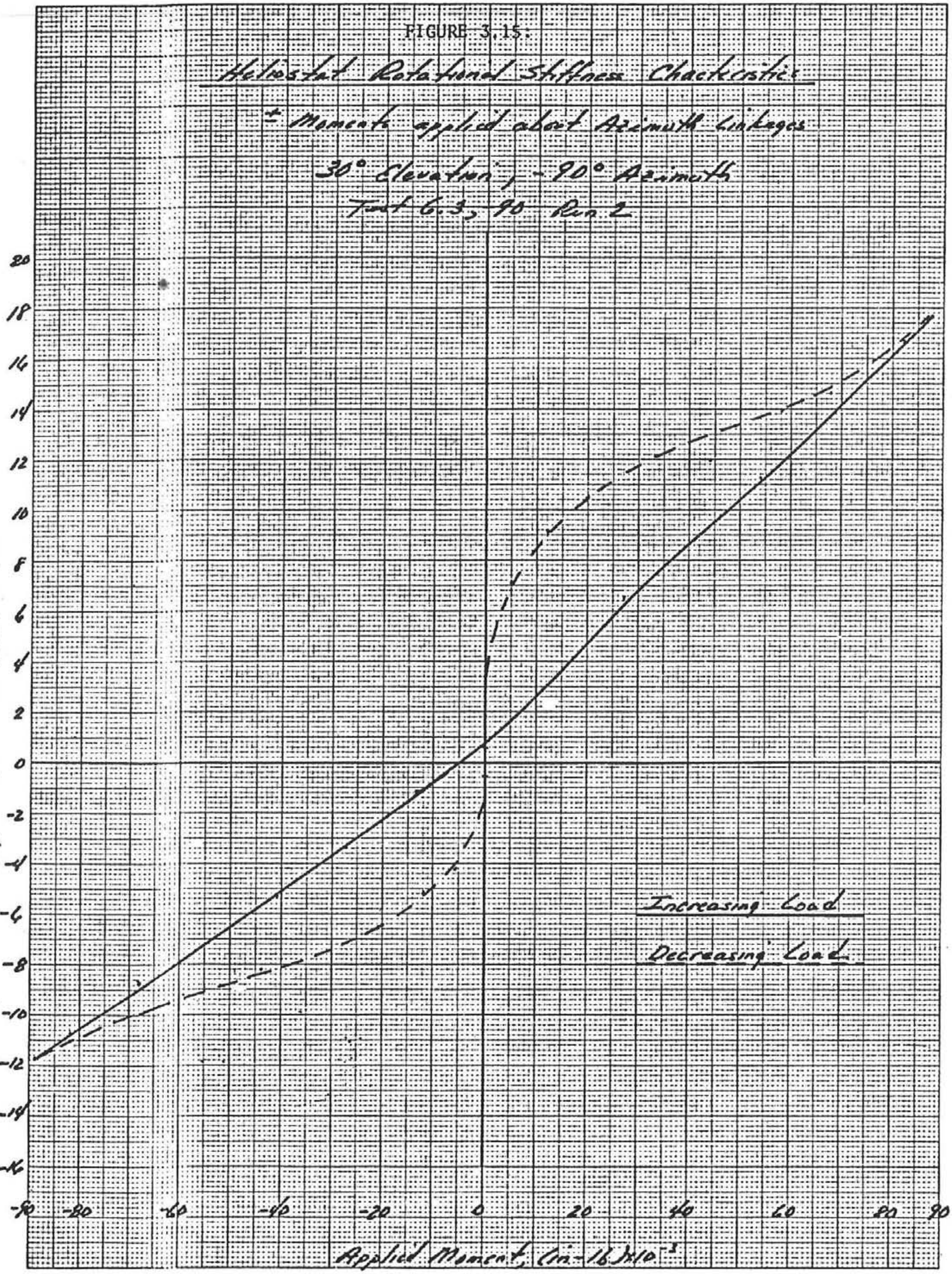
FIGURE 3.15:
Heliostat Rotational Stiffness Characteristic
± Moments applied about Azimuth Linkages
30° Elevation, -90° Azimuth
Test 6.3, 90 Run 2
Increasing Load
Decreasing Load
Angular Rotation (Radians) x10+3
Applied Moment, (in-lb)x10-3
20
18
16
14
12
10
8
6
4
2
0
-2
-4
-6
-8
-10
-12
-14
-16
-90
-80
-60
-40
-20
0
20
40
60
80
90

FIGURE 3.16

Heliostat Rotational Stiffness Characteristics

± Moments applied to Azimuth Linkages

+180° Elevation, 0° Azimuth

Test 6.5, 0 Run 2

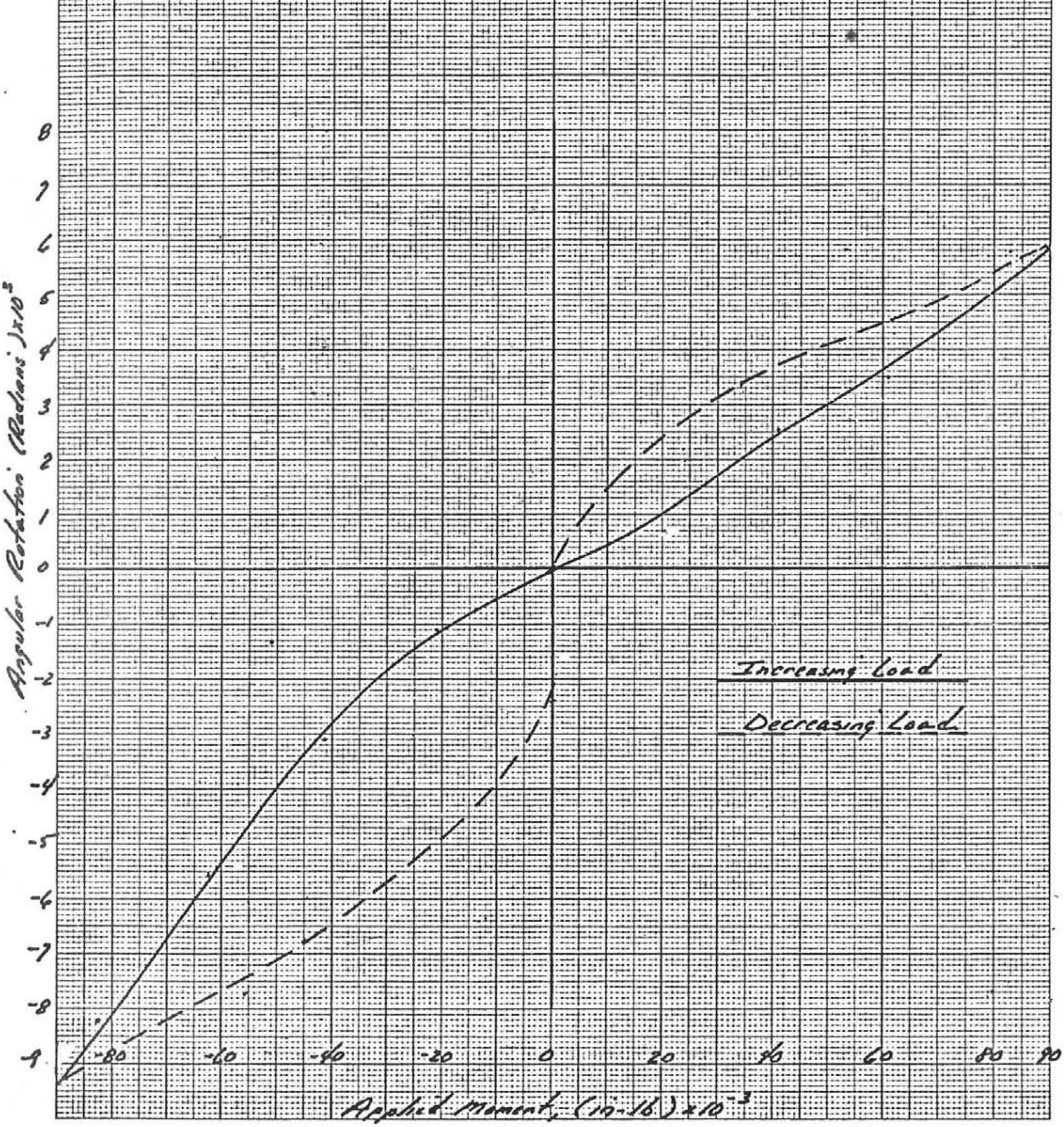

TABLE 3.3:

SHEET ____ OF ____

ANCO ANCO Engineers, Incorporated 1701 Colorado Avenue, Santa Monica, CA 90404 (213) 829-9721, 829-2624	DESCRIPTION Elev = -23°, 0° Azimuth - Moment about y-axis (Elev. mechanism)
MADE BY Atk DATE 2/3/79	CALCULATIONS FOR Solaramics, Inc.
CHECKED BY DJ DATE 12/79	1310-4

(−) Moment against Elevation Linkages
−23° Elevation, 0° Azimuth

moment (in-lb)	θ_x Radians x 10^{-4}	θ_y Radians x 10^{-4}
0	0	0
-13,949	0	-5.5
-27,897	1.1	-12.0
-41,846	1.6	-19.7
-55,795	2.2	-31.7
-69,743	4.4	-38.3
-83,692	5.5	-45.9
-97,640	6.6	-54.7
-83,692	6.6	-51.4
-52,308	6.6	-43.7
-34,872	5.5	-33.9
-17,436	4.4	-27.3
0	0	0

TABLE 3.4:

ANCO Engineers, Incorporated		SHEET ___ OF ___
1701 Colorado Avenue, Santa Monica, CA 90404 (213) 829-9721, 829-2624		DESCRIPTION 0° Elev., 0° Azi. Load applied to Elevation Linkages
MADE BY Ahk	DATE 9/4/79	CALCULATIONS FOR Solaramics, Inc.
CHECKED BY RL	DATE 12/79	1310-4

Σ Moment against Elevation Linkages
0° Elevation, 0° Azimuth

Moment (in-lb)	θ_x radians $\times 10^{-4}$	θ_y Radians $\times 10^{-4}$
0	0	0
10,462	0	6.6
24,410	0	14.2
34,872	0	17.5
41,846	0	24.1
52,308	0	38.3
62,769	0	46.5
48820	0	39.9
17,436	0	33.9
10,462	0	20.8
0	0	0
0	0	-5.5
-10,462	0	-8.7
-27,897	0	-16.4
-34,872	0	-19.7
-41,846	1.1	-23.0
-52,308	2.2	-27.3
-62,769	5.5	-33.9
-48,820	5.5	-26.2
-37,897	3.2	-23.0
-13,949	1.1	-19.7
0	0	-5.5

TABLE 3.5:

SHEET ____ OF ____

ANCO Engineers, Incorporated 1701 Colorado Avenue, Santa Monica, CA 90404 (213) 829-9721, 829-2624	DESCRIPTION 30° Elevation, 0° Azimuth Load applied to Elevation Linkages
MADE BY RSK DATE 8/2/79	CALCULATIONS FOR Solaramics, Inc.
CHECKED BY RL DATE 12/79	1310-4

± Moments against Elevation Linkages

Elevation = 30°, Azimuth = 0°

Moment (in - lb)	θ_x Radians ×10⁴	θ_y Radians ×10⁴	Dial ind. (mils)	$\theta_{Jackstrut}$ Radians ×10⁴
0	0	3.3	0	0
+13949	-1.1	7.7	0	0
+27897	-1.1	16.4	3	2.1
+41846	-2.2	21.9	5.5	3.8
+55795	-2.7	29.5	8.5	6.0
+69743	-3.3	35.5	11	7.7
+83692	-3.8	41.6	13	9.1
+97641	-4.4	48.1	15	10.5
+38359	-3.3	29.5	10	7.0
+24410	-2.7	24.1	9	6.3
+13949	-2.2	20.8	8.5	6.0
+10462	-2.2	18.6	8.0	5.6
0	-1.1	6.6	4.5	4.5

TABLE 3.6:

SHEET ____ OF ____

ANCO

ANCO Engineers, Incorporated
1701 Colorado Avenue, Santa Monica, CA 90404
(213) 829-9721, 829-2624

MADE BY RSK DATE 2/8/79

CHECKED BY PL DATE 12/79

DESCRIPTION Elev = 60°, Azi = 0°
moment about y-axis (Elevation Links)

CALCULATIONS FOR Solaronics, Inc.
1310-4

+ Moments against Elevation Linkages

Elevation = 60°, Azimuth = 0°

moment (in-lb)	θ_x Radians x10^-4	θ_y Radians x10^-4	θ_y actuator. Radians x10^-4
0	0	0	0
6,974	0	2.7	-
13,949	-1.1	4.4	-
20,923	-1.1	5.5	1.1
27,897	-1.6	8.2	1.3
34,872	-2.2	10.9	1.3
41,846	-2.7	13.7	1.4
48,820	-3.3	16.4	1.4
31,385	-2.2	12.0	1.4
17,436	-1.1	8.7	1.4
13,949	-1.1	7.7	1.4
9,764	-1.1	5.5	1.2
0	+1.1	1.1	1.2

TABLE 3.7:

ANCO Engineers, Incorporated
1701 Colorado Avenue, Santa Monica, CA 90404
(213) 829-9721, 829-2624

MADE BY RSK DATE 2/3/79

CHECKED BY RL DATE 12/79

DESCRIPTION 180° Elevation, 0° Azi
± Moments about y axis

CALCULATIONS FOR Solaramics, Inc.

± Moments about y-axis (Elevation Linkages)

Note: No hysteretic Data taken during this Run.

180° Elevation, 0° Azimuth

Moment (in - lb)	θ_y (Radians x 10^{-4})
0	0
17,436	23.9
34,872	38.0
69,743	64.8
139,487	121.0
209,230	173.1
0	0
-17,436	- 19.7
-34,872	- 33.8
-69,743	- 59.1
-139,487	- 126.7
-209,230	- 178.7
0	- 31.1

SHEET ___ OF ___

ANCO Engineers, Incorporated
1701 Colorado Avenue, Santa Monica, CA 90404
(213) 829-9721, 829-2624

MADE BY RSK DATE 7/?/79

CHECKED BY [illegible] DATE 12/79

DESCRIPTION -23° Elevation, 0° Azimuth moments about azimuth linkages

CALCULATIONS FOR Solaronics, Inc 1310-4

± moments against Azimuth Linkages
-23° Elevation, 0° Azimuth

moment (in-lb)	θ_x Radians $\times 10^{-4}$	θ_y Radians $\times 10^{-4}$
0	24.1	1.1
20,923	46.5	2.2
41,846	60.1	2.7
62,769	83.1	3.8
83,692	106.6	4.9
90,666	113.7	4.9
48,820	107.2	4.4
31,385	99.5	4.4
24,410	95.1	3.8
17,436	88.6	3.8
10,462	82.0	3.8
0	19.7	1.1
0	0	0
-20,923	-12.0	1.6
-41,846	-38.3	2.7
-62,769	-55.8	3.3
-83,692	-73.3	4.4
-90,666	-79.8	4.9
-69,743	-77.6	4.4
-24,410	-63.4	3.8
-17,436	-52.5	3.3
-10,462	-48.1	3.3
0	0	0

TABLE 3.9:

SHEET ____ OF ____

ANCO Engineers, Incorporated
1701 Colorado Avenue, Santa Monica, CA 90404
(213) 829-9721, 829-2624

MADE BY RSK DATE 2/8/79

CHECKED BY PL DATE 12/79

DESCRIPTION 0° Elev., 0° Azimuth moments about Azimuth Linkage

CALCULATIONS FOR Solaramics, Inc.

1310-4

± moments about Azimuth Linkages
0° Elevation, 0° Azimuth

moment (in-lb)	θ_x radians×10^{-4}	θ_y radians×10^{-4}
0	0	0
20,923	13.1	1.1
41,846	32.8	2.7
62,769	59.1	4.4
83,692	75.5	5.5
90,666	83.1	6.6
59,282	75.5	6.6
41,848	64.5	5.5
27,897	51.4	3.8
10,462	44.8	3.8
0	-6.6	0
0	-16.4	0
-24,410	-44.8	1.1
-41,846	-59.1	1.6
-62,769	-79.8	2.7
-83,692	-98.4	4.4
-90,664	-109.4	5.5
-52,308	-101.7	4.9
-41,846	-94.1	4.4
-17,436	-85.3	3.3
0	-13.1	0

TABLE 3.10:

SHEET ____ OF ____

ANCO Engineers, Incorporated 1701 Colorado Avenue, Santa Monica, CA 90404 (213) 829-9721, 829-2624	DESCRIPTION *30° Elevation, +90° Azimuth Load applied to Az linkages*
MADE BY *[illegible]* DATE *7/3/79*	CALCULATIONS FOR *Solaronics, Inc.*
CHECKED BY *[illegible]* DATE *12/79*	*1310-4*

± Moments against Azimuth Linkages
30° Elevation 90° Azimuth

	± Moment (in-lb)	θ_x Radians x 10^{-4}	θ_y Radians x 10^{-4}
Load ↓	0	-1.0	+2.0
	+13572	20.7	+2.0
	+28840	49.2	0
	+40715	65.0	-2.0
	+54287	89.6	-3.9
	+67858	114.2	-5.5
	+81430	147.6	-7.9
	+88216	162.4	-9.4
Unload ↓	+72948	135.8	-5.9
	+47501	114.2	-4.4
	+25447	98.4	-3.4
	+15268	85.6	-3.0
	+8482	73.8	-1.5
	0	25.6	+2.0
- moment Load ↓	0	0	0
	-13572	-10.8	-3.0
	-27143	-36.4	-5.9
	-40715	-53.1	-9.8
	-54287	-67.9	-13.3
	-67858	-83.7	-18.7
	-81430	-101.4	-22.1
	-88216	-107.3	-23.6
Unload ↓	-54287	-90.6	-17.7
	-27143	-70.9	-12.8
	-15268	-51.2	-7.9
	-6786	-37.4	-4.9
	0	-3.9	+1.0

TABLE 3.11:

SHEET ____ OF ____

ANCO Engineers, Incorporated 1701 Colorado Avenue, Santa Monica, CA 90404 (213) 829-9721, 829-2624	DESCRIPTION 30° Elev, +90° Azi' moments applied to Azimuth Linkages
MADE BY RSK DATE 2/16/79	CALCULATIONS FOR Solaramics, Inc
CHECKED BY [illegible] DATE 12/79	1310-4

± Moments applied to Azimuth Linkages 30° El, +90° Azi

moment (in-lb)	θ_x rad×10^{-4}	θ_y rad×10^{-4}
0	0	0
18,221	16.6	.8
36,442	43.1	1.5
54,664	72.5	.8
72,885	102.0	0
91,106	130.0	0
54,664	86.9	1.5
23,688	70.3	3.0
9,111	51.4	3.0
0	10.6	3.0
0	0	0
-18,221	-15.9	-4.5
-36,442	-65.0	-18.1
-54,664	-91.4	-24.2
-72,885	-113.3	-31.7
-91,106	-133.0	-39.3
-45,553	-104.2	-28.7
-23,688	-78.6	-20.4
-10,933	-58.9	-13.6
0	+6.0	+3.0

SHEET ____ OF ____

ANCO Engineers, Incorporated
4701 Colorado Avenue, Santa Monica, CA 90404
(213) 829-9721, 829-2624

MADE BY R.S.K. DATE 7/2/79.

CHECKED BY [illegible] DATE 12/79

DESCRIPTION 30° Elev., +45° Azi Moments applied to Azimuth Linkage

CALCULATIONS FOR Solaramics, Inc. 1310-4

30° Elev, 45° Azi

Moment (in-lb)	θ_x radians $\times 10^{-4}$	θ_y radians $\times 10^{-4}$
0	0	0
13,572	12.4	-1.1
27,143	31.7	-2.8
40,715	49.8	-5.7
54,287	64.5	-8.5
67,858	80.3	-11.3
81,430	95.0	-14.7
88,216	103.0	-18.1
64,465	88.2	-13.6
45,804	78.1	-11.3
35,626	70.1	-9.1
22,054	58.8	-8.5
8,482	44.1	-5.7
0	5.7	-1.1
0	0	-2.3
-13,572	-10.7	-3.4
-27,143	-46.4	-6.8
-40,715	-70.1	-11.3
-54,287	-87.1	-15.8
-67,858	-103.0	-20.4
-81,430	-118.8	-23.8
-88,216	-125.6	-26.0
-54,287	-107.5	-21.5
-39,019	-86.0	-15.8
-28,840	-74.7	-12.4
-13,572	-62.2	-11.3
-8,482	-52.0	-7.9
-5,089	-35.1	-5.7
0	0	-2.3

TABLE 3.13:

SHEET ____ OF ____

ANCO

ANCO Engineers, Incorporated
1701 Colorado Avenue, Santa Monica, CA 90404
(213) 829-9721, 829-2624

MADE BY Ahk DATE 2/3/79
CHECKED BY PD DATE 12/79

DESCRIPTION 30° Elev, 0° Az. Moment applied to Azimuth Linkage
CALCULATIONS FOR Solaronics, Inc.
w/# 1310-4

Elev Rate = 140 in/in — I Moment applied to Az. Linkage; 30° El, 0 Az.

Moment (in-lb)	θ_x radians $\times 10^{-4}$	θ_y radians $\times 10^{-4}$	θ_x Actuator radians $\times 10^{-4}$
0	0	0	0
13,572	8.7	-1.6	0
27,143	26.2	-6.6	6.3
40,715	38.3	-10.9	9.8
54,287	51.4	-13.1	13.3
67,858	63.4	-17.5	16.8
81,430	76.6	-20.8	20.3
88,216	83.1	-23.0	21.7
72,948	73.3	-20.8	21.0
42,412	52.5	-14.2	15.4
33,929	41.6	-10.9	12.6
8482	28.4	-8.7	9.1
0	3.3	-2.2	2.1
0	-2.7	0	-7.0
-13,572	-25.2	-1.1	-10.5
-27,143	-44.8	-3.3	-14.0
-40,715	-54.7	-5.5	-15.4
-54,287	-68.9	-7.7	-16.8
-67,858	-82.0	-9.8	-18.2
-81,430	-94.1	-12.0	-20.3
-88,216	-99.5	-14.2	-21.0
-67,858	-86.4	-9.8	-20.3
-42,412	-78.7	-8.7	-19.6
-28,840	-70.0	-7.7	-18.2
-23,750	-64.5	-6.6	-17.5
-20,358	-60.1	-5.5	-16.8
-13,572	-55.8	-4.4	-16.8
-8,482	-50.3	-3.8	-15.4
0	-3.8	+1.1	-4.9

TABLE 3.14:

SHEET ___ OF ___

ANCO ANCO Engineers, Incorporated 1701 Colorado Avenue, Santa Monica, CA 90404 (213) 829-9721, 829-2624	DESCRIPTION 30° Elev, 0° Azimuth moment applied to Azimuth Linkages
MADE BY RSK DATE 7/16/79	CALCULATIONS FOR Schramics Inc
CHECKED BY [signature] DATE 12/79	1310-4

± Moments applied to Azimuth Linkages, 30° Elev, 0° Az.

Moment (in-lb)	θ_x radians x 10^{-4}	θ_y radians x 10^{-4}
0	0	0
18,221	14.2	-3.3
36,442	33.9	-5.5
54,664	49.2	-7.7
72,885	64.5	-12.0
91,106	78.7	-16.4
61,952	55.8	-7.7
54,664	39.4	-4.4
51,019	20.8	0
3,644	13.1	+1.1
0	12.0	+1.1
0 (No Load)	10.9	+1.1
0	0	0
-18,221	-12.0	-4.4
-36,442	-30.6	-6.6
-54,664	-49.2	-13.1
-72,885	-68.9	-21.9
-91,106	-86.4	-35.0
-41,909	-51.4	-7.7
-25,510	-40.5	-5.5
-6,560	-21.9	-3.3
0	-3.3	-3.3
0 (No Load)	+1.1	-1.1

TABLE 3.15:

SHEET ____ OF ____

ANCO ANCO Engineers, Incorporated 1701 Colorado Avenue, Santa Monica, CA 90404 (213) 829-9721, 829-2624	DESCRIPTION 30° Elevation, 0° Azimuth Moment applied to Azimuth Linkage
MADE BY RSK DATE 2/16/79	CALCULATIONS FOR Solaramics, Inc
CHECKED BY PJ DATE 12/79	1310-4

+ Moment Applied to Azimuth Linkage , 30° Elev, 0° Azi
Sightings taken From top of Cross Head & From
Top of Concrete Column.

Moment	θx crosshead rad×10⁻⁴	θz Crosshead rad×10⁻⁴	θx Column rad×10⁻⁴	θz column rad×10⁻⁴
0	0	0	0	0
18,221	5.6	0	1.1	-1.1
36,442	23.5	3.4	3.4	-2.3
54,664	33.6	5.6	5.7	-4.6
72,885	44.7	5.6	6.8	-6.8
91,106	57.0	6.7	9.1	-9.1
43,731			6.8	-4.6
34,620	33.6	3.4		
8,382			5.7	-1.1
7,288	15.7	1.1		
3,644			5.7	-1.1
1,822	8.9	0		
0	1.1	-2.2	5.7	0

TABLE 3.16:

SHEET ____ OF ____

ANCO

ANCO Engineers, Incorporated
1701 Colorado Avenue, Santa Monica, CA 90404
(213) 829-9721, 829-2624

MADE BY RSK DATE 2/3/79

CHECKED BY [illegible] DATE 12/79

DESCRIPTION 30° Elev., -45° Azi Moment applied to Azi Linkages

CALCULATIONS FOR Solaramics, Inc.

1310-4

30° Elev, -45° Azi
± Moments applied against azemuth Linkages

Moment (in-lb)	θ_x radians x 10^{-4}	θ_y radians x 10^{-4}
0	10.3	-1.5
18,661	40.0	-3.6
27,143	49.2	-4.1
40,715	63.6	-7.2
54,287	78.9	-8.2
67,858	93.3	-10.3
81,430	107.7	-12.3
88,216	112.8	-12.8
50,894	87.1	-9.2
27,143	71.8	-7.2
16,965	62.5	-6.7
8,482	55.4	-5.1
0	11.3	-1.0
0	0	0
-13,572	-9.2	-2.1
-27,143	-24.6	-3.6
-40,715	-34.9	-6.2
-54,287	-42.0	-8.2
-67,858	-55.4	-10.3
-81,430	-67.7	-12.3
-88,216	-72.8	-13.8
-57,681	-53.3	-9.2
-45,804	-44.1	-7.7
-20,358	-32.8	-6.2
-13,572	-26.7	-5.6
-6,786	-21.5	-4.1
0	+3.1	-1.0

TABLE 3.17:

SHEET ___ OF ___

ANCO Engineers, Incorporated 1701 Colorado Avenue, Santa Monica, CA 90404 (213) 829-9721, 829-2624	DESCRIPTION 30° Elev. -90° Azi moment applied to azimuth Linkages
MADE BY [illegible] DATE 2/3/79	CALCULATIONS FOR Solaramics, Inc.
CHECKED BY [illegible] DATE 12/79	1310-4

± Moments against Azimuth Linkages, 30° Elev, -90° Azi

	Moment (in-lb)	θx radians x 10⁻⁴	θy radians x 10⁻⁴
Load ↓	0	0	0
	+ 13,572	34.0	- 2.1
	+ 27,143	67.7	-3.1
	+ 40,715	87.5	-6.2
	+ 54,287	113.5	-6.2
	+ 67,858	146.9	-7.3
	+ 81,430	166.6	-8.9
	+ 88,216	176.0	-13.5
Unload ↓	+ 57,680	135.6	-10.4
	+ 44,108	119.8	-7.3
	+ 20,358	105.2	-6.2
	+ 11,875	92.7	-3.6
	+ 5,089	71.9	-3.1
	0	5.2	0
Load ↓	0	5.2	0
	- 13,572	-11.5	-1.0
	- 27,143	-33.3	-4.2
	- 40,715	-53.1	-9.4
	- 54,287	-69.8	-13.5
	- 67,858	-87.7	-8.9
	- 81,430	-106.2	-24.0
	- 88,216	-117.7	-27.1
	- 57,680	-95.8	-18.7
	- 44,108	-82.3	-16.7
	- 20,358	-65.6	-12.5
	- 11,875	-51.0	-7.3
	- 5089	-42.7	-6.2
	0	-5.2	+1.0

TABLE 3.18:

SHEET ____ OF ____

ANCO Engineers, Incorporated 1701 Colorado Avenue, Santa Monica, CA 90404 (213) 829-9721, 829-2624	DESCRIPTION 180° Elev., 0° Azi Load applied to azimuth Linkages
MADE BY [illegible] DATE 2/3/79	CALCULATIONS FOR Solaramics, Inc.
CHECKED BY [illegible] DATE 12/79	1310-4

180° Elev, 0° Azi

± Moments about Azimuth Linkages

moment (in-lb)	θ_x radians x10^{-4}	θ_y Radians x10^{-4}	θ_x actuator Radians x10^{-4}
0	0	0	0
+20,735	6.56	0	2.6
+41,469	25.2	1.1	7.8
+62,203	35.0	2.7	13.0
+82,938	52.5	3.8	17.6
+89,850	57.9	4.4	19.5
+82,938	57.9	4.4	18.8
+62,203	42.6	3.3	15.6
+34,558	33.9	2.2	10.4
+24,190	21.9	1.1	6.5
0	0	0	0
-20,735	-10.9	2.7	-9.1
-41,469	-30.6	4.4	-13.0
-62,203	-53.8	6.6	-15.6
-82,938	-82.0	8.2	-16.9
-89,850	-94.0	8.7	-17.6
-55,292	-78.7	7.7	-15.6
-44,925	-67.8	5.5	-14.3
-33,175	-59.0	4.4	-13.0
-25,573	-52.5	3.8	-12.3
0	-24.0	1.1	-7.6

4.0 ANALYTICAL TECHNIQUES

The finite element method of stress analysis was used to compute the response of the heliostat. A previous model of the heliostat which included idealizations of the mirrors and supporting structure was modified and used to predict the behavior of the structure as tested. The model was modified by replacing the idealizations of the mirrors and supporting structures with idealizations of the concrete filled H-tube. The properties of the concrete filled H-tube was chosen to simulate the mass and inertia properties of the mirrors.

The model consisted of beam elements for the pedestal, linkages and tubes, and shell elements for stiffening flanges and cross tube mounts, and was implemented using the general purpose structural analysis computer program EASE2. A calcomp plot of the model is shown in Figure 4.1.

Both eigenvalue runs for the eigenparameters (frequencies and mode shapes) and static runs for the gravity effects and load deflection characteristics were performed. Only one configuration was modeled with the elevation angle $\alpha = 180°$ and the azimuth angle $\beta = 0°$ (the stowed configuration).

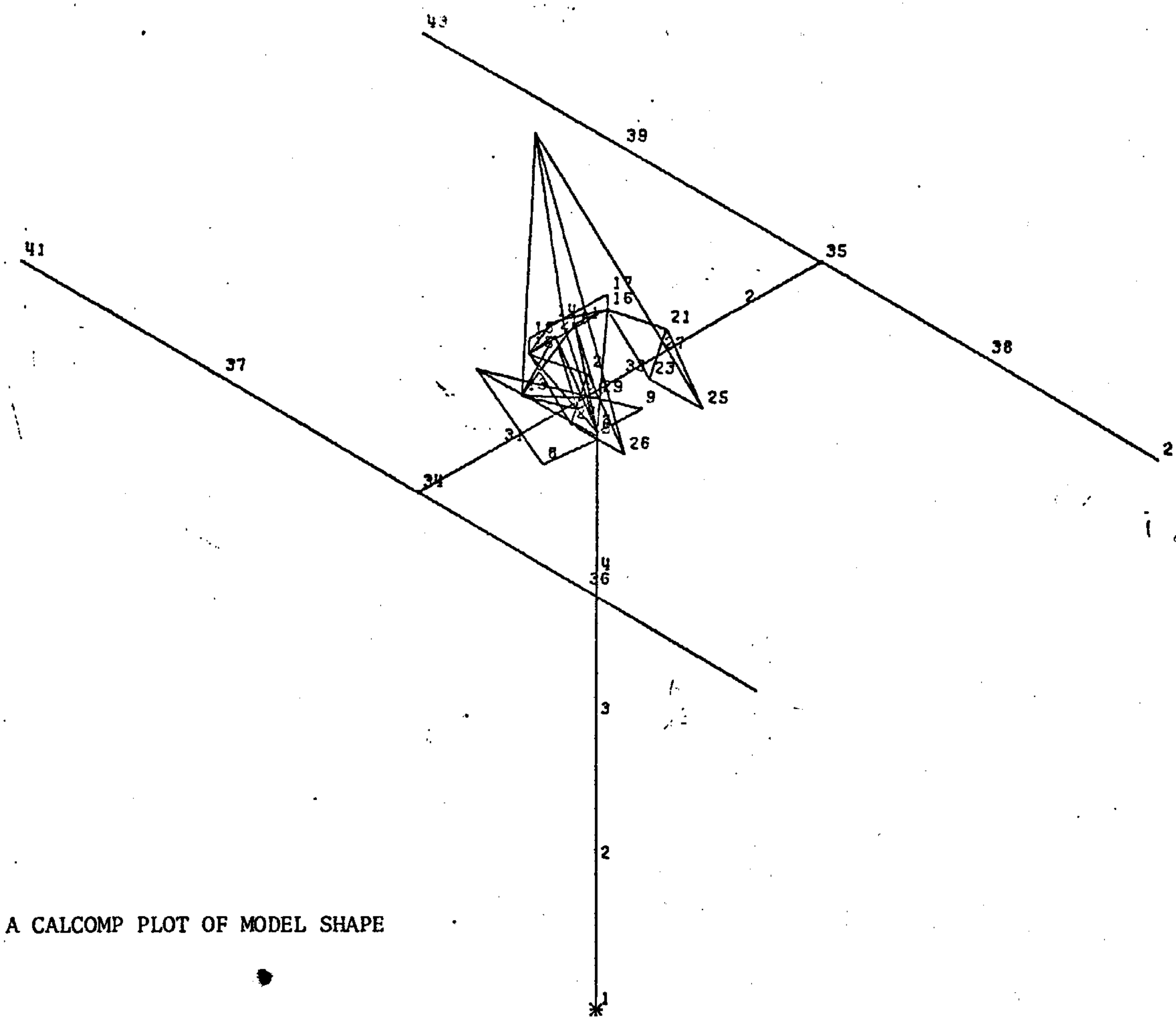

FIGURE 4.1: A CALCOMP PLOT OF MODEL SHAPE

SOLAR CENTRAL RECEIVER PROTOTYPE HELIOSTAT
THE UNDEFORMED SHAPE OF THE SOLAR CENTRAL RECEIVER PROTOTYPE HELIOSTAT

Z

RAME DISPLAYS BEAM AND SHELL ELEMENTS

5.0 ANALYTICAL RESULTS

The eigenvalues (frequencies of vibration) for the first ten modes are given in Table 5.1. Also reported in this table are the eigenvalues for the first six modes for the previous model in which the mirrors and supporting structure were modeled.

Two static runs were performed: (1) gravity loading, and (2) positive elevation moment. Two vertical loads of 1,000 lb were applied at the ends of the cross tubes (nodes 20 and 42 in Figure 4.1) to produce an elevation moment of 219,500 in.-lb about the X-axis. The predicted rotation of the cross tube (node 31) was 10.8 milliradians; the predicted rotation about the hinge line (node 15) was 3.8 milliradians.

TABLE 5.1: EIGENVALUES OF HELIOSTAT

Mode	ω, Hz	
	Lumped Model	Mirrored Model
1	2.67	2.30
2	3.28	3.20
3	4.17	3.72
4	5.31	5.20
5	6.96	6.02
6	7.72	7.12
7	8.52	-
8	13.49	-
9	16.89	-
10	20.18	-

6.0 COMPARISON OF EXPERIMENTAL AND ANALYTICAL RESULTS

The experimental results are compared, where comparison is possible, to the theoretical predictions in Table 6.1. Experimental results for mode 1 were not obtained at $\alpha = 180°$, $\beta = 0°$, but were obtained at $\alpha = 30°$, $\beta = 0°$ and $\alpha = 60°$, $\beta = 0°$. The theoretical prediction at $\alpha = 30°$, $\beta = 0°$ for the mirrored model is $\omega_1 = 2.60$ Hz.

The first mode, observed during manual excitation, was not a structural mode in that it was a "banging against the stops" of the azimuth linkage. The second mode, observed during both manual excitation and snapback, represents a banging against the stops of the elevation linkage. The third and higher modes that were observed were structural modes.

The rotation of the cross tubes due to a positive elevation moment of 220,000 in.-lb for $\alpha = 180°$, $\beta = 0°$ was measured to be 19 milliradians. The predicted value was 10.8 milliradians.

The discrepancy between the measured and theoretical results is a result of:

(1) the clearance in the azimuth and elevation linkages;

(2) the backlash of the two drive mechanisms;

(3) lack of detailed structural modeling of the trunnion assembly and of the kingpin assembly; and,

(4) The lack of soil springs in the structural model.

The clearance in the linkages and the backlash in the mechanisms cannot be modeled using linear structural analysis. Rather, nonlinear analysis to account for the varying stiffness must be used.

The structural model as implemented is adequate to provide estimates at the eigenparameters provided significant nonlinear effects do not occur. Revision of the model is necessary to improve the estimates of the static deflections and predictions of elastic stresses.

TABLE 6.1: COMPARISON OF RESULTS

Mode 1	Frequency		Percentage Difference
	Theory	Experimental	
1	2.67 (2.60)	1.17, 1.91*	122, 36
2	3.28	2.43	35
3	4.17	5.16	-19
4	5.31	3.83	39
5	6.96	9.38	-26
6	7.72	8.95	-14
7	8.52	9.57**	-
8	13.45	20.5**	-
9	16.85	†	-
10	20.18	23.1**	-

*Not measured at $\alpha = 180°$, $\beta = 0°$

**Speculative

†Not observed

APPENDIX A

DRIVE MECHANISM

NATURAL FREQUENCY RESPONSE

ELEVATION MODE @ 0^{o} @ AZIMUTH

EL. ANGLE		HERTZ
-23	-------------	2.59
0	-------------	2.75
30	-------------	2.85
60	-------------	2.62
180	-------------	2.33

AZIMUTH MODE @ 67^{o} ELEVATION

-90^{o}	-------------	1.95
0^{o}	-------------	1.75
$+90^{o}$	-------------	1.95

SIMULATED ARRAY INERTIA

$I_{ELEV.}$ --------- $= 18.9 \times 10^{6}$ LB-IN^2

$I_{AZ.}$ --------- $= 17.9 \times 10^{6}$ LB-IN^2

PERFORMANCE @ 12 M/S WIND

ELEVATION MECHANISM DEFLECTION

Data includes Backlash, Pedestal and Foundation Deflections.

Elevation Angle	Applied Moment	Deflection
-23°	-28,900 in lbs	-1.3 MR
0°	+19,000 in lbs	+1.1 MR
0°	-19,000 in lbs	-1.25 MR
30°	+28,900 in lbs	+1.7 MR
60°	+17,250 in lbs	+ .5 MR

AZIMUTH MECHANISM DEFLECTION

Includes *Backlash, Pedestal & Foundation Deflections

-90°	±28,900 in lbs	±5.4 MR
0°	±28,900 in lbs	±4.1 MR
+90°	±28,900 in lbs	±5.61 MR

Measured Backlash of Azimuth Actuator = .0085 in.

= 1.6 MR

PEDESTAL CHARACTERISTICS

TYPE LOADING	STIFFNESS, Radians/in lb. TEST	ANALYSIS
Cantilever Bending	2.58×10^{-9}	2.99×10^{-9}
Uniform Moment @ Top	13.8×10^{-9}	12×10^{-9}
Torsion @ Top	10×10^{-9}	

Rotation @ Top of Pedestal Due to 12 m/s Wind,

Max. Drag Condition ------------- = 0.34 mr

Max Torsion Condition ------------- = 0.2 mr

Design Properties

Height Above Ground 12.5 ft

Below Ground 12 ft

Torsion Stiffness; $GJ = 1.6 \times 10^{10}$ lb -in^2

Bending Stiffness; $EI = 2.0 \times 10^{10}$ lb -in^2

+90° AZIMUTH, 30° ELEV. 264 TO LARGE READING FROM CENTRAL TORQUE TUBE

Azimuth Stiffness-Mod Linkage

Closed Actuator shaft. C.C. Wise Limit

Gage Pressure	Moment in Lbs	Transit Reading M M	Deflection MR
0	0	0	0
50	19,792	+25	3.11
100	39,584	+63	7.85
150	59,376	+78	9.72
200	79,168	109	13.6
250	98,960	127	15.8
300	118,752	145	18.0
350	138,544	162	20.2
210	83,126	118	14.7
140	55,417	95	11.8
0	0	7	.87
0	0	-8	-1.0
50	-19,792	-24	-2.99
100	-39,584	-50	-6.23
150	-59,376	-75	-9.34
200	-79,168	-98	-12.2
250	-98,960	-125	-15.6
300	-118,752	-150	-18.7
350	-138,544	-180	-22.4
235	-93,022	-146	-18.2
200	-79,168	-135	-16.8
115	-45,521	-104	-12.9
65	-25,729	-73	-9.1
0		-50	-6.2

0^{o} AZIMUTH, 30^{o} ELEV. - 63" LOADARM, 29'4" TO TARGET

READING FROM CENTER TORQUE TUBE

Gage Pressure	Moment	Transit Reading MM	Deflection MR
0	0	0	0
50	19,792	20	2.23
100	39,584	39	4.36
150	59,376	53	5.93
200	79,168	68	7.6
250	98,960	84	9.4
300	118,752	100	11.2
350	138,544	121	13.5
310	122,710	113	12.6
150	59,376	70	7.8
50	19,792	52	5.8
0	0	17	1.9

Reading from top of hub. Same Condition.

0		0	0
50		15	1.7
100		30	3.4
150		44	4.9
200		56	6.3
250		70	7.8
300		80	8.9
350		90	10.0
290		25	2.7
50		15	1.7
0		7	.8

-90° AZIMUTH, 30° ELEV. 63", LOADARM 40'-8" TO TARGET

READING FROM LEFT OF CENTER TORQUE TUBE

Azimuth Stiffness Mod-Linkage

Gage Pressure	Moment	Transit Reading MM	Deflection MR
0	0	0	0
50	-19,792	-14	1.1
100	-39,584	-90	7.26
150	-59,376	-128	10.3
200	-79,168	-180	14.5
250	-98,960	-235	18.9
300	-118,752	-305	24.6
35	-13,800	-96	7.7
0	0	0	0
0	0	0	0
50	19,792	+19	1.53
100	39,584	45	3.63
150	59,376	70	5.65
200	79,168	95	7.6
250	98,960	120	9.68
300	118,752	142	11.45
350	138,544	168	13.55
270	106,870	145	11.7
225	89,064	120	9.68
190	75,209	85	6.85
160	63,334	60	4.8
120	47,500	50	4.0
75	29,688	45	3.63
0	0	+3	.24

TORQUE TO ROTATE PRIMARY WORM GEAR OF ACTUATOR

Actuator Torque Measurement

Elevation Mechanism Actuator 0° Azimuth

Elev. Angle.	Applied Moment	Actuator Torque in Lbs.	
-23°	0	35 clockwise	100 counter clockwise
	-34,850 in lbs	20 clockwise	150 counter clockwise
	-69,900	35 clockwise	210 counter clockwise
	-104,600	45 clockwise	260 counter clockwise
30°	0	10 clockwise	15 counter clockwise
	+104,600 in lbs	10 clockwise	20 counter clockwise
180°	0	60 clockwise	30 counter clockwise
	+34,850	80 clockwise	20 counter clockwise
	+55,800	100 clockwise	20 counter clockwise
	+83,700	90 clockwise	20 counter clockwise
	+111,600	80 clockwise	20 counter clockwise

AZIMUTH ACTUATOR TORQUE MEASUREMENTS

30^{o} ELEVATION

Azimuth Angle	Applied Moment in Lbs.	Actuator Torque	
0^{o}	0	10 clockwise	10 counter clockwise
	39,600	45 clockwise	75 counter clockwise
	59,400	60 clockwise	120 counter clockwise
-90^{o} (shaft extended)	0	20 clockwise	40 counter clockwise
	39,600	60 clockwise	140 counter clockwise
	59,400	95 clockwise	160 counter clockwise
$+90^{o}$ (shaft extended)	0	40 clockwise	20 counter clockwise
	39,600	130 clockwise	60 counter clockwise
	59,400	190 clockwise	95 counter clockwise

UNLIMITED RELEASE

INITIAL DISTRIBUTION

U.S. Department of Energy
600 E Street NW
Washington, D. C. 20585
Attn: W. W. Auer
G. W. Braun
K. Cherian
M. U. Gutstein
L. Melamed
J. E. Rannels

U.S. Department of Energy
San Francisco Operations Office
1333 Broadway
Oakland, CA 94612
Attn: S. D. Elliott
S. Fisk
R. W. Hughey
W. Nettleton

U.S. Department of Energy
Solar Ten Megawatt Project Office
P. O. Box 1449
Canoga Park, CA 91304
Attn: M. Slaminski

U.S. Department of Energy
Solar Ten Megawatt Project Office
5301 Bolsa Ave. MS14-1
Huntington Beach, CA 92649
Attn: R. W. Schweinberg

U.S. Department of Interior
Water & Power Res. Service
P.O. Box 427
Boulder City, NV 89005
Attn: J. Sundberg

Acurex
485 Clyde Avenue
Mountain View, CA 94042
Attn: J. Hull

Aerospace Corporation
Solar Thermal Projects
Energy Systems Group, D-5
Room 1110
P.O. Box 92957
El Segundo, CA 90009
Attn: P. deRienzo
P. Mathur

ARCO
911 Wilshire Blvd
Los Angeles, CA 90017
Attn: J. H. Caldwell, Jr.

Battelle Pacific Northwest Labs
P. O. Box 999
Richland, WA 99352
Attn: M. A. Lind

Bechtel National, Inc.
P. O. Box 3965
San Francisco, CA 94119
Attn: E. Lam
For: J. B. Darnell
R. L. Lessley

Black & Veatch
P. O. Box 8405
Kansas City, MO 64114
Attn: C. Grosskreutz
For: J. E. Harder
S. Levy

Boeing Engineering & Construction
P. O. Box 3707
Seattle, WA 98124
Attn: R. Gillette
J. R. Gintz
R. L. Campbell

Brookhaven National Laboratory
Upton, NY 11973
Attn: G. Cottingham

Busche Energy Systems
7288 Murdy Circle
Huntington Beach, CA 92647
Attn: K. Busche

Corning Glass Works
Advanced Products Dept.
M/S 25
Corning, NY 14830
Attn: W. M. Baldwin
A. Shoemaker

Electric Power Research Institute
P. O. Box 10412
Palo Alto, CA 93403
Attn: J. Bigger

Ford Aerospace
3939 Fabian Way, T33
Palo Alto, CA 94303
Attn: I. E. Lewis
For: H. Sund

Foster-Miller Associates
135 Second Avenue
Waltham, MA 02154
Attn: E. Poulin

General Electric Company
Advanced Energy Programs
P. O. Box 8661
Philadelphia, PA 19101
Attn: A. A. Koenig

General Electric Company
1 River Road
Schenectady, NY 12345
tric Company
1 River Road
Schenectady, NY 12345
Attn: J. A. Elsner
For: R. N. Griffin
R. Horton

GM Transportation System Center
GM Technical Center
Warren, MI 48090
Attn: J. Britt

Jet Propulsion Laboratory
Building 520-201
4800 Oak Grove Drive
Pasadena, CA 91103
Attn: V. Truscello
For: H. Bank
W. Carley
W. Carroll
E. Cuddihy

Lawrence Berkeley National Laboratory
University of California
Berkeley, CA 94720
Attn: A. J. Hunt

Los Alamos National Laboratory
P. O. Box 1663
Los Alamos, NM 87545
Attn: S. W. Moore

Martin Marietta Corporation
P. O. Box 179
Denver, CO 80201
Attn: P. R. Brown
A. E. Hawkins
T. Heaton
L. Oldham
H. C. Wroton

McDonnell Douglas Astronautics Co.
5301 Bolsa Avenue
Huntington Beach, CA 92647
Attn: P. Drummond
R. L. Gervais
D. A. Steinmeyer
L. Weinstein

Northrup, Inc.
302 Nichols Drive
Hutchins, TX 75141
Attn: J. A. Pietsch

Northrup, Inc.
Blake Laboratory
Suite 306
7061 S. University Boulevard
Littleton, CO 80122
Attn: J. Anderson
F. Blake

Pittsburgh Corning
800 Presque Isle Drive
Pittsburgh, PA 15239
Attn: W. F. Lynsavage

Pittsburgh Corning
723 N. Main Street
Port Allegany, PA 16743
Attn: W. J. Binder
For: R. Greene

PPG Industries, Inc.
One Gateway Center
Pittsburgh, PA 15222
Attn: C. R. Frownfelter

Safeguard Power Transmission Co.
Hub City Division
P. O. Box 1089
Aberdeen, SD 57401
Attn: R. E. Feldges

Schumacher & Associates
2550 Fair Oaks Blvd., Suite 120
Sacramento, CA 95825
Attn: J. C. Schumacher

Solar Energy Research Institute
1617 Cole Boulevard
Golden, CO 80401
Attn: L. Duhham, TID
G. Gross
B. Gupta
D. Kearney
L. M. Murphy
R. Ortiz, SEIDB
J. Thornton

Stanford Research Institute
333 Ravenswood Avenue
Menlo Park, CA 94025
Attn: A. Slemmons

Veda, Inc.
400 N. Mobile, Building D
Camarillo, CA 90310
Attn: L. E. Ehrhardt
For: W. Moore

Westinghouse Corporation
Box 10864
Pittsburgh, PA 15236
Attn: J. J. Buggy
For: R. W. Devlin
W. Parker

Winsmith
Division of UMC Industries
Springville, NY 14141
Attn: W. H. Heller

K. R. Miller, 3153
G. E. Brandvold, 4710; Attn: J. F. Banas, 4716
J. A. Leonard, 4717
B. W. Marshall, 4713; Attn: D. L. King
A. B. Maish, 4719
R. G. Kepler, 5810; Attn: L. A. Harrah, 5811
J. G. Curro, 5813
F. P. Gerstle, 5814
J. N. Sweet, 5824; Attn: R. B. Pettit and E. P. Roth
T. B. Cook, 8000; Attn: A. N. Blackwell, 8200
B. F. Murphey, 8300
C. S. Hoyle, 8122; Attn: V. D. Dunder
R. J. Gallagher, 8124; Attn: B. A. Meyer

D. M. Schuster, 8310; Attn: W. R. Hoover, 8312, for M. D. Skibo
A. J. West, 8314
W. R. Even, 8315
R. L. Rinne, 8320
C. T. Yokomizo, 8326; Attn: L. D. Brandt
P. L. Mattern, 8342; Attn: J. Vitko, Jr.
L. Gutierrez, 8400; Attn: R. A. Baroody, 8410
D. E. Gregson, 8440
C. M. Tapp, 8460
C. S. Selvage, 8420
V. Burolla, 8424; Attn: C. B. Frost
R. C. Wayne, 8450
T. D. Brumleve, 8451
W. R. Delameter, 8451
P. J. Eicker, 8451 (5)
R. M. Houser, 8451
C. L. Mavis, 8451
W. L. Morehouse, 8451
H. F. Norris, Jr., 8451
W. S. Rorke, Jr., 8451
D. N. Tanner, 8451
S. S. White, 8451
A. C. Skinrood, 8452
W. G. Wilson, 8453
Publications Division, 8265, for TIC (27)
Publications Division, 8265/Technical Library Processes and Systems Division, 3141
Technical Library Processes and Systems Division, 3141 (2)
M. A. Pound, 8214, for Central Technical File (3)